PETRO-MINERALOGICAL AND GEOCHEMICAL CHARACTERISATION OF RHYOLITIC TUFF AND ASSOCIATED ROCKS AROUND BURIWARA, BARMER DISTRICT, RAJASTHAN AND THEIR POTENTIALITY FOR REE MINERALISATION

by

SANJEEB KUMAR DEHINGIA

ENGG1G201801002

Bhabha Atomic Research Centre, Mumbai

A thesis submitted to the
Board of Studies in Engineering Sciences

In partial fulfillment of requirements

for the Degree of

MASTER OF TECHNOLOGY

of

HOMI BHABHA NATIONAL INSTITUTE

FEBRUARY, 2021

Homi Bhabha National Institute

Recommendations of the Thesis Examining Committee

As members of the Thesis examining Committee, we recommend that the thesis prepared by **Sanjeeb Kumar Dehingia** entitled "Petro-mineralogical and geochemical characterisation of rhyolitic tuff and associated rocks around Buriwara, Barmer district, Rajasthan and their potentiality for REE mineralisation" be accepted as fulfilling the thesis requirement for the Degree of Master of Technology.

	Name	Signature
Member-1	Dr. D. K. Sinha	Sinha
Member-2	Dr. T. S. Sunil Kumar	
Member-3	Dr. Navin Goyal	
Member-4	Dr. Pranesh Sengupta$	P. Sengupta
Member-5	Dr. A. Rama Raju	
Technical advisor	K. L. Mundra	
Examiner	Prof. A.M. Pophare$	
Guide & Convener	Dr. Navin Goyal	
Chairman	Prof. Vivekanand Kain$	

$ Participated through video conferencing

Final approval and acceptance of this thesis is contingent upon the candidate's submission of the final copies of the thesis to HBNI.

I hereby certify that I have read this thesis prepared under my direction and recommend that it may be accepted as fulfilling the thesis requirement.

(Dr. Navin Goyal)
Guide

Date: 15-02-2021

Place: Hyderabad

DECLARATION

I, hereby declare that the investigation presented in the thesis has been carried out by me. The work is original and has not been submitted earlier as a whole or in part for a degree / diploma at this or any other Institution / University.

Dehingia

(SANJEEB KUMAR DEHINGIA)

DEDICATED TO MY FAMILY

ACKNOWLEDGEMENTS

I express my sincere gratitude to Dr. D.K. Sinha, Director, Atomic Minerals Directorate for Exploration and Research for giving me permission and required facility to pursue the M. Tech program.

I am deeply indebted to my guide, Dr. Navin Goyal, AMD/HQ, Hyderabad for his support and relentless co-operation throughout the course of this work. My technical adviser Shri K. L. Mundra, AMD/HQ, Hyderabad is thankfully acknowledged for his suggestion and guidance through the learning process of this thesis.

I acknowledge my sincere gratefulness to Shri Sandeep Hamilton, Additional Director (OP-I); Shri B. Saravanan, Additional Director (OP-II); Dr. T.S. Sunil Kumar, Additional Director (R&D); Dr. B.S. Bisht, Regional Director, AMD/WR who inspired me to pursue the M.Tech programme. I am thankful to the competent authority of HBNI for providing the opportunity to pursue the M. Tech. degree.

I am thankful to Dr. S. K. Srivastava, former Head, BARC training school and Dr. A. Ramaraju, In-charge, BARC Training School, AMD Campus, Hyderabad for their valuable suggestions and support.

I appreciate and acknowledge Shri Kuldeep Nautiyal, SO/G and Mrs. Anubhooti Saxena, SO-E for their guidance in interpretation of thin section studies. I also sincerely thank Incharge, XRF laboratory, AMD/HQ Hyderabad; Incharge, Chemical laboratory, AMD/WR Jaipur and Incharge, Physics laboratory, AMD/WR Jaipur for their timely analytical support.

I wish to convey my special thanks to Shri Sanjay Bagora, SO-G; Shri Atanu Banerjee, SO-D and Shri S.P. Singh, SO-D for their affection and encouragement throughout the work. I also sincerely thank all my colleagues of AMD, Jaipur, batch mates of OCES 2018, BARCTS for their contribution directly or indirectly in preparation of this thesis.

Sanjeeb Kumar Dehingia

CONTENTS

		Page no.
Synopsis		**i**
List of Figures		**ii**
List of Tables		**vi**
Chapter 1	**INTRODUCTION**	**1**
1.1	Background	1
1.2	Previous study	3
1.3	Objective	4
1.4	Methodology	4
1.5	Location and accessibility	5
1.6	Physiography	5
Chapter 2	**REGIONAL GEOLOGY**	**7**
2.1	Malani Igneous Suite (MIS)	7
2.2	Siwana Ring Complex (SRC)	10
Chapter 3	**LOCAL GEOLOGY**	**13**
3.1	Lithology	15
3.1.1	Pyroclastic rock / Rhyolitic tuff	15
3.1.2	Rhyolite	16
3.1.3	Agglomerate	17
3.2	Structure	21
Chapter 4	**PETROGRAPHY**	**25**
4.1	Methodology	25
4.1.1	Preparation of thin section	25
4.1.2	Study in transmitted light microscope	25
4.2	Observations	26
4.2.1	Rhyolitic tuff	27
4.2.2	Rhyolite	29
4.2.3	Agglomerate	32
Chapter 5	**GEOCHEMISTRY OF TUFF AND ASSOCIATED ROCKS**	**35**
5.1	Methodology	35
5.1.1	X-Ray Fluorescence (XRF) laboratory	35

5.1.2	Chemical laboratory: Inductively Coupled Plasma –Optical Emission Spectroscopy (ICP-OES)	38
5.2	Identification of rock types	41
5.3	Geochemical analysis of Rhyolitic tuff	43
5.3.1	Major oxide and Trace Elements in Rhyolitic tuff	43
5.3.2	REE in Tuff	50
5.4	Geochemical analysis of Massive Rhyolite	52
5.4.1	Major oxide and Trace Elements in Massive Rhyolite	52
5.4.2	REE in Massive rhyolite	59
5.5	Geochemical analysis of Agglomerate	61
5.5.1	Major oxide and Trace Elements in Agglomerate	61
5.5.2	REE in Agglomerate	68
5.6	Geochemical analysis of Porphyritic Rhyolite	70
5.6.1	Major oxide and Trace Elements in Porphyritic Rhyolite	70
5.6.2	REE in Porphyritic rhyolite	77
5.7	Alteration studies	79
5.7.1	Elemental behaviour during alteration	80
Chapter 6	**RARE EARTH ELEMENT (REE) MINERALISATION**	**85**
Chapter 7	**RADIOACTIVE ANOMALIES**	**87**
7.1	Radioactive anomaly in rhyolitic tuff	87
7.2	Radioactive anomaly in agglomerate	87
7.3	Anomalous concentration of High Field Strength (HFS) elements in Tuff and Agglomerate	88
Chapter 8	**STUDY OF TECTONIC ENVIRONMENT**	**91**
Chapter 9	**DISCUSSION**	**93**
Chapter 10	**CONCLUSION AND FUTURE SCOPE OF WORK**	**99**
References		**101**

SYNOPSIS

REE mineralisation associated with alkaline igneous complexes represent one of the most economically important resources of heavy REE. Peralkaline granites are important host of such mineralisation. These complexes usually occur in continental within plate tectonic settings associated with rifts, faults or hotspot magmatism. Siwana Ring Complex (SRC) lying in the western part of Aravali range is having a similar setting which comprises of bimodal volcano-plutonic rocks of peralkaline nature. Buriwara area in the western part of SRC exposes rhyolite, tuff and agglomerate. These rocks are characterized by high concentration of SiO_2, Na_2O, K_2O, Zr, Nb, Y & REE and lower concentration of MgO, Fe_2O_3 (t), CaO, Cr, Ni & Sr. Dominance of K-feldspar phenocryst and perthitisation is abundantly observed during petrographic study which is indicating their hypersolvus origin. The pyroclastic rocks: tuff and agglomerate in the area hosts REE mineralisation. The evolution of the rocks are attributed to magmatic fractionation and also the intrinsic REE enrichment was there in the residual magma. The alteration has further enriched the concentration in tuff whereas, mineralisation in agglomerate is suspected to be adsorbed in the matrix part. Average REO concentration of 0.32% and 0.43% was analyzed from tuff and agglomerate samples respectively. Alteration has impacted mobility of alkali elements and as a result of which the peralkalinity was affected. Bivariate plots of Al_2O_3 vs TiO_2, Y vs Nb and Zr vs Nb forms positive correlation irrespective of altered and unaltered rocks suggesting their immobility during alteration. Thus for tectonic discrimination, Pearce et al (1984) was adopted which uses these HFS elements.

LIST OF FIGURES

Figure no.	Description	Page no.
2.1	Geological map of Rajasthan with highlighted MIS and SRC (after Sinha-Roy 1998)	8
2.2	Geological map of Siwana Ring Complex (after Bhushan and Chandrasekharan, 2002)	10
3.1	Geological map of Buriwara	14
3.2	Mixture terms and end-member rock terms for pyroclastic fragments (Fisher, 1966)	15
3.3	a) Sharp and steep boundary between rhyolite and tuff. b) Ferrugenised tuff with vesicular texture. c) A sharp contact between porphyritic and massive rhyolite d) Hematitic chert veins traversing within tuff. e, f) Block sized pyroclastic breccia / agglomerate	19
3.4	a, b) Quartz and calcite growth in lithophysae cavities attaining spherulitic texture c,d) Altered glass attaining rim structure and flattened to attain eutaxitic texture with the surrounding e) Uniform flow lamination in rhyolite f) Flow laminations with alternating cherty and ferrugenised layer	20
3.5	a) Illustration of how circumferential horizontal shortening results as material points move radially inward (reduction of arc length from a1–b1 to a2–b2) and is accommodated by the strike-slip components of fault displacements b) block diagram of centered subsidence with oblique-slip faults related to the camera iris effect. The area of the roof delimited by dashed box is roughly that considered in Figure a.	22
3.6	a) Pentagonal columnar joints in rhyolite: plan and section view b)Flow warping characterized by marker bed c)Slickenside observed in rhyolite d) Slickenside observed in tuff e) Intense warping of flow banding having attitude of axial plane: 10°/70°SE f) View of the warped banding on 130°/35° NE plane	23

4.1 Schematic diagram of transmitted light binocular microscope and its working principle 26

4.2 a) Microcrystalline granular texture of quartz and feldspar b) Preferred oriented texture with masking of ferruginous matter c) Glass fragment attaining devitrification along boundaries d) Magnetite crystal e),f) Ferrugenised band within microcrystalline quartzo and feldspar 28

4.3 a) Perlitic cracks in rhyolite b) Embayed margin along quartz boundaries c)Offset along microfaulting preserved in alternate ferrugenised and cherty bands d)Fracture and offset along quartz grain supporting faulting event e) K-feldspar undergoing perthitisation f)Apatite grain within ferrugenised matrix 31

4.4 a) Perthite phenocryst in quartzo-feldspathic groundmass b) Radiating laths of K-feldspar with impact of ferrugenisation c) Embayed margin interlocking texture forming by quartz and feldspar d) Microlaths of prismatic aegirine within quartzo-feldspathic groundmass. [Fls: Feldspar, Qtz: Quartz] 32

4.5 a) Flow texture in groundmass with quartz and K-Feldspar phenocryst b) Pyroxene phenocryst warped by surrounding flow texture c) Lithic fragments of rhyolite d) Spherulitic texture in quartz e) Altered glass showing perlitic cracks and orthoclase feldspar with Carlsbad twinning f) Devitrification of glass preserved as perlitic cracks. [Fls: Feldspar, Qtz: Quartz, Pxn: Pyroxene, LF: Lithic fragment, M: Matrix] 34

5.1 X-Ray generation principle 35

5.2 Working principle and photograph of ICP-OES instrument 38

5.3 a) Total Alkali Silica (TAS) diagram of acid volcanics of SRC, Most of them fall on the rhyolitic field with a few in trachy-dacite; b) Classification diagram using trace elements, they fall in the alkali rhyolite field (Al-rich Comendite and Fe-rich Pantellerite); c)A/NK vs A/CNK plots altered tuff in peraluminous and other unaltered lithotypes in peralkaline 42

5.4 Bar diagram of mean concentration of major, minor and trace element of tuff 46

5.5 Variation diagrams (Harker type) between major oxides (in %) and trace elements (ppm) in Tuff 48

5.6 Spider diagram for trace elements of Tuff a) Chondrite normalized after (Thompson, 1982); b) Primitive mantle normalized (Sun and Mc Donough 1989) 49

5.7 Spider diagram of REE, Chondrite normalized after (Boynton,1984) for tuff 51

5.8 Bar diagram of mean concentration of major, minor and trace element of massive rhyolite 55

5.9 Variation diagrams (Harker type) between major oxides (%) and trace elements (ppm) in Massive rhyolite 57

5.10 Spider diagram for trace elements in massive rhyolite a) Chondrite normalized (Thompson, 1982); b) Primitive mantle normalized (Sun and Mc Donough 1989) 58

5.11 Spider diagram of REE Chondrite normalized after (Boynton,1984) for massive rhyolite 60

5.12 Bar diagram of mean concentration of major, minor and trace element of Agglomerate 64

5.13 Variation diagrams (Harker type) between major oxides (%) and trace elements (ppm) in agglomerate 66

5.14 Spider diagram for trace elements in agglomerate a) Chondrite normalized (Thompson, 1982) b) Primitive mantle normalized (Sun and Mc Donough 1989) 67

5.15 Spider diagram of REE Chondrite normalized after (Boynton,1984) for agglomerate 69

5.16 Bar diagram of mean concentration of major, minor and trace element of porphyritic rhyolite 73

5.17 Variation diagrams (Harker type) between major, minor oxides (in %) and trace (ppm) for porphyritic rhyolite 75

5.18 Spider diagram for trace elements in porphyritic rhyolite a) Chondrite normalized (Thompson, 1982) b)Primitive mantle normalized (Sun and Mc Donough 1989) 76

5.19 Spider diagram of REE Chondrite normalized after (Boynton,1984) for porphyritic rhyolite 78

5.20 (Na2O+Cao)-Al2O3-CaO diagram of Nesbitt and Young (1984, 1989) showing alteration trends for average rhyolite and average basalt 79

5.21 Bivariate plots of major oxide and trace elemant behavior for altered and unaltered rocks 83

6.1 Chondrite normalized plot (Boynton, 1984) for average REE from different lithotypes from Buriwara 86

7.1 Bar diagram depicting relative enrichment of HFS elements in tuff and agglomerate plotted with respect to average crustal abundance, described in logarithmic scale 89

8.1 Tectonic discrimination diagram by Pearce et. al. (1984) 92

LIST OF TABLES

Table no.	Description	Page no.
5.1	Representative Major Oxide and trace elemental compositions of Rhyolitic tuff from Buriwara	44
5.2	Statistical evaluation of major, minor (in %) and trace (in ppm) elements of tuff	45
5.3	Correlation matrix of geochemical data of major, minor (in %) and trace elements (in ppm) of tuff (n=16)	47
5.4	Representative analysis of REE of Tuff:	51
5.5	Representative Major Oxide and trace elemental compositions of Massive rhyolite from Buriwara	53
5.6	Statistical evaluation of major, minor (in %) and trace (in ppm) elements of Massive rhyolite	54
5.7	Correlation matrix of geochemical data of major oxides (in %) and trace elements (in ppm) in massive rhyolite (n=7)	56
5.8	Representative analysis of REE in Massive rhyolite	59
5.9	Representative Major Oxide and trace elemental compositions of Agglomerate from Buriwara	62
5.10	Statistical evaluation of major, minor (in %) and trace (in ppm) elements of Agglomerate	63
5.11	Correlation of geochemical data of major, minor (in %) and trace elements (in ppm) in agglomerate (n=6)	65
5.12	Representative analysis of REE of Agglomerate	68
5.13	Representative Major Oxide and trace elemental compositions of Porphyritic rhyolite from Buriwara	71
5.14	Statistical evaluation of major, minor (in %) and trace (in ppm) elements of Porphyritic rhyolite	72

5.15 Correlation matrix of geochemical data of major, minor (in %) and trace elements (in ppm) of porphyritic rhyolite (n=7) 74

5.16 Representative analysis of REE in Porphyritic rhyolite 77

5.17 U and Th ratio of rhyolitic tuff samples from Buriwara 82

6.1 Average REO concentration in different lithotypes of Buriwara 85

7.1 Physical assay result of radioactive tuff and agglomerate samples from Buriwara 87

7.2 Average concentration of HFS elements in tuff and agglomerate from Buriwara and average concentration in continental crust 89

CHAPTER 1

INTRODUCTION

1.1 Background

Anorogenic tectonic setting holds significance as the rocks present in such environment are known for enrichment in various mineralisation. They are related to continental rifting events wherein continental lithosphere is thinned as a result of upwelling asthenosphere. The upwelling raises the geothermal gradient leading to a divergent or extensional tectonic setting which is characterized by the generation of A-type or peralkaline igneous rocks (Kochhar, 1984). Peralkaline rocks are defined by high contents of alkali elements relative to alumina, such that molecular (Na_2O+K_2O) exceeds molecular Al_2O_3. Under such circumstances, minerals like the sodic amphiboles (riebeckite and arfvedsonite) and the sodic pyroxene (aegirine) are commonly found in these rocks. In addition, they tend to be relatively Fe-rich and thus fayalitic olivine sometimes occurs. In silica-deficient (undersaturated) peralkaline rocks of mafic composition, common feldspars may be replaced or augmented by feldspathoid minerals. As the felsic peralkaline magmas are highly fractionated, they favor the concentration of Rare Earth Elements (REE) and associated elements. The high concentrations of these elements in residual peralkaline magmas leads to the formation of a wide range of uncommon silicate and oxide minerals. Peralkaline granites and associated volcanic are characterized by concentration of heavy rare metals (Dostal, 2017) for which the peralkaline rocks gain special economic importance.

Apart from this, divergent setting is also a suitable location for volcanogenic Uranium (U) deposits. The thinning of the crust and rise of mafic magmas induce partial melting of U rich upper crustal rocks to create melt compositions that favor enrichment of U and other incompatible elements. Thus felsic rocks have high intrinsic uranium content with granite and its volcanic equivalent rhyolite having the highest. Hydrothermal fluids that are driven by magmatic heat, leach uranium from these rocks and concentrate at sites of deposition within veins, stockworks, breccias, volcaniclastic rocks and lacustrine caldera sediments (Goodell, 1985). Sometimes the rocks proximal to volcanic centers may directly form such deposits. Caldera complexes are often targeted for such kind of deposits because they comprise a large range of magma composition from basalt to highly fractionated rhyolite. Another highly favourable character is because of the development of permeable horizon (in the form of fault systems and collapse structures) and existence of relatively shallow magma chamber inducing convective hydrothermal fluid circulations lasting over a long period of time. Such a geological environment allows alterations of the source rocks, remobilization of U from the volcanic pile (leaching of uranium bearing minerals and glassy matrix) and re-concentration in suitable locales.

In India the Trans-Aravalli igneous activity of Malani Igneous Suite (MIS) in western Rajasthan comprises anorogenic peraluminous to peralkaline granites with bimodal volcanics. The co-genetic pyroclastics and acid lava flows constitute the most voluminous unit of MIS representing the largest felsic volcanic suite in India which are characterized by ring structures. Siwana Ring Complex (SRC) is a classic example of collapse caldera characterized by intrusion of peralkaline granites as ring dyke. The complex is also characterized by presence of faults and fracture system which might acts as conduits for hydrothermal fluid transport that leads to alterations such as ferrugenisation, sericitisation and kaolinization. Considering all these factors, the SRC is identified as a favorable setup for the exploration of REE and Volcanogenic U deposit. The study has been carried out in the western margin of the SRC near Buriwara village where rhyolitic tuff and rhyolite is exposed.

1.2 Previous study

The term 'Malani' was introduced by Blanford (1877) for volcanic series of porphyritic lavas and ash beds occurring in parts of Barmer district, Rajasthan, formerly known as Malani area. Different locations within SRC have been surveyed by Atomic Minerals Directorate for Exploration and Research (AMD) since five decades, in various spells. Exploration started in SRC way back in 1978 by Narayan Das et. al., followed by Jain et. al. in 1996, leading to identification of anomalous radioactivity in agpaitic acid intrusive traversing felsic volcanics. The major emphasis has been on the younger intrusive like microgranites and aplites intruded into the peralkaline granites in the southern margin near Mokalsar-Ramaniya area having substantial amount of REE, Nb, Y, Zr and Siwana fort hill having considerable U anomaly. Nb, Zr, REE rich aplite intrusive and their potential to host REE mineralization have been emphasized by many workers (Narayan Das et al 1978, Jain et al 1996, Vallinayagam G 1998, 1999, 2004 etc). Bidwai (2001), in his PhD thesis, expressed on the geology, structure and geochemical potentiality of SRC for favourable volcanogenic, caldera related U and rare metal mineralization. In the F.S 2011-12, the SRC for its radioactive and related REE potential has been relooked intensively by AMD with the emerging and established concepts on felsic volcanism related volcanogenic U mineralisation being explored globally. From the surveys conducted in different localities within the complex, Bhatikhera, Phulan, Ramaniya, Nal and Dantala were discovered to have economically viable concentrations of Rare Earth Elements (REE) and Rare Metals (RM) with avg. TREE of 0.60%, 0.3%, 0.312%, 1.47% and 0.629% respectively. The mineralization in all the localities except Dantala are hosted by felsic microgranite dyke which is the last phase of intrusions. In Ramania, besides microgranite, brecciated mylonitized granite as well as pegmatitic veins are also behaving as host rock. In Dantala, mineralisation is hosted by pyroclastic tuffaceous rock. Besides that, geological and radiometric surveys carried out by Banerjee and Varughese during 2011-12 brought to light thorium free uranium mineralisation in the intermediate volcanic rocks at Mawri (0.047% U_3O_8) along the southern margin thereby opened a new dimension for the occurrence of possible volcanogenic uranium mineralization in the southern margin of the SRC. An anomalous concentration of 0.022% eU_3O_8 indicating a possible setup of volcanogenic U deposit was also reported in the moat sediments of Siwana fort hill.

1.3 Objective

To identify and map the volcanic sequences in the Buriwara area of SRC, their petro-mineralogical and geochemical characterization to elucidate their potentiality for REE mineralization. Further, an attempt shall be made to understand the tectonic environment based on analytical results.

1.4 Methodology

The project work included detailed geological mapping over an area of 2 sq km to demarcate the contact of various litho-units for preparation of a geological map in 1:2000 scale. Radiometric survey was undertaken with the help of hand held scintillometer. Samples of rhyolitic tuff, different variants of rhyolite and agglomerate were collected for megascopic, microscopic and whole rock geochemical analysis. As extremely fine grained acid volcanics are difficult to characterize in field, petrography and WDXRF and EDXRF data were used primarily to characterize the rock types. Several classification diagrams were made using major oxides and trace elements data for classification of the rocks and understanding their chemical evolution. REE analysis were done by ICP-OES in Chemical laboratory, AMD/WR, Jaipur. U and Th concentration in different rock types were recorded by gamma-ray spectrometry in Physics lab, AMD, Jaipur.

1.5 Location and accessibility

Siwana town in the Barmer district, Rajasthan is located in the centre of the SRC which is at 36 km SE of Balotra and 52 km NW of Jalore. The study area Buriwara is located at about 15 km west of Siwana town and falls in Toposheet no. 45C/2, bounded by Latitude $25^0$38’44.6”N to $25^0$39’50”N and Longitude $72^0$13’40”E to $72^0$14’16”E. The area is well connected by road and the nearest railway station is Balotra.

1.6 Physiography

SRC is a spectacular circular outcrop that lies within aeolian sand and sand dunes in the Marwar plateau towards the western part of Aravalli ranges. The Luni and Sukri river flow in the northern and southern part of SRC which are intermittent in nature and remain dry for maximum duration of the year. Small internal drainage pattern flowing from higher topography and ending within the soil are also common. The circular outcrop pattern resembles collapse caldera structure with the volcanic vent located at the centre of Siwana fort hill. The ring structure is detached by soil cover and at many places steep sloped hillocks are noticed. It is exposed over an area of 750 sq km with a dimension of 30 km along E-W and 25 km N-S. The southern part of the ring is having the highest width and in the other directions it varies from 600m-1km. In the study area near Buriwara, highest elevation is 306m with average ground elevation of 150m.

CHAPTER 2

REGIONAL GEOLOGY

2.1 Malani Igneous Suite (MIS)

Neoproterozoic MIS spreading over 51,000 sq km area to the west of Aravalli mountain ranges in Rajasthan represents the largest bimodal anorogenic (A-Type) acid volcanism in India. The magmatism is associated with post-Erinpura granitic activity and pre-Marwar sedimentation covering a span of 850Ma to 550 Ma. Since the area forms a part of the Thar desert, the rocks occur as tors, inselbergs and sometimes residual hill ranges within aeolian sand and sand dunes. The best outcrop areas are scattered around Jalore, Siwana, Jasol, Jodhpur, Barmer, Bisala, Jasai, Chautan, Mungaria and Taratara *(Figure 2.1).* Blanford (1877) first coined the term "Malani beds" for a series of volcanic rocks in western Rajputana (presently Rajasthan). La Touche in 1902 and Coulson in 1933 subsequently termed these rocks as "Malani Volcanic Series" and "Malani System" respectively. Pascoe in 1960 again termed them as "Malani granites and volcanic suite". They are presently referred to as "Malani Igneous Suite" (MIS) to cover all the volcanic and associated rocks. MIS is extended over an area of 51,000 sq km and another possible extension of 1,00,000 sq km is estimated to be underlying the sedimentary rocks of Cambrian and Jurassic. Hence it might have a total spread of more than 1,51,000 sq km. (Pareek, 1981). The Malani magmatism is controlled by NE-SW trending lineaments which is the most prominent trend of Aravalli craton and owes its origin to hotspot magmatism and related tectonics (Kochar, 1984). The Siwana, Jalore and Tusham igneous complexes respectively represent peralkaline, mildly peralkaline and peraluminous granites associated with co-genetic acid volcanic rocks. Malani volcanism has been postulated to originate in an extensional tectonic setting where geotherm was raised by the repeated influx of basaltic magma and crustal extension triggered by buoyant rise of silicic magma (Kochar 2001). The migration of the Indian supercontinent during the Malani magmatism to high northern latitudes may be due to mantle activity some 750 Ma, which gave rise to the MIS (Kochar, 2001).

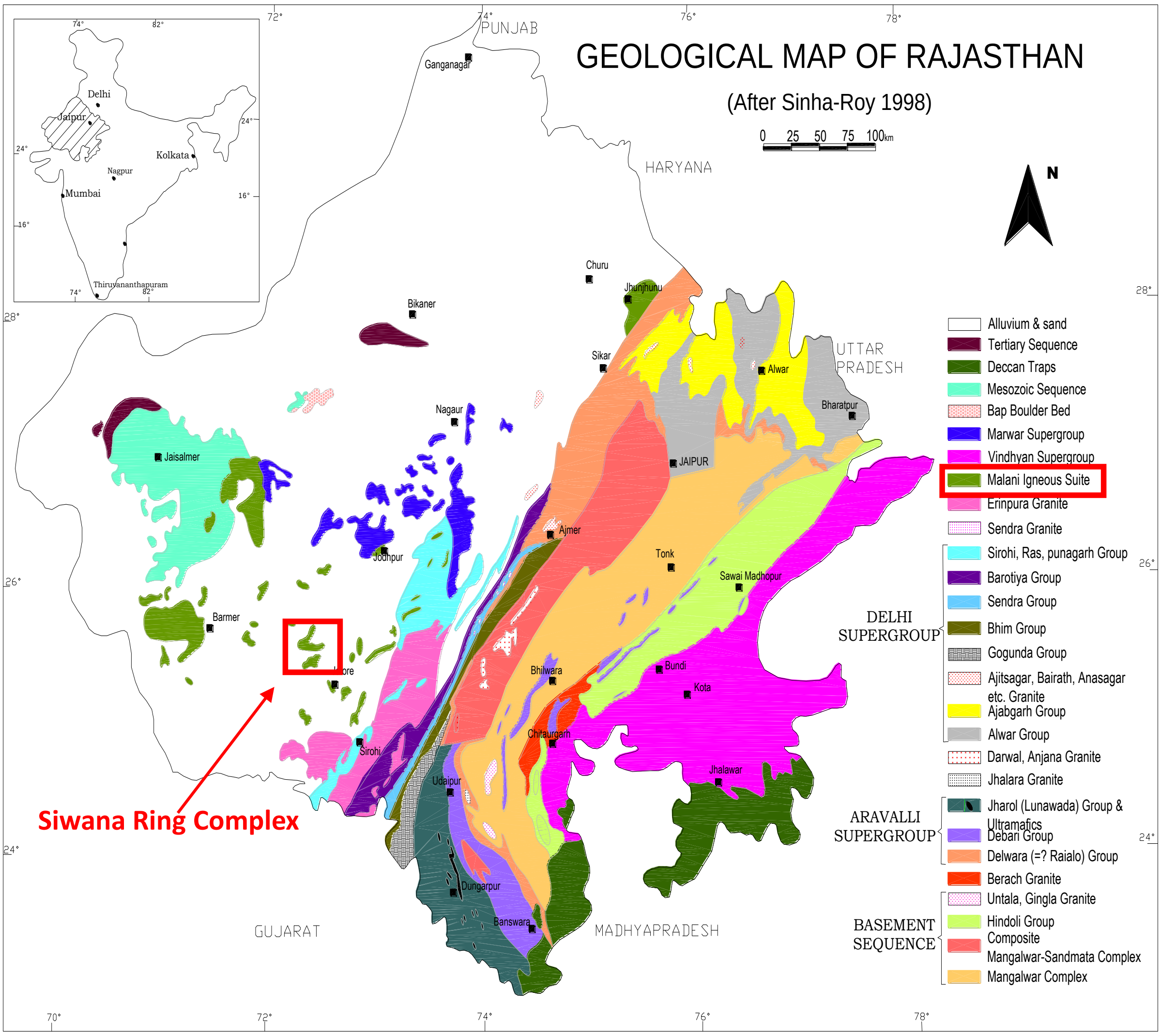

Figure 2. 1 Geological map of Rajasthan with highlighted MIS and SRC (after Sinha-Roy 1998)

The Malani volcanic rocks have erupted in three (3) phases (Bhushan 2000). The first phase commenced with the eruption of basic flows, followed by voluminous acid flows which culminated with ash flow deposits. The second phase experienced intrusion of discordant peraluminous and peralkaline granites, rhyodacite and trachyte flows as plutons, ring dykes and bosses. The third phase corresponds to intrusion of mafic and felsic dyke swarms. The dominant felsic volcanics of MIS are rhyolites and rhyodacites spreading over 31,000 km^2. The other rock types associated with rhyolite are trachytes, dacites, pitchstone, welded tuff, ignimbrite, volcanic breccias and volcanic conglomerate. The cumulative thickness of felsic volcanic rocks exceeds 3.5 km in 45 cumulative flows at Siwana caldera.

The stratigraphic succession of MIS (after Bhusan, 2000):

Supergroup	**Group**	**Formation**	**Mode of Magmatism**	**Lithology**
Marwar Supergroup (Vendian to Lower Cambrian)				Sandstone, shale, limestone, evaporites
		------Unconformity-----		
Malani Igneous Suite (Upper Proterozoic)	Dyke swarm	Basic dykes, acid dykes, trachyte porphyry, andesite and porphyry dykes, aplite and diorite plugs.	Intrusive dyke Phase-III	Gabbro, dolerite, basalt, granite, rhyolite porphyry, trachyte porphyry, andesite porphyry, aplite veins
	Granitoid plutonism	Malani granite Siwana granite Jalor granite	Intrusive Phase II	Hornblende granite, riebeckite/aegirine granite, biotite/ hornblende granite
	Bimodal volcanism	Rhyolite, trachyte and basalt flows	Extrusive Phase I	Rhyolite, trachyte, dacite and rhyodacite flows, Basalt and trachy andesite flows
		------Unconformity-----		
Pre Malani basement (middle to lower Proterozoic)	Aravalli - Delhi Supergroup			

2.2 Siwana Ring Complex (SRC)

Siwana Ring Complex (SRC) is the most prominent geomorphic feature in the MIS which represents a classic collapse caldera structure having a near circular outcrop pattern with volcanic centre around Siwana. The Siwana caldera spread over 750 sq km has a dimension of 30 km along E-W and 25 km along N-S. This caldera structure was intruded by detached ring dykes of younger peralkaline granites along the fractures developed in the periphery during caldera collapse (Nelson Eby and Kochhar, 1990).

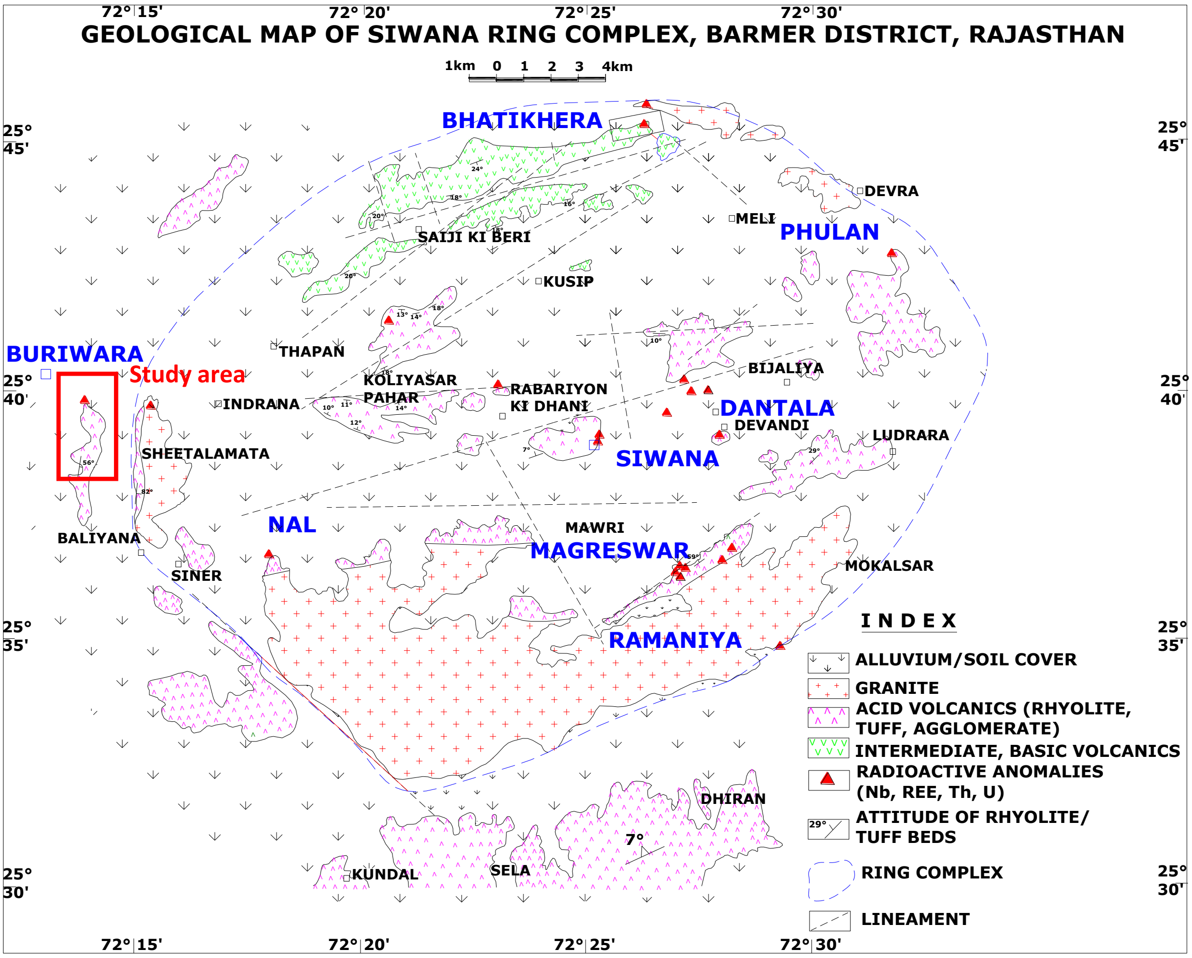

Figure 2. 2 Geological map of Siwana Ring Complex (after Bhushan and Chandrasekharan, 2002)

The granites are attributed to A-type chemistry and within plate origin. The low whole rock $\delta^{18}O$ values (-10 to +1.8 permil) has been interpreted in terms of interaction with a low ^{18}O rift related meteoric/hydrothermal system, generated by Siwana granites of High Heat Producing (HHP) nature which acted as heat engines (Kochar 2001). HHP nature of the granite is due to higher intrinsic U, Th and K content i.e. heat generated due to radioactive decay is high. The inward pitching of these ring dykes with dips varying from 10° to 50° indicate collapse nature of the caldera. The SRC owes its origin to extensional tectonism and represents bimodal volcanism. Multiple phases of magmatism are deciphered in SRC, manifested by basalt-rhyolite-tuff sequences, volcano-sedimentary assemblages intruded by ring dykes of granite. Micrograinite dykes and veins occur as intrusives within the bimodal volcanics and granite. Three sets of lineaments are identified, the prominent being the NE-SW one which has got a bearing with the trend of the Aravalli-Delhi Mobile belt. The other major lineaments trend in E-W and NW-SE directions, most being faults traversing the caldera and thereby offering suitable locales for uranium mineralization. The Luni and Sukri river flowing in the north and south of SRC also merges with the E-W and NE-SW lineaments. Volcanic landforms such as lava channels and tubes have been identified in SRC, which have been interpreted to be the former sites of volcanic vents (Bidwai, 1997). Rhyolites and tuff of SRC show intense hydrothermal alterations especially along fault/fracture zones.

CHAPTER 3

LOCAL GEOLOGY

Siwana Ring Complex (SRC) having peralkaline igneous rocks is being explored for its potential REE mineralisation. Atomic Minerals Directorate for Exploration and Research has covered major part of the area through detailed survey and reconnoitory drilling. However, the western part was not well explored and hence this part has been considered for detailed study and characterization of lithotypes. Buriwara area, which lies in the westernmost part of the ring, exposes felsic volcanic and pyroclastic rocks. The pyroclastic tuff from Dantala area in SRC has been established as host to REE mineralisation. Hence, the pyroclastic rocks in Buriwara were considered to be studied in detail to understand its REE potential. Based on the previous studies carried out in the area, initial approach was made by following the geological map of *Bhushan and Chandrasekharan, 2002 (Figure 2.2)* as a base map. Geomorphologically, the area is an isolated hillock surrounded by aeolian sand. Drainage system is mainly intermittent in nature. Also, minor drainage patterns flowing from higher to lower topography is also common which eventually end up internally within sand. The highest topographic elevation is 306 m and the average ground elevation is 140 m. Detailed mapping was carried out in 1:2000 scale over an area of 2 sq km. All the lithotypes have been sampled in detail and the results for the individual lithology have been studied separately in order to decipher their genesis, geochemistry and REE potentiality. Basically, it exposes two lithotypes: rhyolite and rhyolitic tuff. But detailed field observations concluded different variations within rhyolites, viz. massive and porphyritic separated by a thin layer of agglomerate. The litho-structural map of Buriwara is shown in *Figure 3.1.*

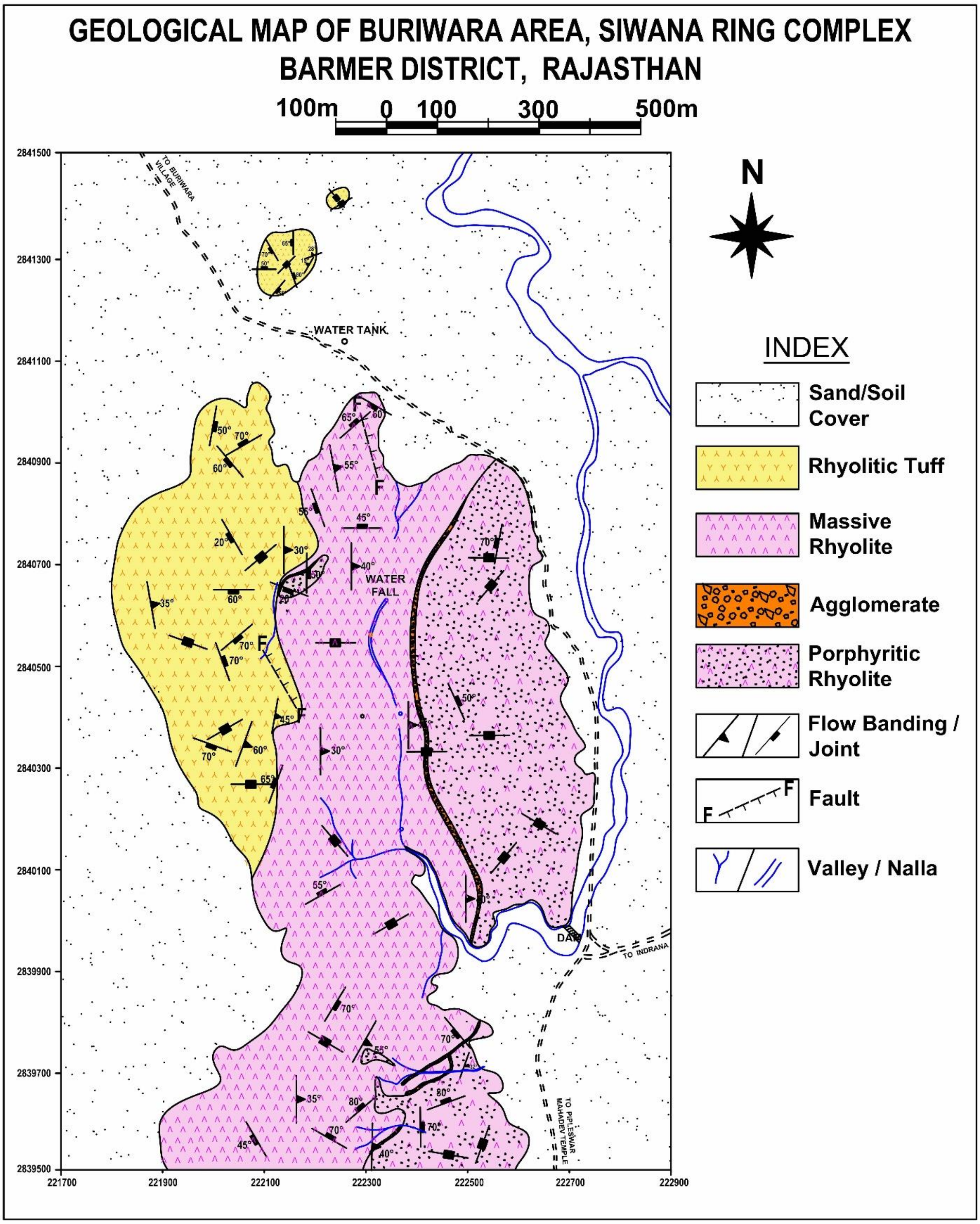

Figure 3. 1 Geological map of Buriwara

3.1 Lithology

3.1.1 Pyroclastic rock / Rhyolitic tuff

The pyroclastic rocks are exposed towards the western and northern part of the area. The exposures in the northern part occur as two small hillock separated by soil cover. It consists of very fine grained quartz, feldspar, biotiote, tiny glass fragments along with a minor concentration of heavy mineral such as magnetite.

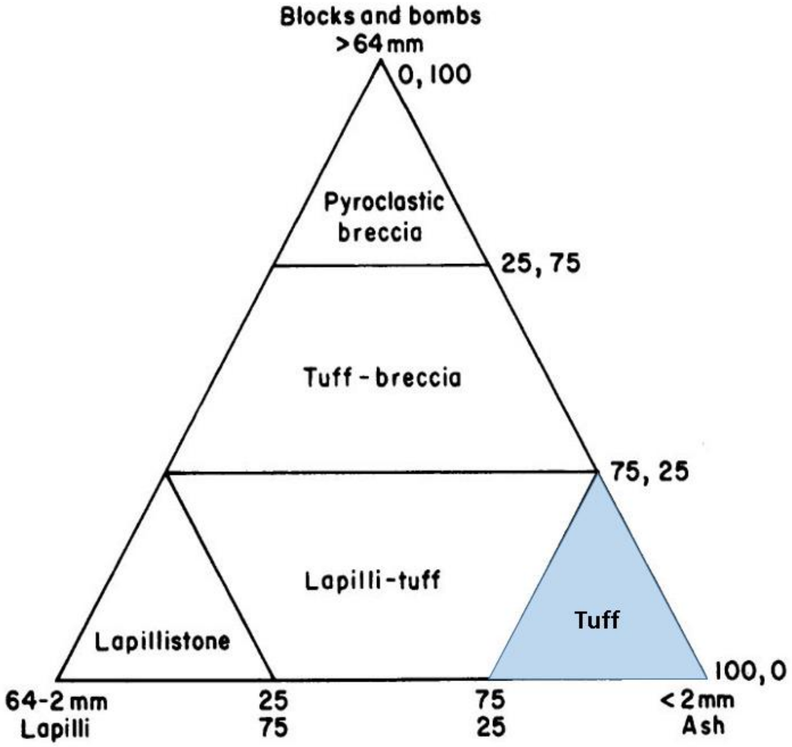

Figure 3. 2 Mixture terms and end-member rock terms for pyroclastic fragments (Fisher, 1966)

The grain size is too fine to distinguish all the compositions in hand specimen. Thus, the pyroclastic grain size corresponds to ash (<2mm) and the lithology is identified as tuff as per classification by Fisher 1966 *(Figure 3.2)*. The composition of the tuff is rhyolitic and hence the lithotype has been distinguished as rhyolitic tuff. At few places gradation of grain size is observed. Silicification, kaolinisation and ferruginisation are prominent alterations observed in the tuff. Specs of kaolin are also found in the pore spaces. The tuff is intensely fractured and hematitic chert is noticed as intrusions along the fractures in the southern part *(Figure 3.3d)*.

These factors are cumulatively imparting reddish appearance of the tuff. Detailed radiometric survey suggested that the activity in the tuff ranges from *0.06 to 0.12 µR/hr* (2 to 4xBG). This activity was due to a relatively higher concentration of U, Th and Rare Earth elements (REE). The tuff is layered in which flow banding are distinguished by alternating compositional difference of highly ferrugenised and siliceous layers *(Figure 3.4f)*. They occur as fine laminations signifying the S_0 plane planes. Warping of flow banding are also observed at places indicating compressive stress after the consolidation of pyroclastic ash material. However, it can also be due to deformation as result of the NW-SE fault. The average strike of flow banding is N-S, dipping 40°-70° towards east. Frequent slickensides are noticed within the tuffaceous zone which implies a fault zone. Disseminations and veins of pyrite are noticed at places, particularly within dark brown chert veins.

3.1.2 Rhyolite

The major part of the area is exposed by rhyolite. Towards the eastern part, rhyolites show a varying nature from fine-equigranular to porphyritic *(Figure 3.3c),* altered to unaltered. It is composed predominantly of quartz, alkali feldspar, alkali amphibole, alkali pyroxene as major minerals along with zircon, apatite, sphene and Fe-Ti oxides as accessories. Vitreous grains are also observed which might be sulphides. Light pink colored welded tuffs and quartz veins are found to be associated with rhyolite at places. The radioactivity in fine grained massive variety shows *0.06 to 0.10 µR/hr* (nearly 2xBG), relatively higher activity being shown by aegirine bearing rhyolite whereas the porphyritic variety shows background RA. Flow is almost similar to the tuff i.e. 40° to 70° easterly dipping *(Figure 3.4 e, f).* Original glassy texture is well preserved at places. Altered glass shards are observed often as lensoid shape which tend to have eutaxitic texture with alternating silicic banding *(Figure 3.4 c,d).* Lithophysae cavities are observed in the rhyolite which are nearly 2-10cm in diameter and in few places they are seemed to have filled by spherilitic intergrowth of quartz and calcite within them *(Figure 3.4 a,b).*

These features indicates devitrification of the metastable glass content that were originally consolidated. Vesicles are present in both the variants which indicates escape of gas bubbles during cooling *(Figure 3.3b).*

The equigranular varieties are very fine in size, massive and compact, however at some places medium sized angular phenocrysts of feldspar are encountered. It is present in various shades i.e. dark grey, light pink, brick red and dark brown. The reddish appearance is due to alteration. Compositional flow bandings are distinctly observed in this variety of rhyolite and also flow warping is commonly observed. These flow warping or deformation in the banding is interpreted to be penecontemporaneous deformation *(Figure 3.6 b, e, f).* At few places lithology of intermediate composition was encountered which is assumed as trachyte. Minor quartz vein traverses the groundmass at places. The porphyritic variety of rhyolite consists of coarse to medium phenocryst within siliceous groundmass. The colour of the groundmass varies from light pink to grey and the phenocrysts are of flesh-coloured alkali feldspar and minute blebs of quartz. The phenocryst are angular and brecciated, but at few locations they shows preferred orientation which might be due to flow action. Ferrugenisation of porphyritic rhyolite is observed in the outcrop near the northern contact of tuff which is signified by reddish groundmass and phenocryst.

3.1.3 Agglomerate

Agglomerate layer of about 10 m in thickness is present within rhyolites where the nature of rhyolite changes from massive to porphyritic. They are characterised by more than 60% block sized particles (>64mm) (Figure 3.2) which consists of tabular, rectangular, angular to subrounded fragments of felsic volcanics and tuffaceous fragments, possibly of the underlying formation *(Figure 3.3 e,f).* Mostly the size ranges 1cm to 20 cm and looks like the broken pieces of wall rocks and intrusives during forceful eruption. They are embedded within matrix of silicic composition and are poorly sorted. So, they correspond to pyroclastic breccia as per classification by Fisher *(Figure 3.2)*. However, for finer size lapilli at some places they fall under tuff breccia. At some places reddish appearance is observed which may be due to ferrugenisation. Towards south of the area the matrix of aegirine rich composition imparting green colour is observed. Apart from grain size, the agglomerate doesnot show any contrasting character in terms of flow direction or composition. So, it is inferred that they are genetically similar. Also, the angular shape of the clast, its interlocking nature with the matrix signify its in-situ igneous origin. Activity within the agglomerate is also high (nearly 3x BG). The attitude of the flow is measured to be N-S trending, dipping 30°-50° towards east. At some places cross cutting joints trending E-W are observed. Towards the southern part of the area, the joints show south-westerly trends. The agglomerate is present consistently throughout the study area in roughly NS trend which has been demarcated in the geological map *(Figure 3.1)*.

Figure 3. 3 a) Sharp and steep boundary between rhyolite and tuff. b) Ferrugenised tuff with vesicular texture. c) A sharp contact between porphyritic and massive rhyolite d) Hematitic chert veins traversing within tuff. e, f) Block sized pyroclastic breccia / agglomerate

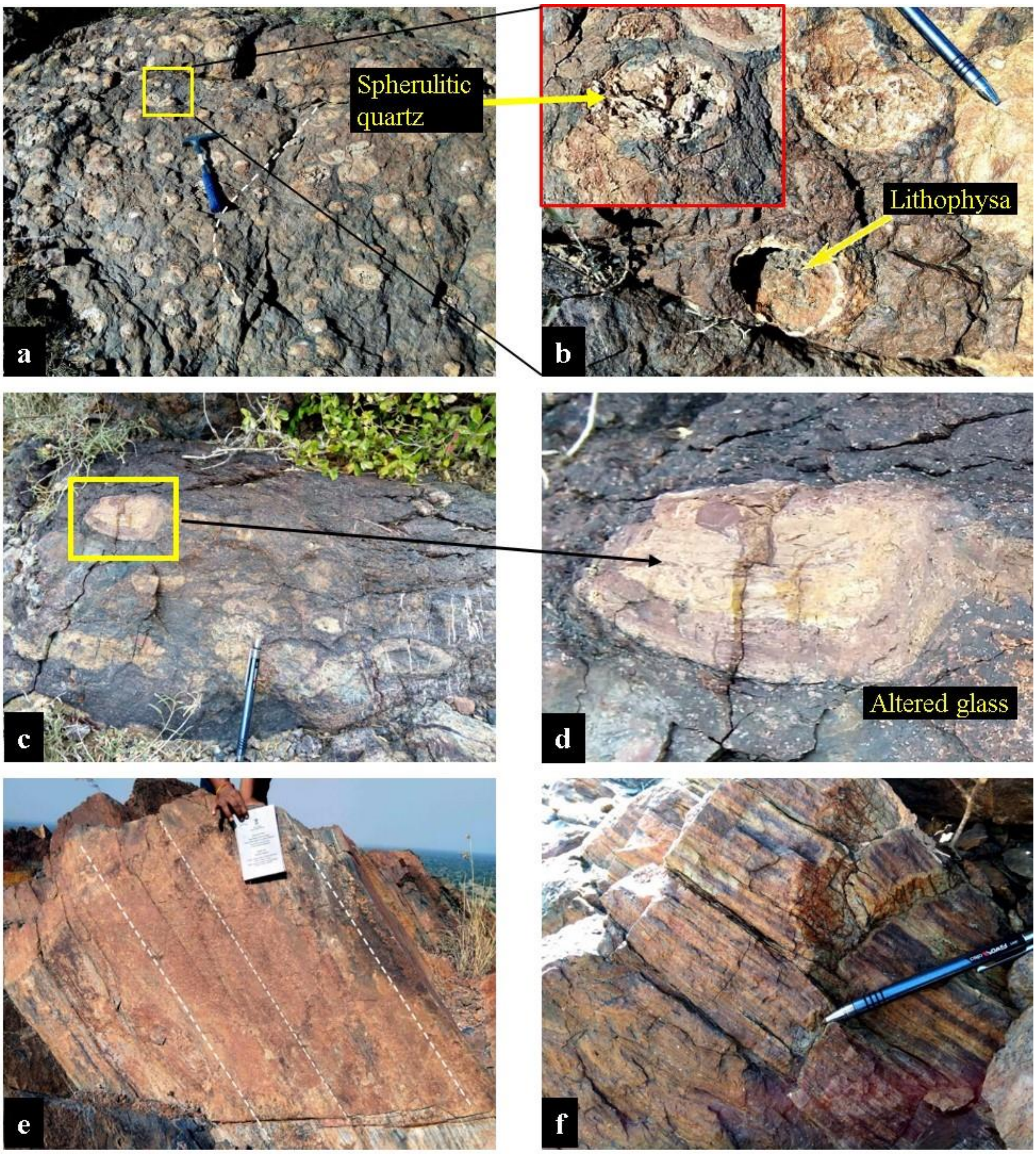

Figure 3. 4 a, b) Quartz and calcite growth in lithophysae cavities attaining spherulitic texture c,d) Altered glass attaining rim structure and flattened to attain eutaxitic texture with the surrounding e) Uniform flow lamination in rhyolite f) Flow laminations with alternating cherty and ferrugenised layer

3.2 Structure

Joints are the most prominent structural feature observed in the area. Both the tuff and rhyolite show a similar variation of joints and fracture trends. Three major joint trends are **NE-SW, E-W** and **NW-SE** with dips varying from 45° to 70°. Major dip directions for **NE-SW, E-W** and **NW-SE** sets are SE, vertical and SW respectively. Columnar joint which is also a characteristic feature of volcanic rock is encountered in rhyolite. Columnar pattern is formed by pentagonal set of joints which is clearly observed in planar outcrop *(Figure 3.6a).*

Evidence of faulting is drawn from the slickensides encountered on planar surfaces. These slickensides are preserved as striations and grooves having an oblique sense of slip on the surface resembling the fault plane. The slickensides are plunging towards east (direction of the caldera centre with respect to the study area). As the fault planes are NNW-SSE oriented, so the rake of the slip on the plane, i.e. the pitch is reflected as nearly 70° from SSE. Two such observations from different locations are: Rake of straition in a) tuff: 70° from SSE on 330°/45°NE plane *(Figure 3.6c)* and b) rhyolite: 70° from SSE on 345°/50°NE plane *(Figure 3.6d).* Thus, from the slickenside orientation, it is concluded that their sense of slip is oblique in nature. The oblique sense of slip generated in caldera subsidence setting is described by Holohan et.al. (2013) through a kinematics known as "Camera Iris" effect. The inward radial movement generates a concentric shortening and a related compressive stress in the horizontal plane. In order to accommodate this concentric shortening a strike-slip displacement component on an obliquely trending fault emerges to relax the compressive stress *(Figure 3.5a).* A dip-slip component on such a fault then accommodates either shortening (oblique-reverse) or extension (oblique-normal) in the radial direction. Oblique slip faults hence enable sections of the caldera periphery to move horizontally inward by sliding past each other, in a manner that is analogous to the closure of a camera "iris" *(Figure 3.5b)*

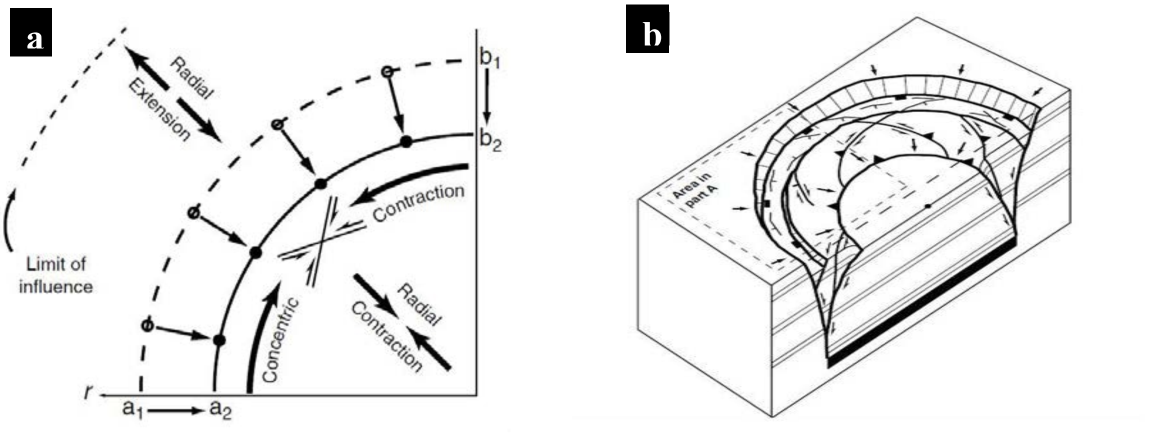

Figure 3. 5 a) Illustration of how circumferential horizontal shortening results as material points move radially inward (reduction of arc length from a1–b1 to a2–b2) and is accommodated by the strike-slip components of fault displacements b) block diagram of centered subsidence with oblique-slip faults related to the camera iris effect. The area of the roof delimited by dashed box is roughly that considered in Figure a.

Warping of flow laminations are commonly observed both in tuff and rhyolite. The intensity of warping is low and is reflected by bending of flow foliations. At few places, warp is distinctly characterised by marker flow layers of contrasting compositional difference which are mainly hematitic chert veins *(Figure 3.6b).* A rare intense warping of flow laminations is encountered in rhyolite towards northern part in the vicinity of the measured fault plane *(Figure 3.6 e,f).* It might have warped during penecontemporaneous deformation that generates due to compressive stress regime soon after the consolidation of pyroclastic ash material. The attitude of the general open folds varies greatly whereas in case of the intense fold attitude of axial plane: 10°/70°SE and the fold axis plunges 40° towards N10°E.

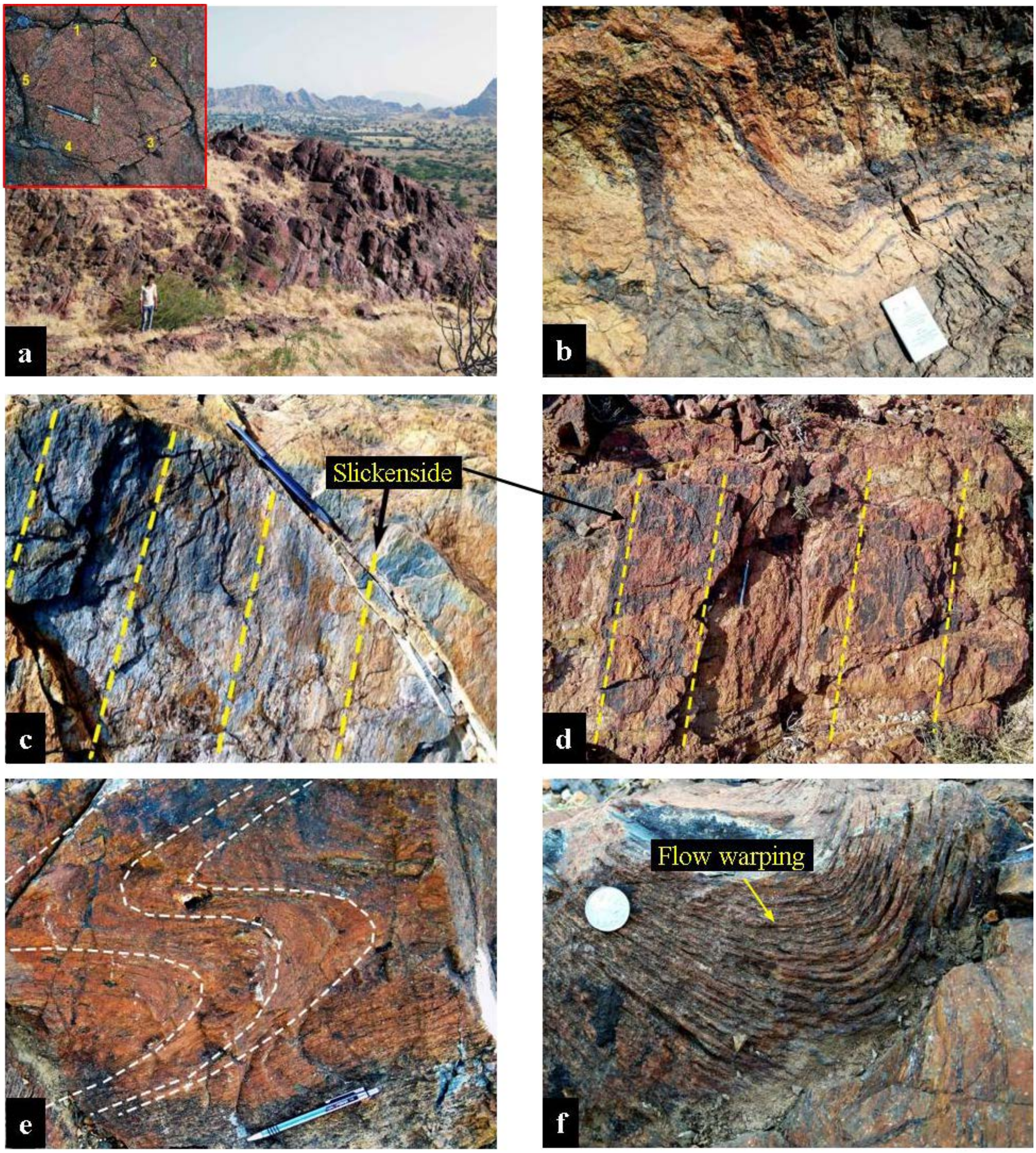

Figure 3. 6 a) Pentagonal columnar joints in rhyolite: plan and section view b)Flow warping characterized by marker bed c)Slickenside observed in rhyolite d) Slickenside observed in tuff e) Intense warping of flow banding having attitude of axial plane: 10°/70°SE f) View of the warped banding on 130°/35° NE plane

CHAPTER 4

PETROGRAPHY

4.1 Methodology

4.1.1 Preparation of thin section

From the grab samples collected from field, proper representative part is determined which is then cut into thin-section size with a diamond-blade circular saw. Friable samples are treated in Canada balsam and diluted with xylene before slicing. Treated thin slice is fine polished on one side using silicon carbide (Carborundum powder) of 400#, 600# & 800#. The fine polished side of the specimen is bonded with thin micro slide using epoxy (cold mounting). The rock specimen on thin slide is ground to reduce its thickness to 0.03mm using silicon carbide (Carborundum powder) of 220#, 400#, 600# & 800#. It is then fine polished on a polishing machine using nylon cloth and diamond paste. Hifin fluid is used to avoid the sticking of the paste to the polishing cloth. Polished thin section is cleaned in mild soap solution and is ready for microscopic observations.

4.1.2 Study in transmitted light microscope

The prepared thin section is observed under a mineralogical microscope for different optical properties of the constituting minerals. The transmitted light from the illuminator are polarized after passing through the lower polarizer. The polarized light gets refracted after incidence upon the mineral grains *(Figure 4.1).* The optical phenomenon of the refracted rays is studied with or without the upper polarizer (analyser), each being used for study of the following properties:

Under plane polarized conditions (PPL): Colour and pleochorism (if any), relief, mineral habit, texture and alterations, cleavage.

Under crossed polars (XPL) (upper polarizer inserted): Isotropism, birefringence and interference colour, interference figures, extinction angle, twinning, zoning and dispersion.

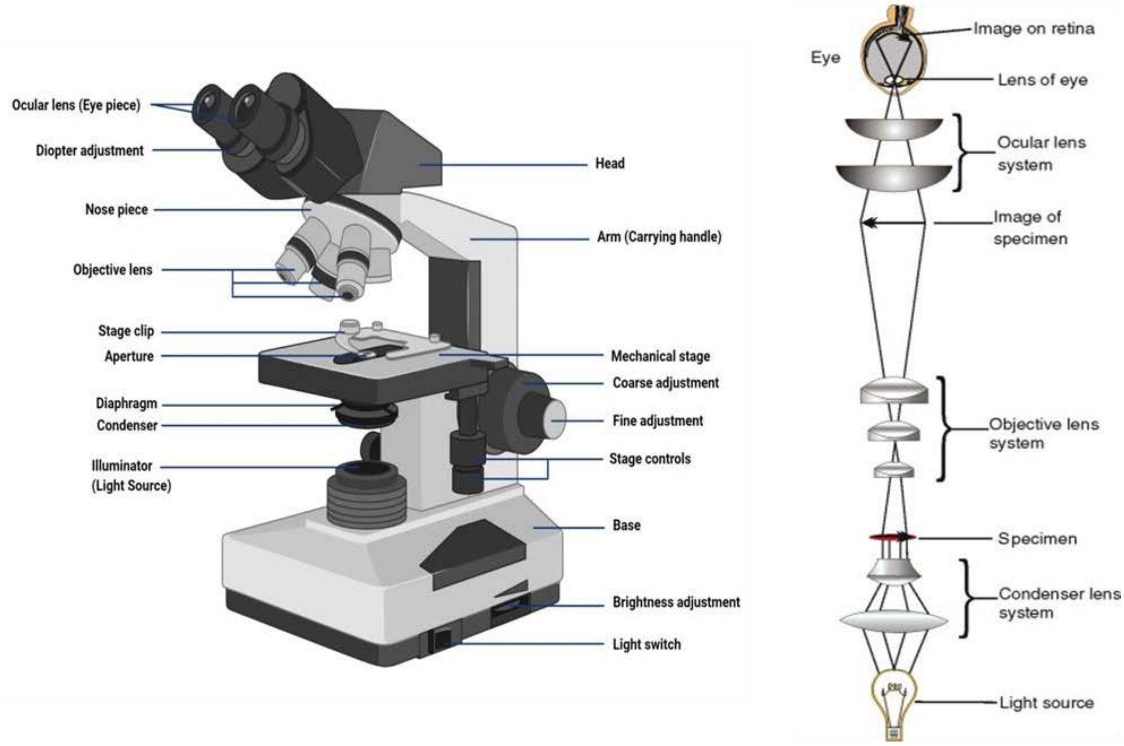

Figure 4. 1 Schematic diagram of transmitted light binocular microscope and its working principle

4.2 Observations

Petrographic studies of different litho-units collected during traverse in Buriwara area of Siwana Ring Complex have been carried out in petrology laboratory, AMD/WR. The main emphasis was upon texture, mineralogy, alteration studies and eventually rock nomenclature. Microscopic studies of tuff, rhyolite and agglomerate were studied by using OLYMPUS BX 50 petrographic microscope and detailed descriptions of these litho-units are described below.

4.2.1 Rhyolitic tuff

Megascopic properties of rhyolitic tuff

Megascopically, tuff is brick red colour, homogeneous, fine grained and variable colour intensity flow layers could be seen. Tiny vesicles are also observed on the surfaces. The grains are compacted and the reddish appearance is imparted due to impact of ferrugenisation. At few places pale greenish appearance is also observed. Very thin siliceous veins are also seen.

Microscopic properties of rhyolitic tuff

Microscopically, the tuff is composed dominantly of quartz and feldspar with minor mica content. Quartz grains are non-undulose, characteristic of volcanic origin. The grain size is very fine and grain boundary is mostly hazy *(Figure 4.2a, b).* Microcrystalline granular texture is most commonly observed. At places elongated grains with preferred orientation is also common which resembles pyroclastic flow before consolidation. The tuff has undergone intense ferrugenisation that imparts dominance of brownish red colour throughout major portion of the sample *(Figure 4.2b).* The ferrugenisation is an impact of post depositional Fe rich hydrothermal activity. Massive Fe oxide is present in the intergranular spaces within the unwelded pyroclast of tuff. The ferrugenised material is also observed to form distinct alternate bands of 2-5 mm thickness where quartzo-feldspathic composition is stained by ferruginous matter indicating minor periods of Fe oxidation on the groundmass. Fe oxidation is more prominent over feldspar dominated parts. Fe oxides are mainly hematite with few other hydrated iron oxides viz. limonite and goethite. They are massive, lumpy or acicular and rarely form euhedral crystals of magnetite *(Figure 4.2d).* Very minor quantity of isotropic magnetite crystal is observed. Due to the masking of ferrugenised matter over the very fine grain size, individual minerals properties could hardly be studied. However, quartz is found to be dominant over feldspar and nearly absence of mafic mineral phases signify that the tuff is rhyolitic. Tiny glass fragments are observed where devitrification is observed along the boundary as a result of which the glass fragment is eventually merging with surrounding quartzo-feldspathic texture *(Figure 4.2c).*

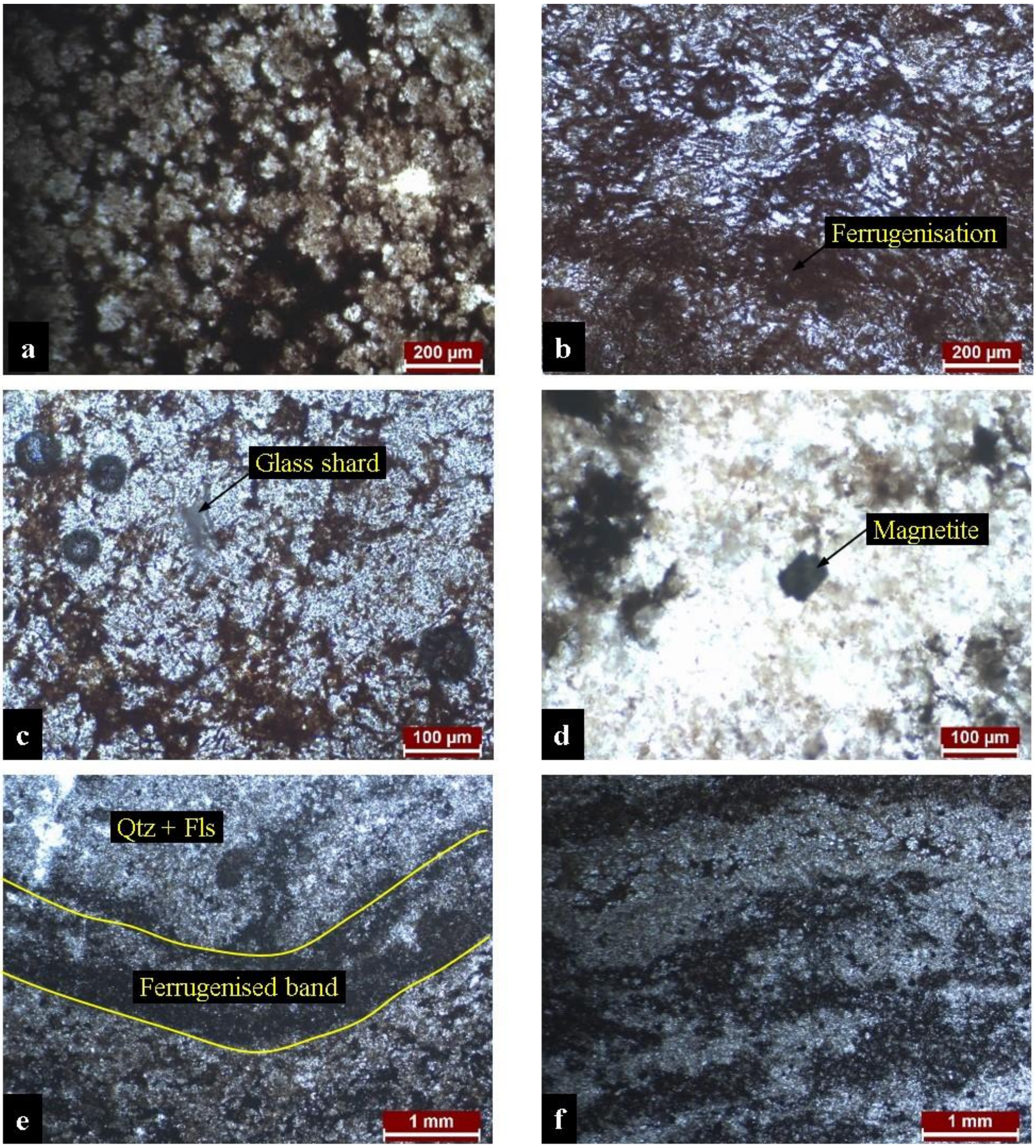

Figure 4. 2 a) Microcrystalline granular texture of quartz and feldspar b) Preferred oriented texture with masking of ferruginous matter c) Glass fragment attaining devitrification along boundaries d) Magnetite crystal e),f) Ferrugenised band within microcrystalline quartzo and feldspar.

4.2.2 Rhyolite

Megascopic properties of rhyolite

Megascopically, massive rhyolite is fine-equigranular, compact, homogeneous and devoid of any phenocryst. They show variation in colour from grey to reddish pink. Alternate ferrugenised bands are also observed in few samples.

Porphyritic rhyolite have angular feldspar grains as phenocryst within the quartzo-feldspathic groundmass. They range in size from 2 mm to 6 mm mostly occurring as tabular form. Brownish tints are also observed within such phenocryst which are iron oxides formed due to ferrugenisation.

Microscopic properties of rhyolite

Massive rhyolite: In thin section massive rhyolite exhibits homogenous microcrystalline granular quartz and feldspar. Quartz grains show mildly undulose extinction. Quartz micro-phenocrysts having embayed margin is occasionally present. Blebs of alkali feldspar transforming to perthite is also observed. Presence of volcanic glass indicated by perlitic cracks is the characteristic devitrification texture *(Figure 4.3a).* Also along such cracks greenish appearance is imparted by the formation of palagonite, which indicates alteration of volcanic glass by fluid activity. Microfaulting is also observed along a straight plane where offset of flow banding is very clear *(Figure 4.3c).* Signatures of faulting or an existed stress regime is also supported by the relative distortion along cracks formed in the mineral grains *(Figure 4.3d).* Very minor occurrence of apatite was also identified.

Porphyritic Rhyolite: In the porphyritic rhyolite, phenocryst of alkali feldspar and quartz are embedded within microcrystalline granular groundmass. Quartz form medium sized anhedral grains and show mild undulose extinctions. Feldspar forms fine lath shaped crystals (2-6mm) of random orientations. Sometime laths are arranged in radiating pattern *(Figure 4.4b).* They are cloudy in appearance due to impact of ferrugenisation. Presence of alkali feldspar phenocryst and transformation to perthite *(Figure 4.4a)* can be attributed to hypersolvus origin. Feldspar forming interlocking boundary along embayed margin in quartz is also commonly observed *(Figure 4.4c)*. Groundmass is also made up of microcrystalline quartz and feldspar. Very fine aegirine and riebeckite laths occurring as prismatic and longitudinal crystals are also common in the groundmass *(Figure 4.4d)*. Aegirine is light green with mild pleochroism while riebeckite is dark greenish blue and strongly pleochoric.

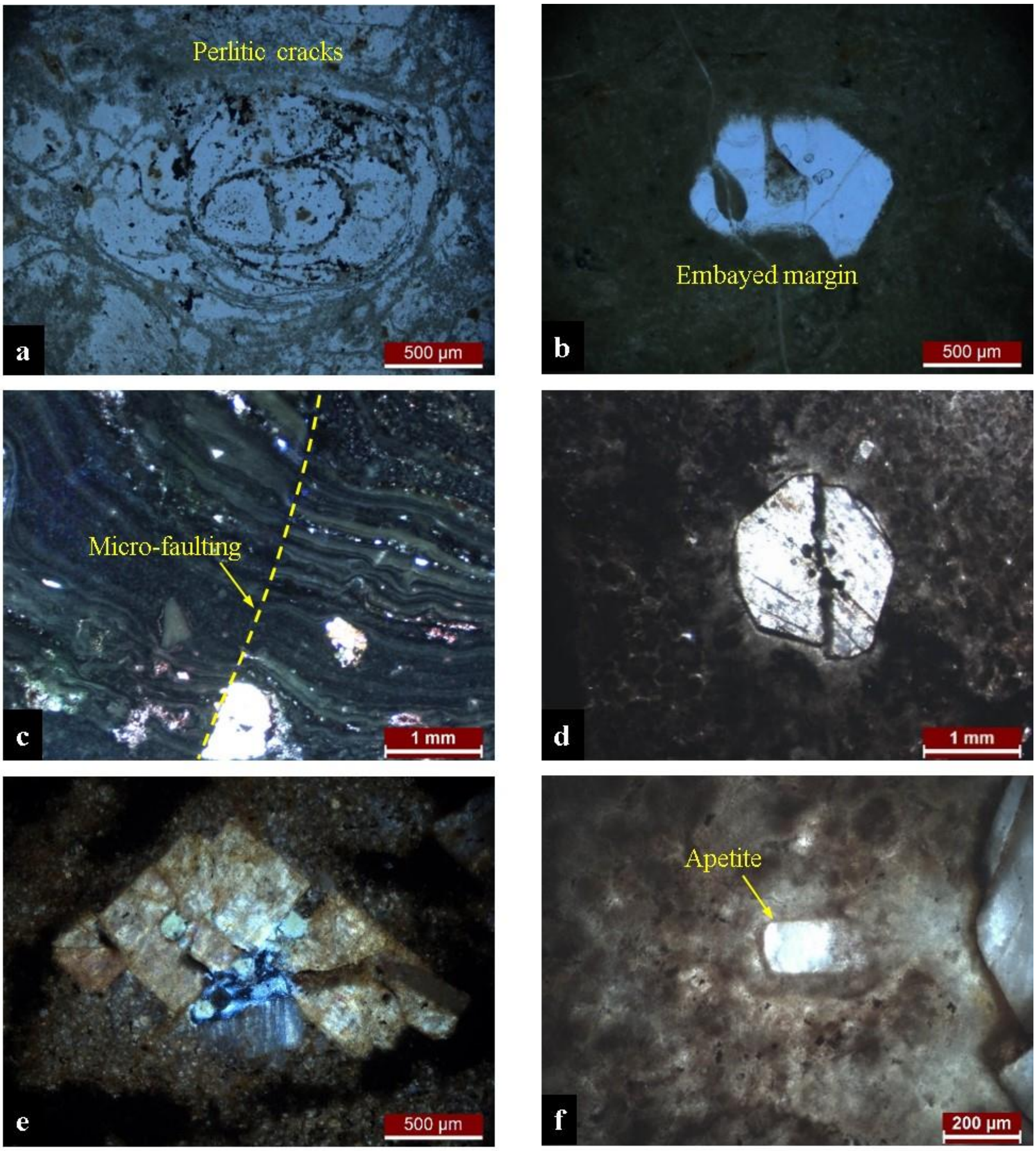

Figure 4. 3 a) Perlitic cracks in rhyolite b) Embayed margin along quartz boundaries c)Offset along microfaulting preserved in alternate ferrugenised and cherty bands d)Fracture and offset along quartz grain supporting faulting event e) K-feldspar undergoing perthitisation f)Apatite grain within ferrugenised matrix

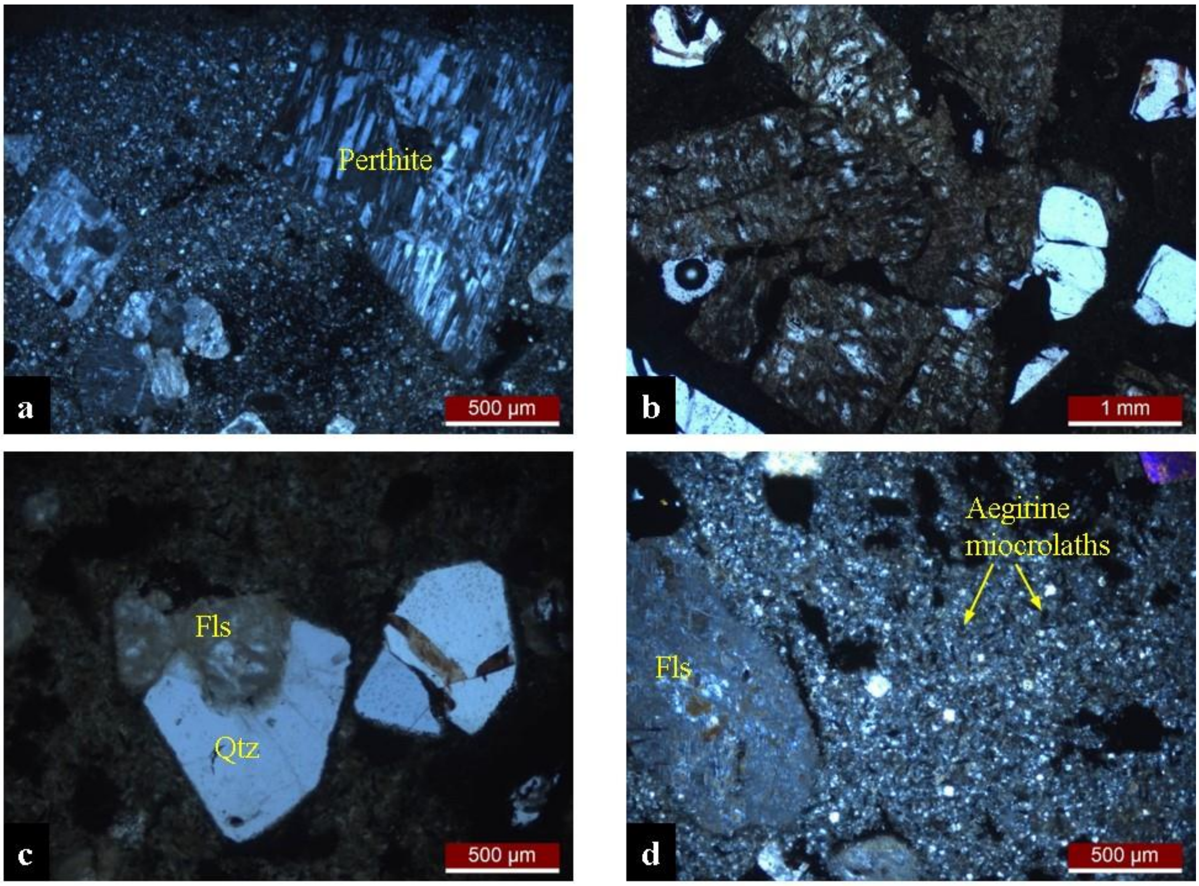

Figure 4. 4 a) Perthite phenocryst in quartzo-feldspathic groundmass b) Radiating laths of K-feldspar with impact of ferrugenisation c) Embayed margin interlocking texture forming by quartz and feldspar d) Microlaths of prismatic aegirine within quartzo-feldspathic groundmass. [Fls: Feldspar, Qtz: Quartz]

4.2.3 Agglomerate

Megascopic properties of agglomerate

The agglomerate bed lying between porphyritic and massive variety of rhyolite has distinctive megascopic properties. It comprises of lithic fragments and porphyritic crystal fragments as medium to large size phenocryst (upto 2 cm in the studied samples) embedded within matrixes of silicic composition and are poorly sorted. They are angular in shape and mostly occur in tabular form. Thin colour bandings can also be seen in the matrix portion and impact of ferrugenisation is also clearly visible at few samples.

Microscopic properties of agglomerate

Microscopic observation of agglomerate is very unique and diverse than that of rhyolite and tuff. It appears as unsorted, non-homogeneous fragments within fine matrix and also occurrence of flow banding *(Figure 4.5a)* as well as glassy texture is very conspicuous. All these observations are characteristics of pyroclastic breccia which are result of deflation zones (zone of gas escape) during turbulent eruption. The large fragments are mainly lithic fragments of pre-existing rhyolite having similar characteristics as studied in rhyolite which are embedded within dark matrix *(Figure 4.5c).* Mineral crystal fragments mainly comprise of dominantly of alkali feldspar phenocryst *(Figure 4.5e).* Quartz crystal are found as anhedral grains, some of which occur as polycrystalline and cryptocrystalline form. Perlitic cracks signifying devitrification texture is prominent in the matrix part *(Figure 4.5f).* Spherulitic texture in quartz phenocryst is also commonly observed *(Figure 4.5d).* Phenocryst of pyroxene is also occasionally seen, being wraped by groundmass which is mainly quartzo-feldspathic with some greenish unidentifyable prismatic laths. These laths are assumed to be the crypto crystalline fragments of the pyroxene, which is supported by the presence of phenocryst.

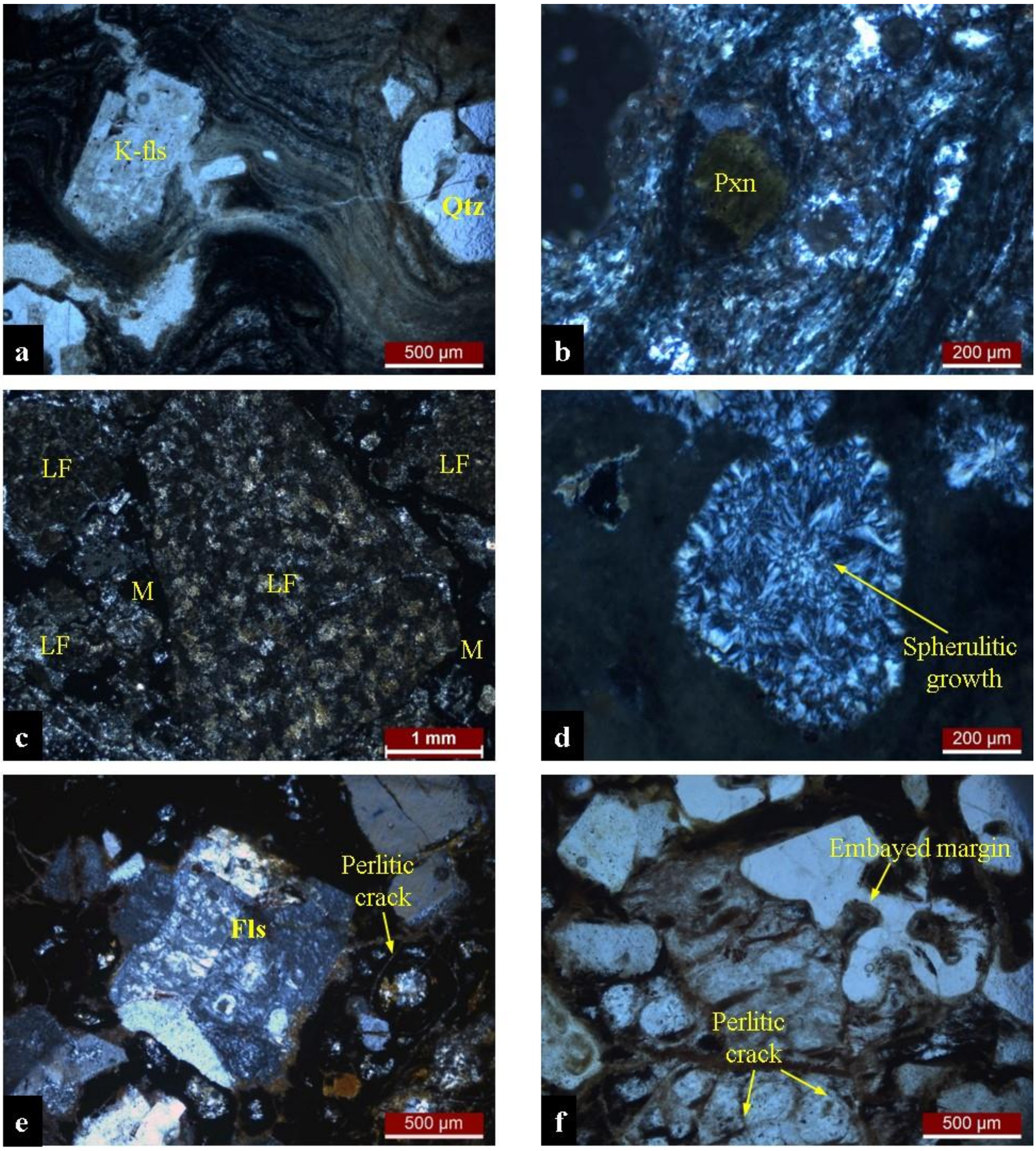

Figure 4. 5 a) Flow texture in groundmass with quartz and K-Feldspar phenocryst b) Pyroxene phenocryst warped by surrounding flow texture c) Lithic fragments of rhyolite d) Spherulitic texture in quartz e) Altered glass showing perlitic cracks and orthoclase feldspar with Carlsbad twinning f) Devitrification of glass preserved as perlitic cracks. [Fls: Feldspar, Qtz: Quartz, Pxn: Pyroxene, LF: Lithic fragment, M: Matrix]

CHAPTER 5

GEOCHEMISTRY OF TUFF AND ASSOCIATED ROCKS

5.1 Methodology

5.1.1 X-Ray Fluorescence (XRF) laboratory

Introduction to XRF

X-rays are a type of electromagnetic wave having short wavelength that measures from 100A to 0.1A. X-ray fluorescence analysis is a method that uses characteristic X-rays (fluorescent X-rays) generated when X-rays irradiate a substance. Fluorescent X-rays are electromagnetic waves that are created when irradiated X-rays force inner-shell electrons of the constituent atoms to an outer shell and outer shell electrons promptly move to inner shells to fill the vacancies *(Figure 5.1)*. These fluorescent X-rays possess energies that are characteristic to each type of element enabling qualitative analysis by using Moseley's law and quantitative analysis by using the intensity (number of photons) of each X-ray energy

.

Moseley's Law: $1/\lambda = K (Z-\sigma)^2$

K : constant of particular series (K, L, M)

Z : Atomic Number, λ : wave length

σ : shielding constant

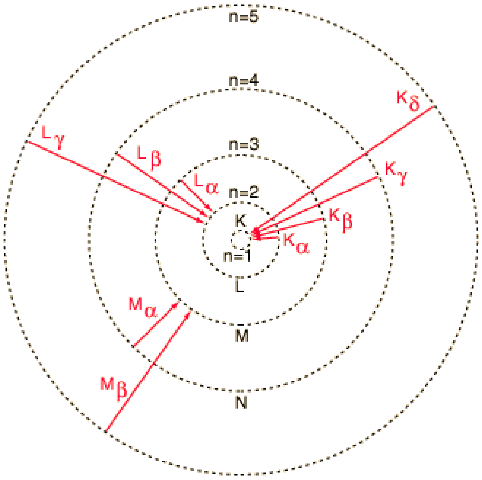

Figure 5. 1 X-Ray generation principle

XRF analysis instruments can be largely categorized into wavelength-dispersive X-ray spectroscopy (WDX) and energy-dispersive X-ray spectroscopy (EDX).

Principle of EDXRF

- A high-energy X ray is focused into the sample
- Ground state (unexcited) electrons in sample are stimulated
- Electrons are excited from lower energy shells to higher energy shell
- The difference in energy between the shells may be released in the form of an X-ray
- The number and energy of the X-rays emitted from a specimen can be measured by an energy dispersive spectrometer.

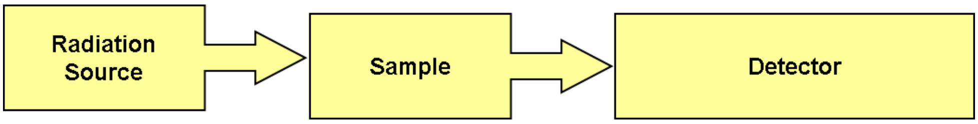

Principle of WDXRF

- A high-energy X ray is focused into the sample and ground state electrons are stimulated
- Electrons are excited from lower energy shells to higher energy shell resulting in the release of secondary X-ray
- The secondary X-rays are collected by the collimator and directed to the analysing crystal which together determine the wavelength or spectral resolution
- The X-rays go to the detector and to the pulse height analyser to be measured

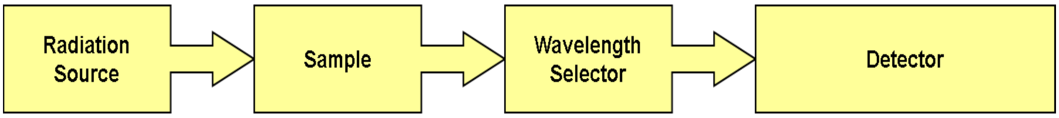

Sample preparation for XRF

The blank sample is coarse powder containing larger chips and was grinded to fine powder with a grinding vessel as fine powder gives higher intensities and more stable results. The sample (powder) is pressed to pellets as pressed samples give higher intensities than loose powder samples. For the base of the pressed pellets, 10 ml (~3.4 g) of Borax was used as a backing material in a 40 mm aluminium cup. Borax is an organic material which is highly stable under X-rays and is used to prevent X-rays from reaching the aluminium cup.

Sample analysis method was developed by the following steps:

a. **Preparation of the reliable calibration samples:**. The method included twelve elements to be calibrated: K, Ca, Cr, Mn, Co, Cu, Zn, Cd, Sn, Sb, Tl and Pb with concentration range of 0-100 ppm. The elements were from quite wide atomic number (Z) spectrum: K (Z= 19) and Pb (Z = 82).

b. **Qualitative analysis:** By measuring the energies (determining the colours) of the radiation emitted by the sample it is possible to determine the element.

c. **Quantitative method:** By measuring these intensities of the emitted energies (colours) it is possible to determine how much of each element is present.

Accuracy and Precission of the analysis:

Element/Oxide	**Accuracy (%error)**	**Precission**	**Detection Limit**
Si, Al, Ti, Fe, Ca, K	<5%	<1%	0.01%
Na_2O and MgO	4-5%		
Mn and P	5-10 % (if conc is <0.1%)		
Trace Elements	<5% (if conc>100 ppm) ± 5% (if conc is >30 ppm but <100 ppm) ± 10 %(if conc is <30ppm).		10 ppm

5.1.2 Chemical laboratory: Inductively Coupled Plasma –Optical Emission Spectroscopy (ICP-OES)

Introduction to ICP-OES

Inductively coupled plasma/optical emission spectroscopy (ICP/OES) is a powerful tool for the determination of metals in a variety of different sample matrices. With this technique, liquid samples are injected into a radiofrequency (RF)-induced argon plasma using one of a variety of nebulizers or sample introduction techniques. The sample mist reaching the plasma is quickly dried, vaporized, and energized through collisional excitation at high temperature. The atomic emission emanating from the plasma is viewed, collected with a lens or mirror, and imaged onto the entrance slit of a wavelength selection device. Single element measurements can be performed cost effectively with a simple monochromator/ photomultiplier tube (PMT) combination, and simultaneous multielement determinations are performed for up to 70 elements with the combination of a polychromator and an array detector *(Figure 5.2)*. The analytical performance of such systems is competitive with most other inorganic analysis techniques, especially with regards to sample throughout and sensitivity.

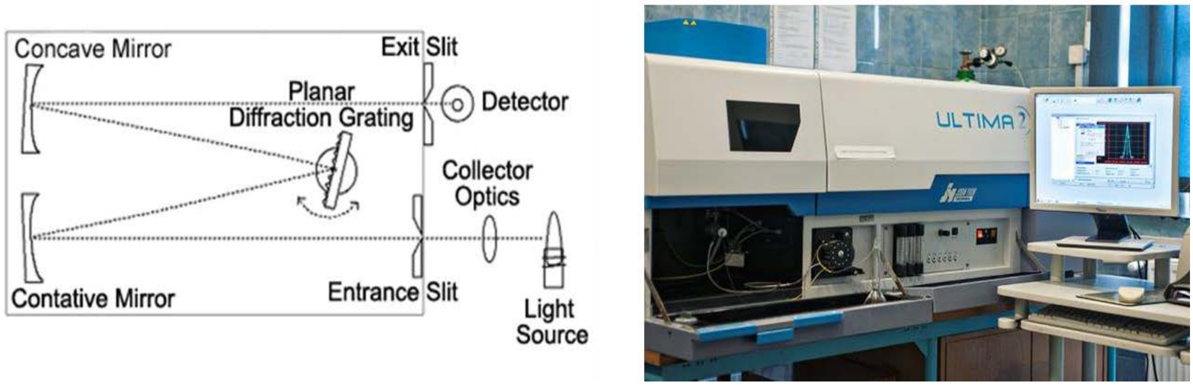

Figure 5. 2 Working principle and photograph of ICP-OES instrument

Principle of ICP-OES

- Plasma is generated by supplying argon gas to torch coil, and high frequency electric current is applied to the work coil at the tip of the torch tube which creates an electromagnetic field in the torch tube.
- Argon gas is ionized by the electromagnetic field and plasma is generated.
- This plasma has high electron density and temperature (10000K) and this energy is used in the excitation-emission of the sample.
- Solution samples are introduced into the plasma in an atomized state through the narrow tube in the centre of the torch tube.
- When the excited atoms return to low energy position, emission rays (spectrum rays) are released and the emission rays that correspond to the photon wavelength are measured.
- The element type is determined based on the position of the photon rays, and the content of each element is determined based on the rays intensity.

Advantages of ICP-OES

- High temperature (7000–8000 K)
- High electron density (1014–1016cm$_3$)
- Appreciable degree of ionization for many elements simultaneous multi element capability (over 70 elements including P and S)
- Low background emission and relatively low chemical interference
- High stability leading to excellent accuracy and precision
- Excellent detection limits for most elements (0.1 –100 ng mL1)
- Wide linear dynamic range (LDR) (four to six orders of magnitude)
- Cost-effective analyses.

Sample preparation

- Samples should be delivered in 12 – 15 ml tubes.
- Samples should be acidified (preferably with 1-5 % HNO_3 in order to keep metals in solution).
- The content of salts in samples should be kept below 3%, preferably below 2% (= 20 g/l).
- Solid material should be destructed, preferably with nitric acid only (concentration HNO_3 below 10%, ideally 1%), or if necessary, with HNO_3/H_2O. This step can be performed as a closed destruction in a microwave-oven.
- HCl can cause precipitates and the sulphur in sulfuric acid interferes in the analysis.
- The torches present at the GI are not resistant to HF.
- For the ICAP samples should not contain any organic solvents.
- Indicate as far a possible what concentration level may be expected in the samples.

Blank and standard used

Standard: Pure metal oxides (99.999% purity) of Sigma Aldrich make.

Blank: 3 % HNO_3: the standard is dissolved in 3 % HNO_3 and prepared to 1000 ppm with distilled water. Further dilution upto 100ppm, 1ppm and 0.1ppm was done

Accuracy and precission: Reserves are within 95%-98% confidence interval and precission is within 3-5% RSD (Relative Standard Deviation). Reference materials used are SY-4 (diorite genesis) and NCSDC 86318 (REE ore).

5.2 Identification of rock types

From megascopic and petrographic study the lithotypes have been classified as tuff, rhyolite and agglomerate. For geochemical characterization, values are collectively processed in order to attain a comparative discrimination between them. The samples show high SiO_2 (68.12-82%), $Al_2 O_3$ (6.15-8.71%) and Fe_2O_3 (1.52-14.10). Enrichment of Nb, Y, Zr, Ce, Rb and depletion in Ba, Sr and Ti is characteristic of the rocks. In total alkali-silica diagram (Middlemost, 1994) it has been observed that all the sample value fall predominantly in rhyolite field irrespective of tuff, rhyolite and agglomerate with a few in trachydacite *(Figure 5.3a)*. According to Nb/Y- vs. Zr/TiO_2 classification diagram (Winchester and Floyd,1977), the samples plot in the comendite-pantellerite field which are Al-Fe rich variety of rhyolite *(Figure 5.3b)*. This indicates that geochemically the pyroclastic tuffs and agglomerate are similar to rhyolites, hence may be concluded that they are rhyolitic in composition. Discrimination based on the molecular ratio of alumina to alkali [$Al_2O_3/(Na_2O+K_2O)$] versus alumina to lime and alkali [$Al_2O_3/(CaO+Na_2O+K_2O)$] after Shand (1943) shows that the samples are forming a distinct linear correlation from peralkaline to peraluminous field where the tuff samples tend to attain peraluminous nature *(Figure 5.3c)*. It illustrates that the parental magma was peralkaline and the tuff has attained peraluminous nature because of alteration (studied in detail in the alteration section).

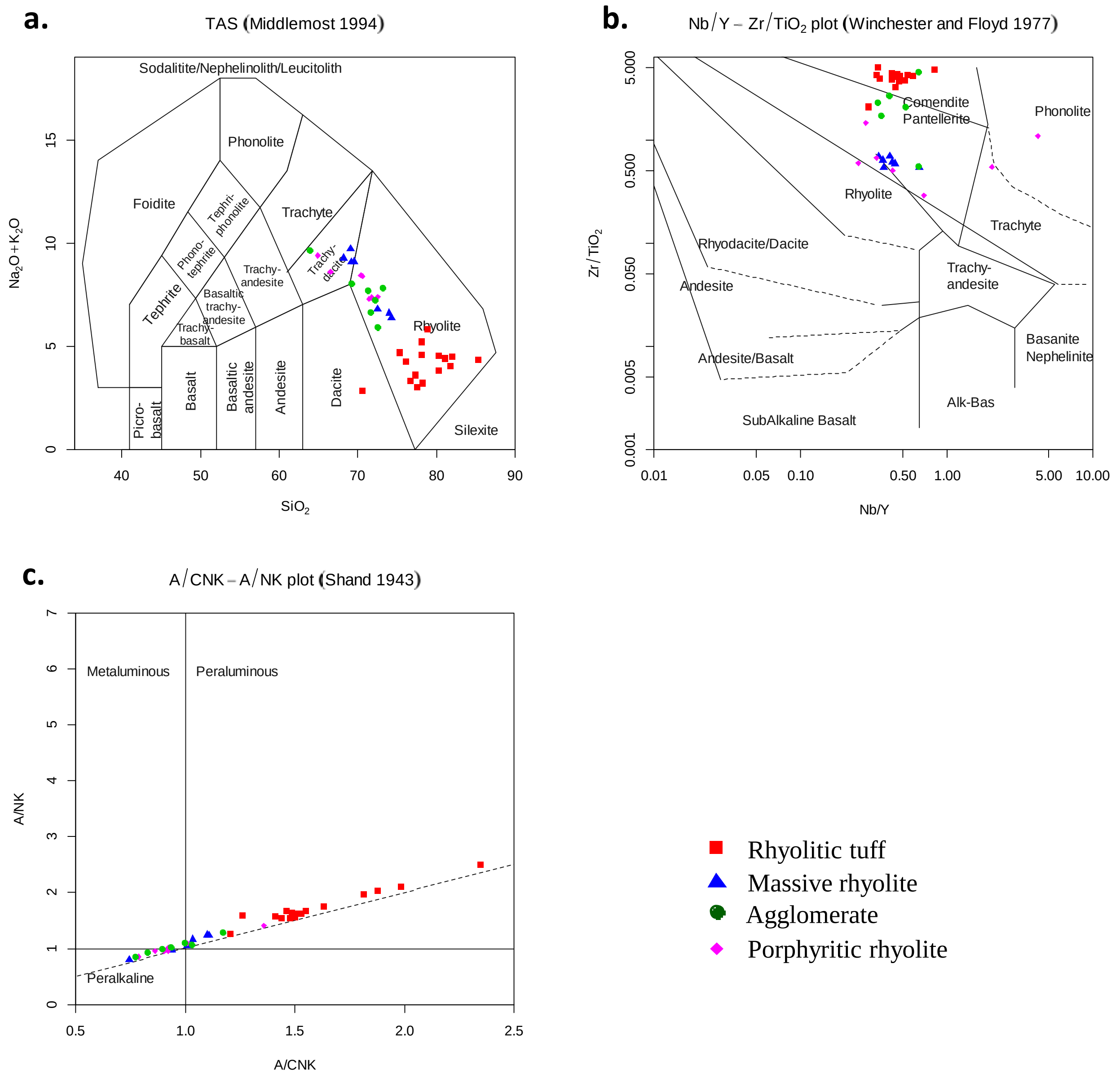

Figure 5. 3 a) Total Alkali Silica (TAS) diagram of acid volcanics of SRC, Most of them fall on the rhyolitic field with a few in trachy-dacite; b) Classification diagram using trace elements, they fall in the alkali rhyolite field (Al-rich Comendite and Fe-rich Pantellerite); c)A/NK vs A/CNK plots altered tuff in peraluminous and other unaltered lithotypes in peralkaline.

5.3 Geochemical analysis of Rhyolitic tuff

The chemical data with major, minor and trace elements of rhyolitic tuff are tabulated in *Table 5.1* depicting the major and trace element while REE data is tabulated in *Table 5.4.*

5.3.1 Major oxide and Trace Elements in Rhyolitic tuff

Sixteen samples (n=16) for rhyolitic tuff have been considered for analyzing geochemistry. These samples are characterized by high concentration of SiO_2, Na_2O, K_2O, Zr, Nb, Y &REE and lower concentration of MgO, Fe_2O_3 (t), CaO, Cr, Ni & Sr. SiO_2 from 68.12 to 80.00%; Al_2O_3 from 6.15 to 8.71%; Fe_2O_3t from 1.52 to 14.1%; MgO from 0.01 to 0.33%; CaO from 0.11 to 0.63%; Na_2O from 0.27 to 1.18%; K_2O from 2.28 to 4.66%; MnO from 0.02 to 0.14%; TiO_2 from 0.17 to 0.28% and P_2O_5 values from 0.21 to 0.45%. Among the trace elements U varies from 20 to 50ppm, Th varies from 58 to 104ppm; Zn from 96 to 2000 ppm; Pb from 40 to 484ppm; Ba from 24 to 79ppm; Nb from 162 to 378 ppm; Rb from 300 to 542ppm; Cr from 34 to188 and Zr in range of 5200 to 10220 ppm *(Table 5.2).*

Range (maxima- minima), median and standard deviation has been calculated for the major, minor and trace element in tuff (n=16). The statistical data is given in *Table 5.2* and its graphical representation given in the bar diagram *(Figure 5.4)*

Table 5. 1 Representative Major Oxide and trace elemental compositions of Rhyolitic tuff from Buriwara

Major elements analysis (wt% oxide) of Rhyolitic tuff of Buriwara																
	BDW 1	**BDW 2**	**BDW 3**	**BDW 4**	**BDW 5**	**BDW 6**	**BDW 7**	**BDW 8**	**BDW 9**	**BDW 10**	**BDW 11**	**BDW 12**	**BDW 13**	**BDW 14**	**BDW 15**	**BDW 16**
SiO_2	68.1	76.12	74.5	77.84	79.52	74.9	76.14	74.22	76.92	72.65	74.4	82	77.95	76.23	77.35	78.15
Al_2O_3	8	7.59	7.23	7.03	7	8.71	8.25	8.17	7.98	7.9	6.15	7.27	7.8	8.5	6.97	7.94
Fe_2O_3 (t)	16.9	9.89	11.4	11.78	5.59	6.61	7.61	10.14	5.81	10.58	11.41	1.8	4.04	5.3	7.56	4.85
MgO	0.04	0.03	0.04	0.06	0.03	0.01	0.15	0.2	0.05	0.08	0.07	0.27	0.25	0.11	0.06	0.33
CaO	0.11	0.13	0.17	0.15	0.63	0.13	0.28	0.18	0.16	0.14	0.26	0.19	0.21	0.18	0.19	0.37
Na_2O	0.45	0.38	0.38	0.34	0.29	0.32	0.38	0.38	0.37	0.36	0.27	0.34	0.37	1.18	0.33	0.32
K_2O	2.28	2.74	2.82	2.69	3.63	4.66	4.08	3.75	3.99	4.16	3.18	3.83	3.89	4.43	3.34	3.91
MnO	0.14	0.02	0.08	0.03	0.06	0.05	0.04	0.05	0.02	0.03	0.04	0.02	0.02	0.06	0.09	0.04
TiO_2	0.24	0.24	0.23	0.24	0.22	0.24	0.28	0.22	0.23	0.23	0.18	0.2	0.21	0.25	0.17	0.19
P_2O_5	0.28	0.26	0.32	0.23	0.35	0.28	0.27	0.24	0.23	0.29	0.23	0.21	0.33	0.45	0.31	0.28
Trace elements analysis (in ppm) of Rhyolitic tuff from Buriwara																
U	25	26	31	30	50	25	32	25	22	20	40	30	43	25	31	34
Th	104	98	90	80	86	90	96	94	88	100	72	80	84	58	76	92
Mo	<10	<10	<10	<10	<10	<10	<10	<10	<10	<10	<10	<10	<10	<10	<10	<10
V	<10	<10	<10	<10	<10	<10	<10	<10	<10	<10	<10	<10	<10	<10	<10	<10
Cu	6	6	6	6	20	10	<5	6	<5	<5	<5	<5	10	6	8	8
Ni	<10	<10	<10	<10	<10	<10	<10	<10	<10	<10	<10	<10	<10	<10	<10	<10
Co	<10	<10	<10	<10	<10	<10	<10	<10	<10	<10	<10	<10	<10	<10	<10	<10
Zn	594	268	530	308	206	2000	1050	1390	254	370	348	96	1090	522	450	1150
Pb	190	40	156	160	74	484	97	72	116	64	54	46	150	78	80	92
Ba	38	26	40	26	79	28	36	40	34	24	44	50	48	54	52	76
Sr	<10	<10	<10	<10	<10	<10	<10	<10	<10	<10	<10	<10	<10	<10	<10	<10
Nb	378	322	288	312	286	310	310	318	296	316	258	260	312	162	232	260
Ta	<25	<25	<25	<25	<25	<25	<25	<25	<25	<25	<25	<25	<25	<25	<25	<25
Rb	300	376	408	380	346	542	412	374	410	504	334	380	470	380	350	522
Cr	64	44	104	122	176	84	96	44	48	34	170	116	90	188	118	134
Zr	10220	9928	8596	9066	9042	9242	9060	9422	10212	9644	7824	7828	10100	5200	7270	9660
Total	97.8	98.52	98.20	101.4	98.36	97.20	98.60	98.73	96.91	97.53	97.11	97.02	96.31	97.36	97.24	97.59

Table 5. 2 Statistical evaluation of major, minor (in %) and trace (in ppm) elements of tuff

Tuff (n=16)	**Range**		**Mean**	**Std dev**
	Min	**Max**		
Major oxide (wt%)				
SiO_2	68.12	82.00	76.06	3.01
Al_2O_3	6.15	8.71	7.66	0.65
Fe_2O_3	1.52	14.10	7.61	3.31
FeO	0.20	2.84	0.60	0.61
MgO	0.01	0.33	0.11	0.10
CaO	0.11	0.63	0.22	0.12
Na_2O	0.27	1.18	0.40	0.20
K_2O	2.28	4.66	3.59	0.66
MnO	0.02	0.14	0.05	0.03
TiO_2	0.17	0.28	0.22	0.03
P_2O_5	0.21	0.45	0.29	0.06
Trace element (ppm)				
U	20.00	50.00	30.56	7.77
Th	58.00	104.00	86.75	11.31
Mo	0.00	0.00		
V	0.00	0.00		
Cu	6.00	20.00	8.36	3.98
Ni	0.00	0.00		
Co	0.00	0.00		
Zn	96.00	2000.00	664.13	508.54
Pb	40.00	484.00	122.06	102.96
Ba	24.00	79.00	43.44	15.80
Sr	0.00	0.00		
Nb	162.00	378.00	288.75	46.50
Ta	0.00	0.00		
Rb	300.00	542.00	405.50	67.46
Cr	34.00	188.00	102.00	47.16
Zr	5200.00	10220.00	8894.63	1282.09

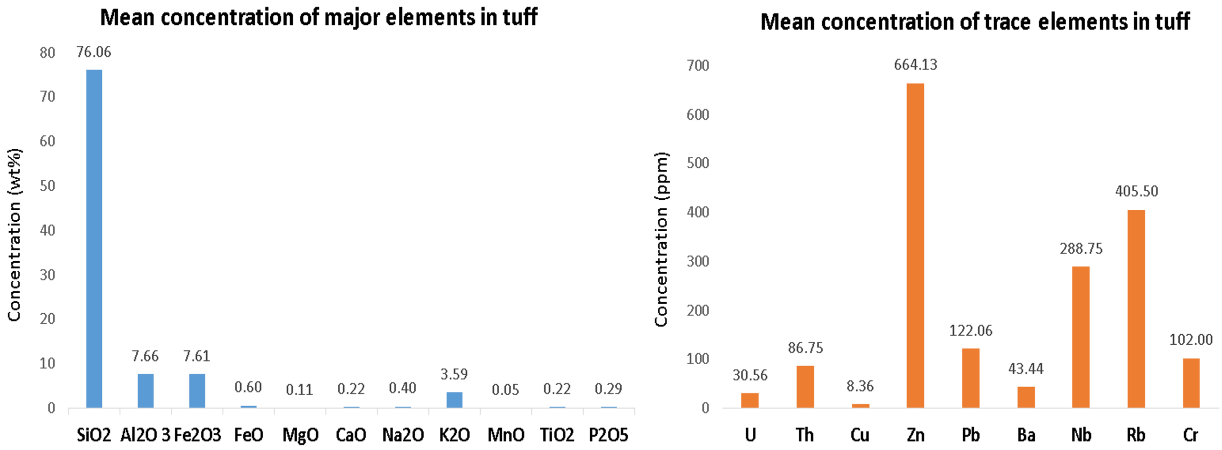

Figure 5. 4 Bar diagram of mean concentration of major, minor and trace element of tuff

In between the different major and trace element of tuff the correlation matrix *Table 5.3* has been prepared and those pairs of elements which is showing the strong positive or negative correlation has been plotted in Harker diagram *(Figure 5.5).* Very strong positive correlation has been observed in between CaO vs Ba; Nb vs Th; Zr vs Th and Nb vs Zr, Moderate positive correlation is observed betweenAl_2O_3 vs TiO_2; K_2O vs Al_2O_3; Al_2O_3 vs Zn, Al_2O_3 vs Rb; Fe_2O_3 vs Nb; K_2O vs Rb; U vs Ba; Zn vs Pb while the very weak positive correlation is observed between SiO_2 vs MgO; SiO_2 vs K_2O, SiO_2 vs CaO; Al_2O_3 vs Na_2O_3; K_2O vs Zn and strong negative correlation between SiO_2 vs Fe_2O_3; moderately negative correlation between Al_2O_3 vs U; Fe_2O_3 vs MgO; Fe_2O_3 vs K_2O; Fe_2O_3 vs Ba; Na_2O vs Nb; Na_2O vs Zr and weak negative correlation between SiO_2 vs Nb; K_2O vs Nb and Ba vs Nb is observed.

The spider diagram of trace elements are plotted in order to understand their relative concentration with respect to Chondrite (Chondrite values after Thompson 1982) and Primitive mantle (Primitive mantle values after Sun and Mc. Donough 1989) *(Figure 5.6).* It has been noticed that Ba, Sr, K and Ti shows a negative anomaly which indicates mobility of these elements. Other trace elements like Mo, V, Ni, Co and Ta are also very low in concentration which supports element mobility. This may lead to the conclusion that events like magma

mixing or heterogeneity in magma had been taken place where these elements had escaped from the system.

Table 5. 3 Correlation matrix of geochemical data of major, minor (in %) and trace elements (in ppm) of tuff (n=16).

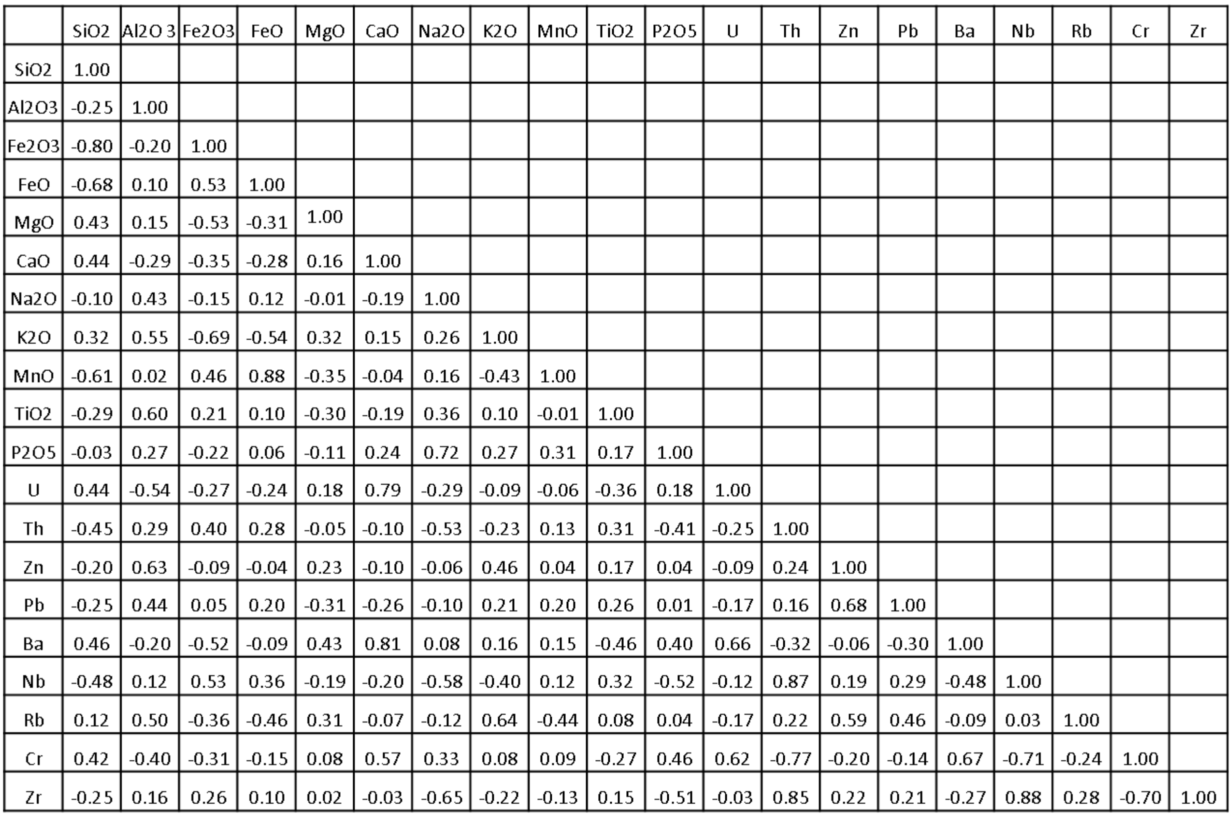

	SiO_2	Al_2O_3	Fe_2O_3	FeO	MgO	CaO	Na_2O	K_2O	MnO	TiO_2	P_2O_5	U	Th	Zn	Pb	Ba	Nb	Rb	Cr	Zr
SiO_2	1.00																			
Al_2O_3	-0.25	1.00																		
Fe_2O_3	-0.80	-0.20	1.00																	
FeO	-0.68	0.10	0.53	1.00																
MgO	0.43	0.15	-0.53	-0.31	1.00															
CaO	0.44	-0.29	-0.35	-0.28	0.16	1.00														
Na_2O	-0.10	0.43	-0.15	0.12	-0.01	-0.19	1.00													
K_2O	0.32	0.55	-0.69	-0.54	0.32	0.15	0.26	1.00												
MnO	-0.61	0.02	0.46	0.88	-0.35	-0.04	0.16	-0.43	1.00											
TiO_2	-0.29	0.60	0.21	0.10	-0.30	-0.19	0.36	0.10	-0.01	1.00										
P_2O_5	-0.03	0.27	-0.22	0.06	-0.11	0.24	0.72	0.27	0.31	0.17	1.00									
U	0.44	-0.54	-0.27	-0.24	0.18	0.79	-0.29	-0.09	-0.06	-0.36	0.18	1.00								
Th	-0.45	0.29	0.40	0.28	-0.05	-0.10	-0.53	-0.23	0.13	0.31	-0.41	-0.25	1.00							
Zn	-0.20	0.63	-0.09	-0.04	0.23	-0.10	-0.06	0.46	0.04	0.17	0.04	-0.09	0.24	1.00						
Pb	-0.25	0.44	0.05	0.20	-0.31	-0.26	-0.10	0.21	0.20	0.26	0.01	-0.17	0.16	0.68	1.00					
Ba	0.46	-0.20	-0.52	-0.09	0.43	0.81	0.08	0.16	0.15	-0.46	0.40	0.66	-0.32	-0.06	-0.30	1.00				
Nb	-0.48	0.12	0.53	0.36	-0.19	-0.20	-0.58	-0.40	0.12	0.32	-0.52	-0.12	0.87	0.19	0.29	-0.48	1.00			
Rb	0.12	0.50	-0.36	-0.46	0.31	-0.07	-0.12	0.64	-0.44	0.08	0.04	-0.17	0.22	0.59	0.46	-0.09	0.03	1.00		
Cr	0.42	-0.40	-0.31	-0.15	0.08	0.57	0.33	0.08	0.09	-0.27	0.46	0.62	-0.77	-0.20	-0.14	0.67	-0.71	-0.24	1.00	
Zr	-0.25	0.16	0.26	0.10	0.02	-0.03	-0.65	-0.22	-0.13	0.15	-0.51	-0.03	0.85	0.22	0.21	-0.27	0.88	0.28	-0.70	1.00

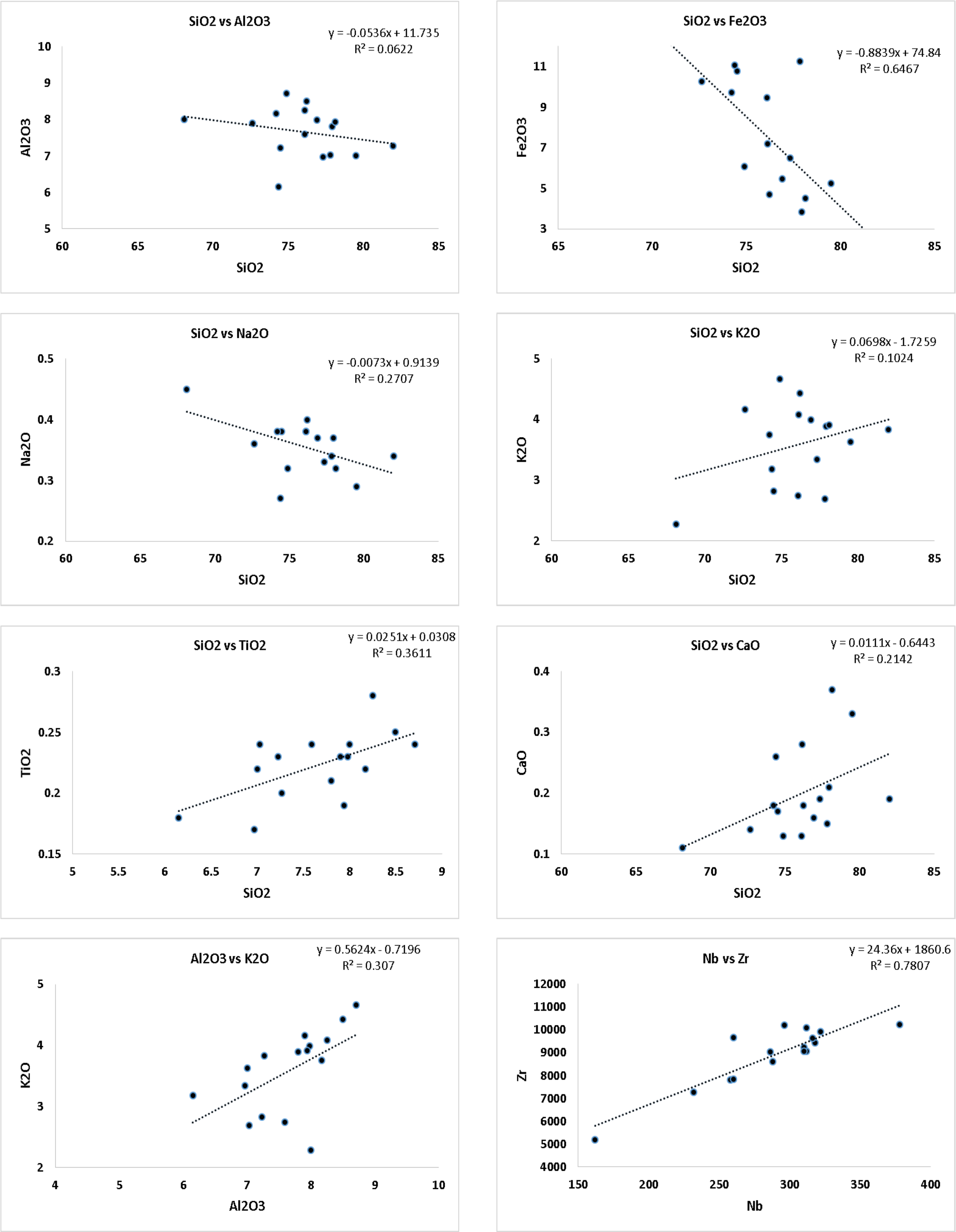

Figure 5. 5 Variation diagrams (Harker type) between major oxides (in %) and trace elements (ppm) in Tuff

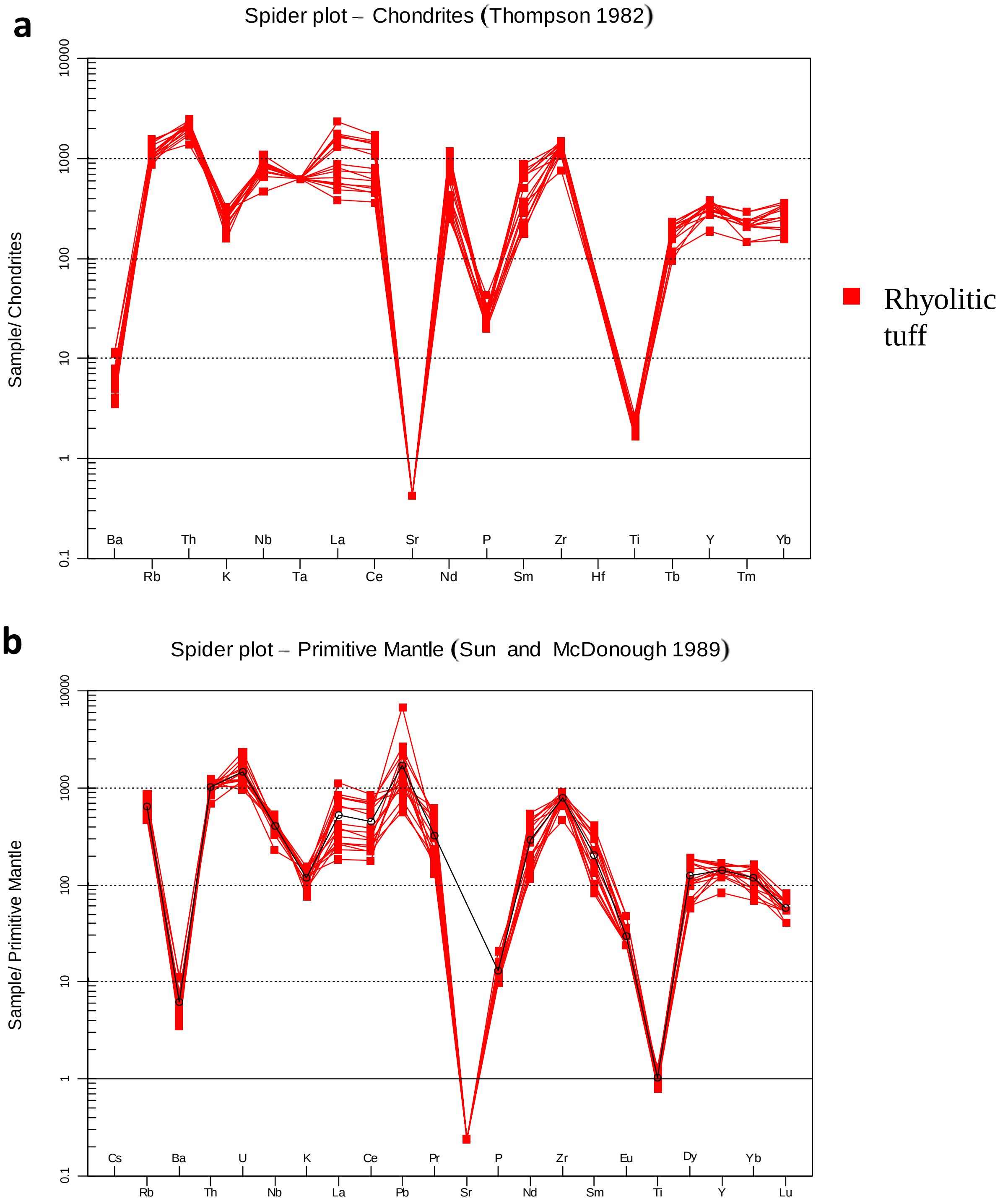

Figure 5. 6 Spider diagram for trace elements of Tuff a) Chondrite normalized after (Thompson, 1982); b) Primitive mantle normalized (Sun and Mc Donough 1989)

5.3.2 REE in Tuff

REE value raw data of (n=16) sample of tuff has been tabulated in the *Table 5.4*. All the samples display uniform REE patterns, parallel to sub-parallel, slightly LREE enriched over HREE. The REE fractionation pattern *(Figure 5.7)* having $(La/Yb)_N$= 2.14-6.87, $(La/Sm)_{N=}$1.81-3.80 and $(Gd/Yb)_N$=0.64-1.17 is forming a slightly negative slope which suggest about magmatic fractionation. Again such a lower slope is entitled to enrichment of HREE, which also means that no significant fraction of HREE bearing phase such as garnet had taken place. The presence of minerals like monazite and alanite could be a reason for such pattern (Rollinson,1993). Negative Eu anomaly, Eu/Eu*=0.12-0.36 could be attributed to plagioclase fractionation which is also being supported by negative strontium anomaly *(Figure5.6).* Previous R&D work reported REE minerals like bastnaesite and monazite in tuff samples from Buriwara (Upadhyay and Banerjee, 2011). The average TREO (total rare earth oxide) of 16 samples is 3200ppm varying from 1464ppm to 5376ppm. The HREO concentration of 1186 ppm accounts to 37% of TREO.

Table 5. 4 Representative analysis of REE of Tuff:

REE	BDW 1	BDW 2	BDW 3	BDW 4	BDW 5	BDW 6	BDW 7	BDW 8	BDW 9	BDW 10	BDW 11	BDW 12	BDW 13	BDW 14	BDW 15	BDW 16
La	548	184	538	266	290	456	186	774	158	584	214	178	126	250	560	428
Ce	1208	456	1256	534	685	932	428	1498	402	1296	516	394	314	612	1196	1072
Pr	134	54	148	48	84	92	44	172	40	140	62	46	36	65	138	112
Nd	606	246	664	190	370	444	210	746	184	604	275	173	156	272	590	524
Sm	142	64	156	44	75	102	46	180	44	130	59	39	36	72	138	132
Eu	8	4	5	4	6	6	4	8	4	4	4	4	4	4	5	6
Gd	94	67	96	52	59	91	58	105	55	80	46	30	35	51	84	86
Tb	12	10	11	11	10	11	12	12	10	10	6	5	6	8	9	8
Dy	136	82	124	80	78	138	72	140	52	124	48	42	45	74	108	134
Ho	28	16	24	22	24	28	16	28	15	25	11	10	12	14	20	18
Er	80	52	70	54	58	82	48	78	45	80	38	28	34	42	56	76
Tm	10	7	8	8	8	7	7	10	7	8	7	5	5	7	7	7
Yb	80	58	68	56	56	76	54	76	45	74	45	38	34	42	58	72
Lu	6	5	5	4	4	4	5	5	4	4	5	4	4	3	4	3
Y	698	678	610	602	632	730	696	712	700	540	562	742	376	554	702	768
$(La/Sm)_N$	2.43	1.81	2.17	3.80	2.43	2.81	2.54	2.70	2.26	2.83	2.28	2.87	2.20	2.18	2.55	2.04
$(La/Yb)_N$	4.62	2.14	5.33	3.20	3.49	4.05	2.32	6.87	2.37	5.32	3.21	3.16	2.50	4.01	6.51	4.01
$(Tb/Yb)_N$	0.66	0.76	0.71	0.87	0.79	0.64	0.98	0.70	0.98	0.60	0.59	0.58	0.78	0.84	0.68	0.49
Eu/Eu*	0.02	0.01	0.01	0.02	0.02	0.01	0.02	0.01	0.02	0.01	0.02	0.03	0.03	0.01	0.01	0.01
TLREO	3086	1174	3231	1266	1759	2370	1069	3943	969	3222	1317	971	781	1487	3067	2653
THREO	**1407**	1206	1246	**1098**	**1150**	**1435**	**1200**	**1434**	**1161**	**1154**	**954**	**1132**	**683**	**984**	1294	1445
TREO	4493	2380	4477	2364	2909	3805	2269	5376	2129	4376	2271	2104	1464	2471	4361	4098

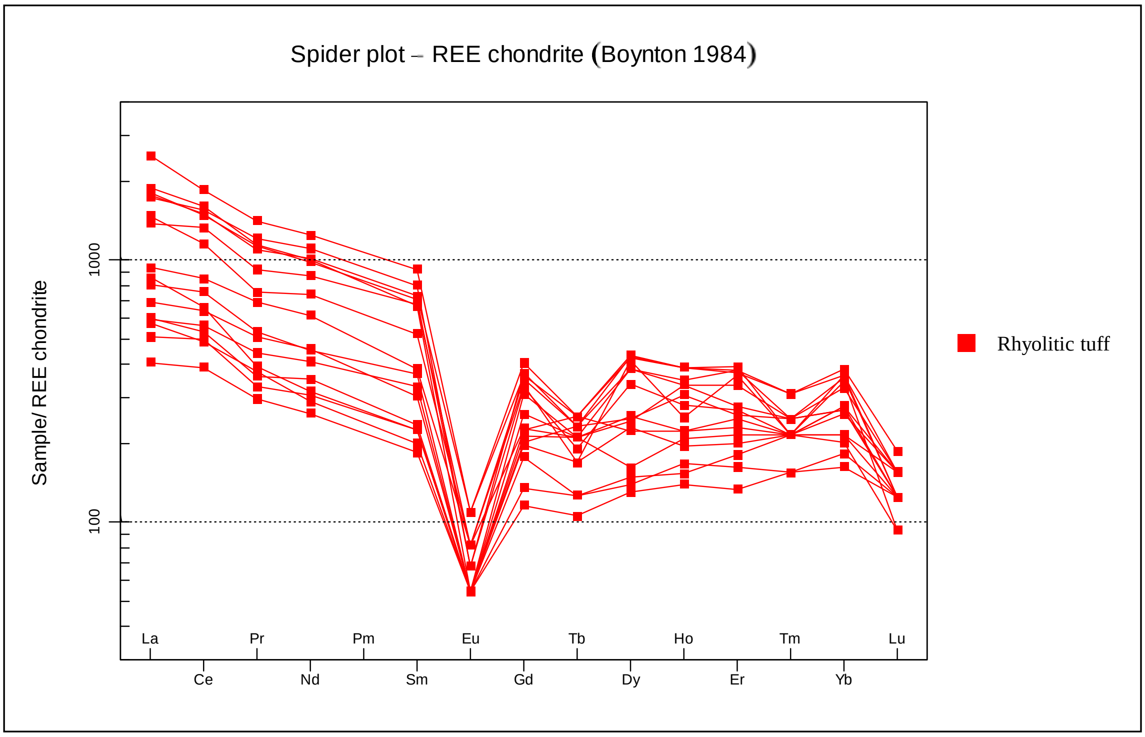

Figure 5. 7 Spider diagram of REE, Chondrite normalized after (Boynton,1984) for tuff

5.4 Geochemical analysis of Massive Rhyolite

The chemical data with major, minor and trace elements of massive rhyolite are tabulated which in *Table 5.5* depicting the major and trace element while analyzed REE data is tabulated in *Table 5.8*.

5.4.1 Major oxide and Trace Elements in Massive Rhyolite

Seven samples (n=7) for massive rhyolite have been considered for analyzing geochemistry. These samples are characterized by high concentration of SiO_2, Na_2O, K_2O, Zr, Nb, Y &REE and lower concentration of MgO, Fe_2O_3 (t), CaO, Cr, Ni &Sr. SiO_2 varies from 67.26 to 73.91%; Al_2O_3 from 9.22 to12.24%; $Fe_2O_{3(}$t) from 7.91 to 9.42%; MgO from 0.08 to 0.36%; CaO from 0.26 to 0.58; Na_2O from 1.21 to 6.33%; K_2O from 3.17 to 5.43%; MnO from 0.02 to 0.16; TiO_2 from 0.39 to 0.48% and P_2O_5 values from 0.02 to 0.05%. Among the trace elements U varies from 6 to 10ppm, Th varies from 36 to 43ppm Zn from 251 to 446 ppm; Pb from 44 to 52ppm; Ba from 28 to 297ppm; Nb from 106 to 163 ppm; Rb from 164 to 307ppm; Cr from 45 to184 and Zr in range of 2100 to 3052 ppm *(Table 5.6).*

Range (maxima- minima), median and standard deviation has been calculated for the major, minor and trace element in massive rhyolite (n=7). The statistical data is given in *Table 5.6* and its graphical representation given in the bar diagram *(Figure 5.8)*

Table 5. 5 Representative Major Oxide and trace elemental compositions of Massive rhyolite from Buriwara

	BDW 17	**BDW 18**	**BDW 19**	**BDW 20**	**BDW 24**	**BDW 29**	**BDW 30**
Major oxides (wt%) of Massive rhyolite							
SiO_2	72.17	69.08	67.26	70.23	73.91	67.59	68.03
TiO_2	0.43	0.45	0.45	0.39	0.44	0.48	0.48
Al_2O_3	9.51	12.1	11.89	10.31	9.22	11.08	12.24
Fe_2O_3(t)	8.08	7.91	9.42	8.59	8.55	8.27	8.15
MgO	0.16	0.22	0.08	0.22	0.36	0.18	0.19
MnO	0.16	0.14	0.11	0.02	0.12	0.11	0.09
CaO	0.56	0.35	0.27	0.55	0.56	0.58	0.26
Na_2O	1.21	4.61	4.02	2.13	1.83	6.33	3.51
K_2O	5.22	4.42	5.12	4.44	4.51	3.17	5.43
P_2O_5	0.05	0.04	0.02	0.04	0.02	0.03	0.04
Trace elements (ppm) of massive rhyolite							
Cr	84	174	126	45	93	121	184
Ni	<10	<10	<10	<10	<10	<10	<10
Cu	<5	17	<5	5	<5	<5	<5
Zn	331	294	364	251	446	340	316
Ga	17	21	19	20	19	19	17
Rb	273	231	286	166	228	164	307
Sr	12	11	16	21	12	10	<10
Y	354	339	374	273	422	314	298
Zr	2995	2648	2740	2100	3052	2593	3040
Nb	123	113	133	163	140	106	114
Pb	<25	<25	44	52	<25	<25	<25
Ba	57	28	297	35	<25	28	40
Ce	624	712	750	1315	1213	788	860
Th	39	39	43	39	36	40	41
U	10	6	8	6	6	6	7
Total	98.04	99.79	99.16	97.37	100.09	98.27	98.94

Table 5. 6 Statistical evaluation of major, minor (in %) and trace (in ppm) elements of Massive rhyolite

Massive rhyolite (n=7)	**Range**		**Mean**	**Std dev**
	Min	**Max**		
Major oxide (wt%)				
SiO_2	67.26	73.91	69.75	2.32
TiO_2	0.39	0.48	0.45	0.03
Al_2O_3	9.22	12.24	10.91	1.16
Fe_2O_3(t)	7.91	9.42	8.42	0.47
MgO	0.08	0.36	0.20	0.08
MnO	0.02	0.16	0.11	0.04
CaO	0.26	0.58	0.45	0.14
Na_2O	1.21	6.33	3.38	1.66
K_2O	3.17	5.43	4.62	0.70
P_2O_5	0.02	0.05	0.03	0.01
Trace element (ppm)				
Cr	45.00	184.00	118.14	45.79
Ni	0.00	0.00		
Cu	5.00	17.00	11.00	6.00
Zn	251.00	446.00	334.57	56.44
Ga	17.00	21.00	18.86	1.36
Rb	164.00	307.00	236.43	52.21
Sr	10.00	21.00	13.67	3.77
Y	273.00	422.00	339.14	46.29
Zr	2100.00	3052.00	2738.29	314.42
Nb	106.00	163.00	127.43	18.21
Pb	44.00	52.00	48.00	4.00
Ba	28.00	297.00	80.83	97.17
Ce	624.00	1315.00	894.57	244.41
Th	36.00	43.00	39.57	1.99
U	6.00	10.00	7.00	1.41

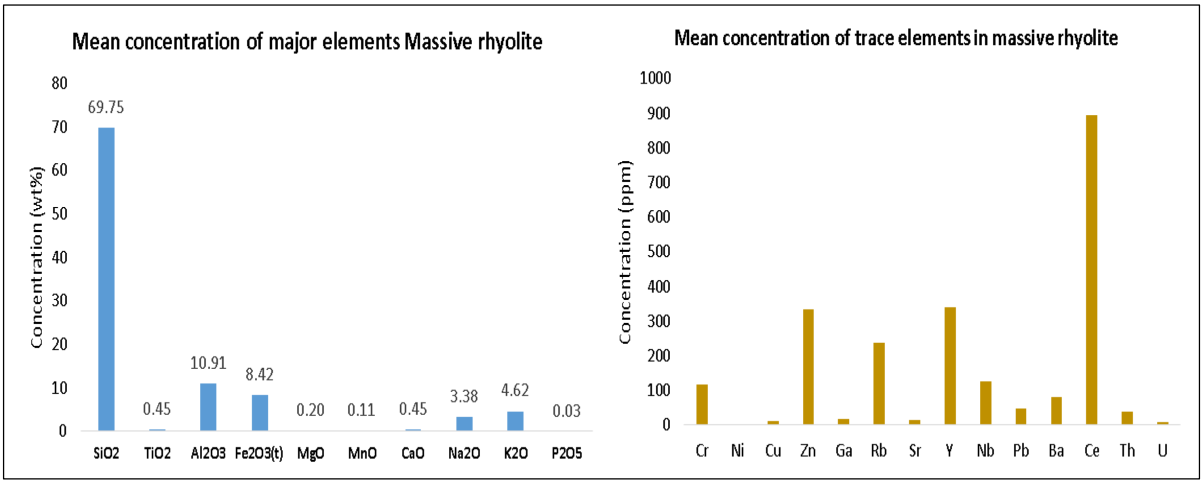

Figure 5. 8 Bar diagram of mean concentration of major, minor and trace element of massive rhyolite

In between the different major and trace element of tuff the correlation matrix *Table 5.7* has been prepared and those pairs of elements which is showing the strong positive or negative correlation has been plotted in Harker diagram *(Figure 5.9).* Very strong positive correlation has been observed in between Fe_2O_3 vs Ba; Al_2O_3 vs Cr; K_2O vs Rb; Sr vs Nb and Zn vs Y. Moderate positive correlation betweenAl_2O_3 vs TiO_2; TiO_2 vs Na_2O; SiO_2 vs CaO, TiO_2 vs Zr; Al_2O_3 vs Th; K_2O vs U; Rb vs Zr; Ba vs Th and strong negative correlation between SiO_2 vs Al_2O_3; SiO_2vsNa_2O; Al_2O_3 vs CaO; TiO_2vs Sr; TiO_2 vs Nb; SiO_2vsTh while moderately negative correlation between Na_2O vs K_2O; CaO vs K_2O; CaO vs Rb; Na_2O vs Nb is observed.

The spider diagram of trace elements are plotted in order to understand their relative concentration with respect to Chondrite (Chondrite values after Thompson 1982) and Primitive mantle (Primitive mantle values after Sun and Mc. Donough 1989) *(Figure 5.10).* It has been noticed that Ba, Sr, K and Ti shows a negative anomaly which indicates mobility of these elements. Other trace elements like Mo, V, Ni, Co and Ta are also very low in concentration which supports element mobility. This may lead to the conclusion that events like magma

mixing or heterogeneity in magma had been taken place where these elements had escaped from the system.

Table 5. 7 Correlation matrix of geochemical data of major oxides (in %) and trace elements (in ppm) in massive rhyolite (n=7).

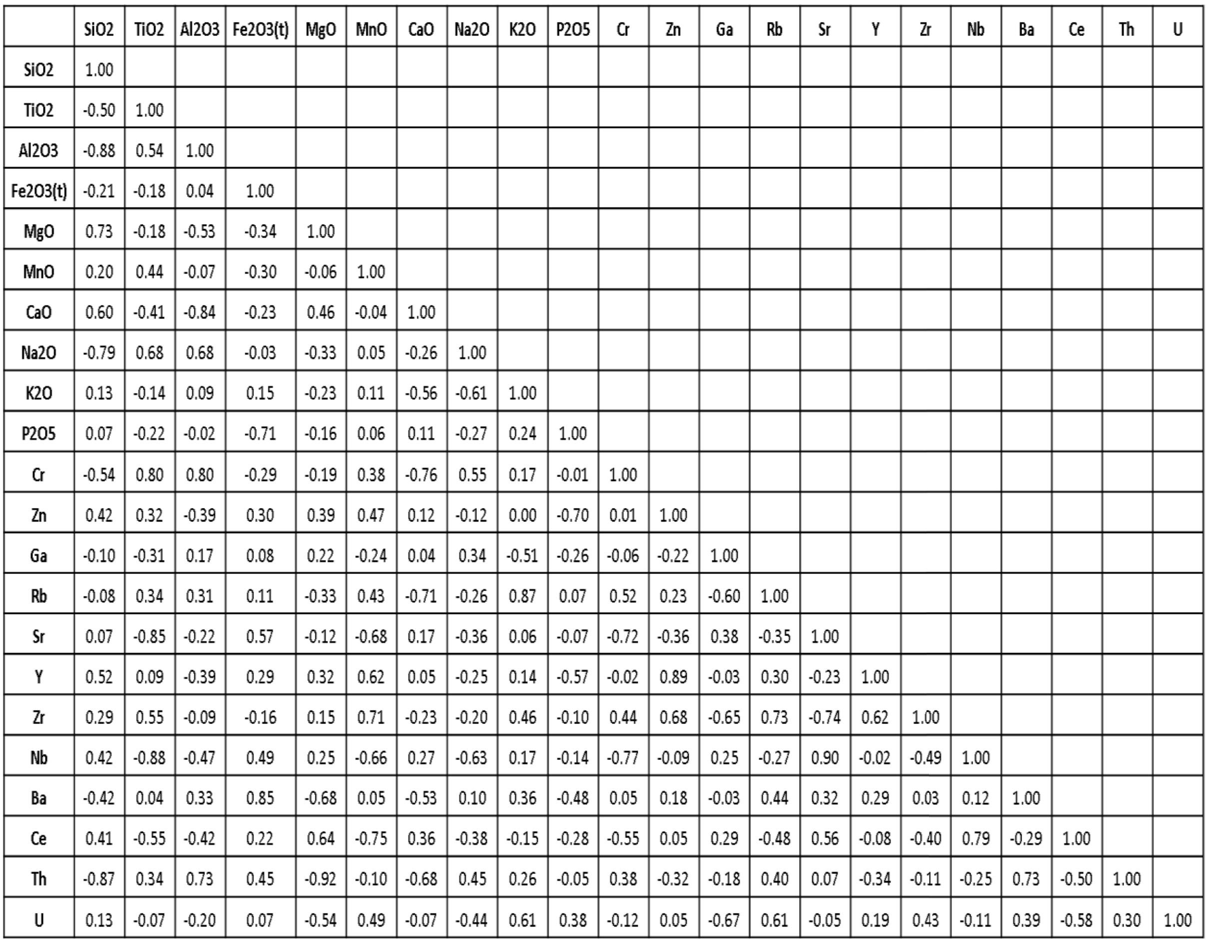

	SiO2	TiO2	Al2O3	Fe2O3(t)	MgO	MnO	CaO	Na2O	K2O	P2O5	Cr	Zn	Ga	Rb	Sr	Y	Zr	Nb	Ba	Ce	Th	U
SiO2	1.00																					
TiO2	-0.50	1.00																				
Al2O3	-0.88	0.54	1.00																			
Fe2O3(t)	-0.21	-0.18	0.04	1.00																		
MgO	0.73	-0.18	-0.53	-0.34	1.00																	
MnO	0.20	0.44	-0.07	-0.30	-0.06	1.00																
CaO	0.60	-0.41	-0.84	-0.23	0.46	-0.04	1.00															
Na2O	-0.79	0.68	0.68	-0.03	-0.33	0.05	-0.26	1.00														
K2O	0.13	-0.14	0.09	0.15	-0.23	0.11	-0.56	-0.61	1.00													
P2O5	0.07	-0.22	-0.02	-0.71	-0.16	0.06	0.11	-0.27	0.24	1.00												
Cr	-0.54	0.80	0.80	-0.29	-0.19	0.38	-0.76	0.55	0.17	-0.01	1.00											
Zn	0.42	0.32	-0.39	0.30	0.39	0.47	0.12	-0.12	0.00	-0.70	0.01	1.00										
Ga	-0.10	-0.31	0.17	0.08	0.22	-0.24	0.04	0.34	-0.51	-0.26	-0.06	-0.22	1.00									
Rb	-0.08	0.34	0.31	0.11	-0.33	0.43	-0.71	-0.26	0.87	0.07	0.52	0.23	-0.60	1.00								
Sr	0.07	-0.85	-0.22	0.57	-0.12	-0.68	0.17	-0.36	0.06	-0.07	-0.72	-0.36	0.38	-0.35	1.00							
Y	0.52	0.09	-0.39	0.29	0.32	0.62	0.05	-0.25	0.14	-0.57	-0.02	0.89	-0.03	0.30	-0.23	1.00						
Zr	0.29	0.55	-0.09	-0.16	0.15	0.71	-0.23	-0.20	0.46	-0.10	0.44	0.68	-0.65	0.73	-0.74	0.62	1.00					
Nb	0.42	-0.88	-0.47	0.49	0.25	-0.66	0.27	-0.63	0.17	-0.14	-0.77	-0.09	0.25	-0.27	0.90	-0.02	-0.49	1.00				
Ba	-0.42	0.04	0.33	0.85	-0.68	0.05	-0.53	0.10	0.36	-0.48	0.05	0.18	-0.03	0.44	0.32	0.29	0.03	0.12	1.00			
Ce	0.41	-0.55	-0.42	0.22	0.64	-0.75	0.36	-0.38	-0.15	-0.28	-0.55	0.05	0.29	-0.48	0.56	-0.08	-0.40	0.79	-0.29	1.00		
Th	-0.87	0.34	0.73	0.45	-0.92	-0.10	-0.68	0.45	0.26	-0.05	0.38	-0.32	-0.18	0.40	0.07	-0.34	-0.11	-0.25	0.73	-0.50	1.00	
U	0.13	-0.07	-0.20	0.07	-0.54	0.49	-0.07	-0.44	0.61	0.38	-0.12	0.05	-0.67	0.61	-0.05	0.19	0.43	-0.11	0.39	-0.58	0.30	1.00

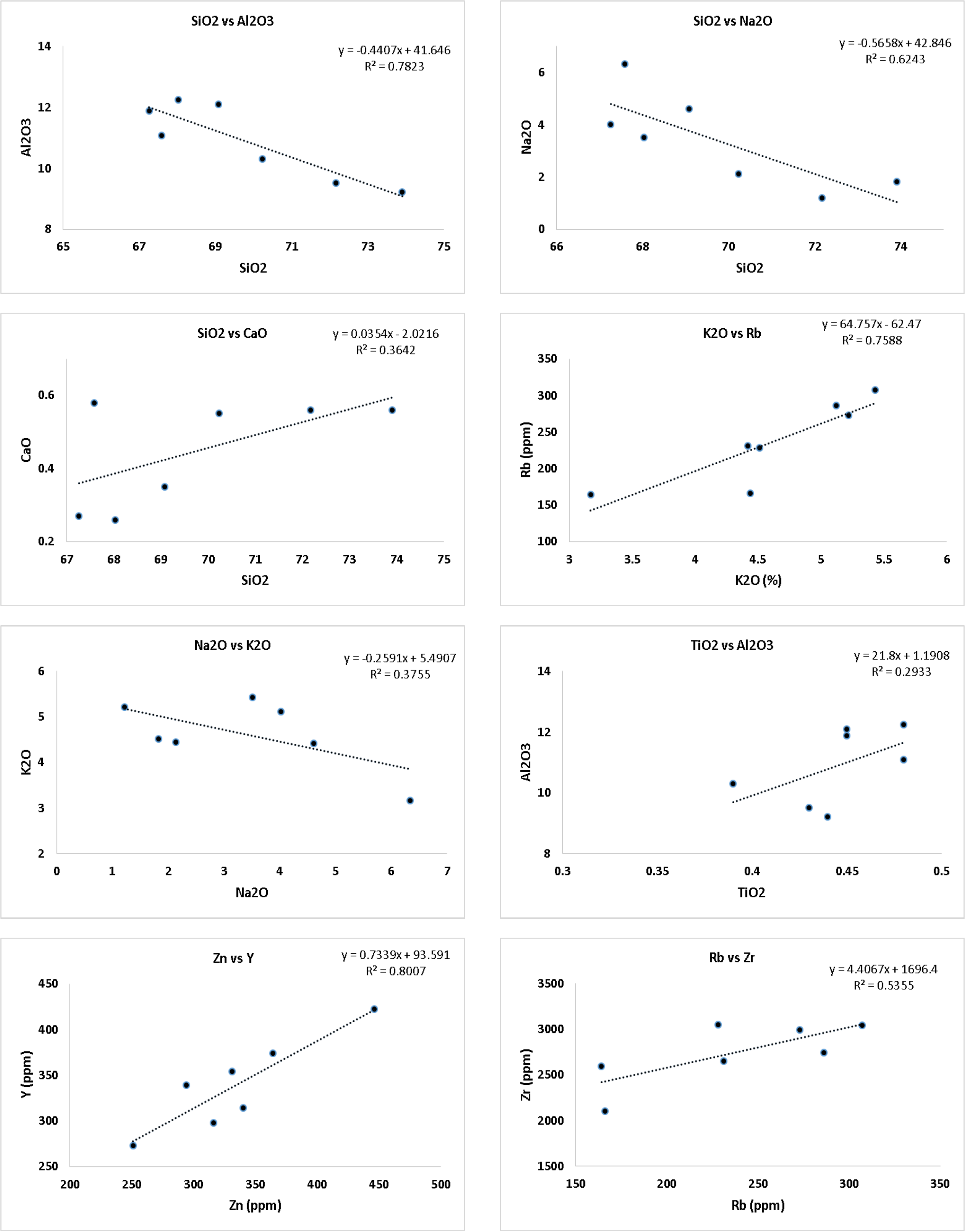

Figure 5. 9 Variation diagrams (Harker type) between major oxides (%) and trace elements (ppm) in Massive rhyolite.

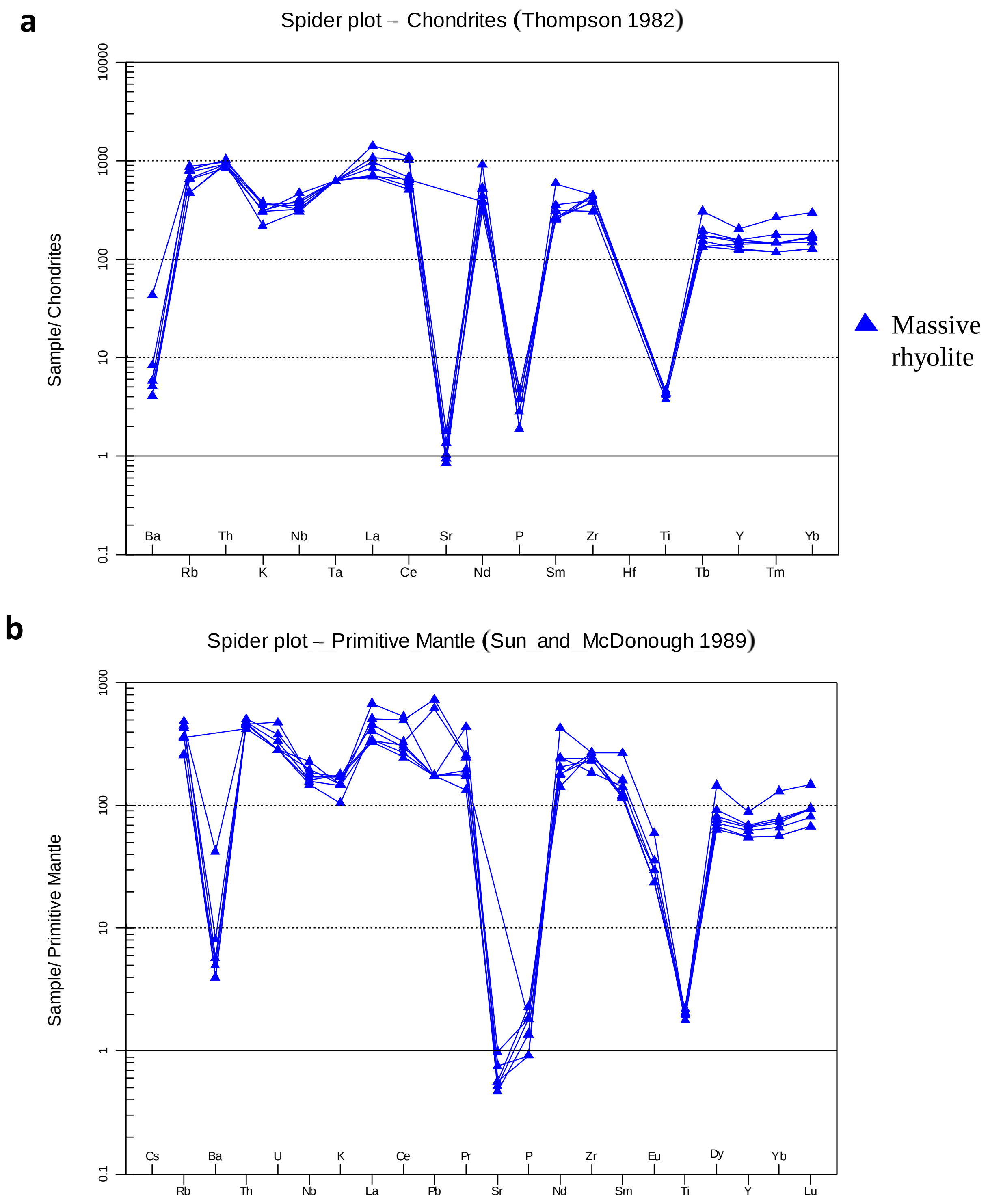

Figure 5. 10 Spider diagram for trace elements in massive rhyolite a) Chondrite normalized (Thompson, 1982); b) Primitive mantle normalized (Sun and Mc Donough 1989)

5.4.2 REE in Massive rhyolite

REE value raw data of (n=7) sample of massive rhyolite has been tabulated in the table. All the samples display uniform REE patterns, parallel to sub-parallel, slightly LREE enriched over HREE. The REE fractionation pattern *(Fig 5.11)* having $(La/Yb)_N$= 4.19-8.43, $(La/Sm)_{N=}$2.47-3.49 and $(Gd/Yb)_N$=1.24-1.47 is almost showing a similar pattern with tuff but a slight higher $(La/Yb)_N$ indicates higher HREE fraction than tuff. Negative Eu anomaly, Eu/Eu*=0.22-0.28 could be attributed to plagioclase fractionation which is also being supported by negative strontium anomaly *(Figure 5.10).* The average TREO of 7 samples is 2271ppm varying from 1744ppm to 3586ppm. The HREO concentration of 659ppm accounts to 29% of TREO

Table 5. 8 Representative analysis of REE in Massive rhyolite

REE in Massive rhyolite							
REE	**BDW 17**	**BDW 18**	**BDW 19**	**BDW 20**	**BDW 24**	**BDW 29**	**BDW 30**
La	226	235	318	350	468	280	230
Ce	438	480	590	888	946	532	552
Pr	37	50	68	71	121	54	48
Nd	193	245	327	335	580	277	240
Sm	51	52	72	63	119	55	53
Eu	5	4	6	5	10	4	4
Gd	59	51	66	49	103	54	57
Tb	9	8	10	7	16	7	9
Dy	57	50	68	47	108	53	60
Ho	12	10	14	10	21	11	12
Er	33	28	38	25	55	32	37
Tm	5	4	6	4	9	5	5
Yb	36	28	39	28	65	33	37
Lu	7	5	7	5	11	6	7
Y	301	254	314	251	407	285	312
$(La/Sm)_N$	2.79	2.84	2.78	3.49	2.47	3.20	2.73
$(La/Yb)_N$	4.23	5.66	5.50	8.43	4.85	5.72	4.19
$(Gd/Yb)_N$	1.32	1.47	1.37	1.41	1.28	1.32	1.24
Eu/Eu*	0.28	0.24	0.27	0.28	0.28	0.22	0.22
TLREO	1106	1242	1609	1997	2613	1402	1314
THREO	638	538	690	525	973	597	658
TREO	1744	1781	2299	2523	3586	1999	1971

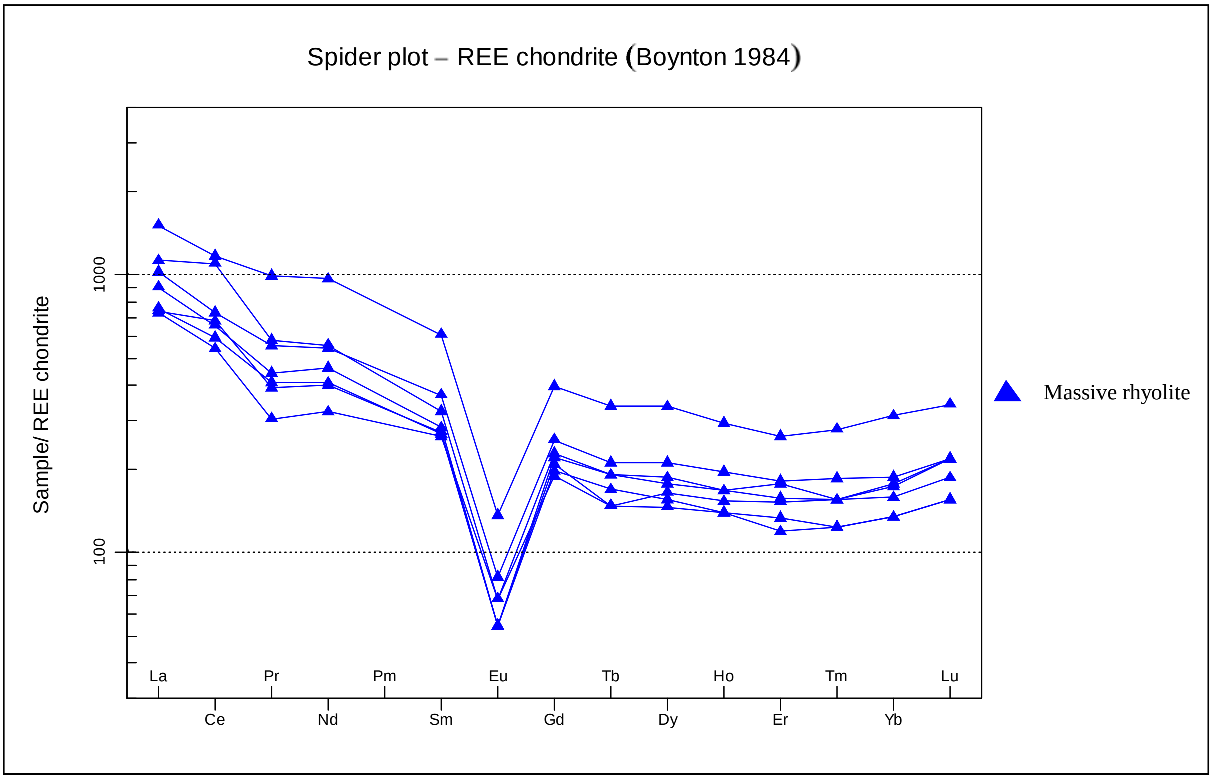

Figure 5. 11 Spider diagram of REE Chondrite normalized after (Boynton,1984) for massive rhyolite

5.5 Geochemical analysis of Agglomerate

The chemical data with major, minor and trace elements of agglomerate are tabulated which in *Table 5.9* depicting the major and trace element while REE data is tabulated in *Table 5.12.*

5.5.1 Major oxide and Trace Elements in Agglomerate

Seven samples (n=6) for Agglomerate have been considered for analyzing geochemistry. These samples are characterized by high concentration of SiO_2, Na_2O, K_2O, Zr, Nb, Y &REE and lower concentration of MgO, Fe_2O_3 (t), CaO, Cr, Ni &Sr. SiO_2 from 62.76 to 72.44%; Al_2O_3 from 7.74 to 13.70; Fe_2O_3(t) from 8.11 to 11.82%; MgO from 0.13 to 0.63%; CaO from 0.28 to 0.61; Na_2O from 2.54 to 4.77%; K_2O from 2.50 to 5.01%; MnO from 0.05 to 0.21; TiO_2 from 0.13 to 0.56% and P_2O_5 values from 0.04 to 0.10%. Among the trace elements U is <10ppm, Th varies from 40 to 102ppm Zn from 134 to 642 ppm; Pb from 17 to 112ppm; Nb from 145 to 290 ppm; Rb from 171 to 389ppm; and Zr in range of 3100 to 7400 ppm (Table 5.10)

Range (maxima- minima), median and standard deviation has been calculated for the major, minor and trace element in agglomerate (n=6). The statistical data is given in *Table 5.10* and its graphical representation given in the bar diagram *(Figure 5.12).*

Table 5. 9 Representative Major Oxide and trace elemental compositions of Agglomerate from Buriwara

	BDW 23	**BDW 28**	**BDW 31**	**BDW 32**	**BDW 33**	**BDW 34**	**BDW 35**
Major oxides (%) in Agglomerate							
SiO_2	70.95	67.31	62.76	69.59	70.63	70.89	72.44
TiO_2	0.26	0.56	0.45	0.22	0.24	0.2	0.13
Al_2O_3	10.4	12.23	13.7	7.74	9.8	9.82	8.46
Fe_2O_3(t)	9.61	8.11	11.14	11.82	9.13	9.8	9.07
MgO	0.13	0.49	0.36	0.63	0.37	0.28	0.39
MnO	0.21	0.14	0.07	0.12	0.05	0.14	0.09
CaO	0.43	0.61	0.28	0.53	0.51	0.58	0.57
Na_2O	3.27	4.77	4.53	2.54	3.34	2.87	2.73
K_2O	2.5	3.06	4.96	3.89	3.75	4.79	5.01
P_2O_5	0.1	0.09	0.06	0.07	0.04	0.04	0.08
Trace elements (ppm) in Agglomerate							
Cr	<10	<10	<10	<10	<10	<10	<10
Ni	<10	<10	14	<10	<10	<10	<10
Cu	<10	<10	<10	37	<10	<10	<10
Zn	196	134	472	160	642	411	373
Ga	24	21	22	16	17	23	14
Rb	171	218	389	213	237	297	328
Sr	11	22	<10	<10	<10	<10	<10
Y	674	244	893	491	762	661	468
Zr	5400	3100	7400	3800	5500	5400	5900
Nb	285	145	NA	226	290	273	250
Pb	82	30	112	40	48	60	17
Ba	<10	129	<10	<10	<10	<10	<10
Ce	1318	851	2355	932	1272	970	369
Th	53	40	102	48	57	40	52
U	<10	<10	<10	<10	<10	<10	<10
Total	98.68	97.87	99.51	97.75	98.75	100.23	99.75

Table 5. 10 Statistical evaluation of major, minor (in %) and trace (in ppm) elements of Agglomerate

Agglomerate (n=7)	Range		Mean	Std dev
	Min	Max		
Major oxide (wt%)				
SiO_2	62.76	72.44	69.22	3.02
TiO_2	0.13	0.56	0.29	0.14
Al_2O_3	7.74	13.70	10.31	1.92
Fe_2O_3(t)	8.11	11.82	9.81	1.18
MgO	0.13	0.63	0.38	0.15
MnO	0.05	0.21	0.12	0.05
CaO	0.28	0.61	0.50	0.11
Na_2O	2.54	4.77	3.44	0.81
K_2O	2.50	5.01	3.99	0.91
P_2O_5	0.04	0.10	0.07	0.02
Trace element (ppm)				
Cr	0.00	0.00		
Ni	14.00	14.00	14.00	0.00
Cu	37.00	37.00	37.00	0.00
Zn	134.00	642.00	341.14	173.34
Ga	14.00	24.00	19.57	3.58
Rb	171.00	389.00	264.71	70.61
Sr	11.00	22.00	16.50	5.50
Y	244.00	893.00	599.00	199.04
Zr	3100.00	7400.00	5214.29	1302.12
Nb	145.00	290.00	244.83	49.66
Pb	17.00	112.00	55.57	30.10
Ba	129.00	129.00	129.00	0.00
Ce	369.00	2355.00	1152.43	570.01
Th	40.00	102.00	56.00	19.70
U	0.00	0.00		

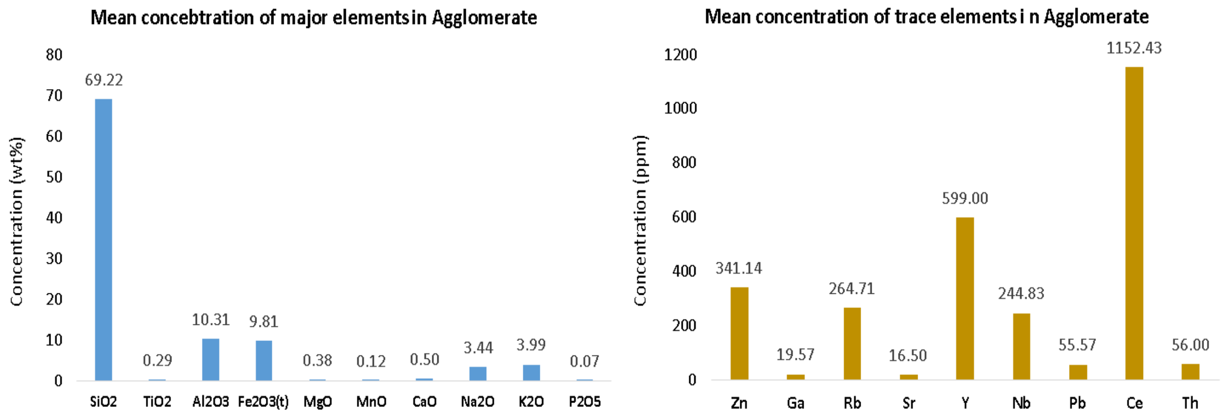

Figure 5. 12 Bar diagram of mean concentration of major, minor and trace element of Agglomerate

In between the different major and trace element of agglomerate the correlation matrix *Table 5.11* has been prepared and those pairs of elements which is showing the strong positive or negative correlation has been plotted in Harker diagram *(Figure 5.13).* Very strong positive correlation has been observed in between Na_2O vs TiO_2; Al_2O_3 vs TiO_2; Al_2O_3 vs Na_2O and K_2O vs Rb, Zr vs Y; Nb vs Y; Zr vs Nb; Pb vs Ce; Pb vs Th; Ce vs Th and Zr vs Rb. Moderate positive correlation between SiO_2 vs CaO; Al_2O_3 vs Pb, Ce, Th; K_2O vs Zr; Y vs Pb, Ce, Th while the very weak positive correlation is observed between Al_2O_3 vs Rb, Zr; Fe_2O_3 vs K_2O, Y, Nb; K_2O vs Y, Nb; and strong negative correlation between SiO_2 vs Al_2O_3, Na_2O, TiO_2, Ce; CaO vs Pb, Ce, Th, Y moderately negative correlation between SiO_2 vs Pb, Th; CaO vs Al_2O_3, Fe_2O_3(t); CaO vs Zr, Nb; K_2O vs P_2O_5 and weak negative correlation between SiO_2 vs Fe_2O_3, Rb is observed.

The spider diagram of trace elements are plotted in order to understand their relative concentration with respect to Chondrite (Chondrite values after Thompson 1982) and Primitive mantle (Primitive mantle values after Sun and Mc. Donough 1989) *(Figure 5.14).* It has been noticed that Ba, Sr, K and Ti shows a negative anomaly which indicates mobility of these elements. Other trace elements like Mo, V, Ni, Co and Ta are also very low in concentration which supports element mobility. This may lead to the conclusion that events like magma

mixing or heterogeneity in magma had been taken place where these elements had escaped from the system.

Table 5. 11 Correlation of geochemical data of major, minor (in %) and trace elements (in ppm) in agglomerate (n=6)

Correlation between different major and trace elements in agglomerate																			
	SiO2	TiO2	Al2O3	Fe2O3(t)	MgO	MnO	CaO	Na2O	K2O	P2O5	Zn	Ga	Rb	Y	Zr	Nb	Pb	Ce	Th
SiO2	1.00																		
TiO2	-0.79	1.00																	
Al2O3	-0.84	0.84	1.00																
Fe2O3(t)	-0.33	-0.19	-0.14	1.00															
MgO	-0.19	0.17	-0.25	0.28	1.00														
MnO	0.27	0.03	-0.06	-0.12	-0.42	1.00													
CaO	0.66	-0.23	-0.56	-0.53	0.32	0.16	1.00												
Na2O	-0.79	0.96	0.93	-0.30	-0.01	-0.09	-0.34	1.00											
K2O	-0.15	-0.30	-0.04	0.32	0.17	-0.63	-0.12	-0.19	1.00										
P2O5	0.04	0.26	0.06	-0.22	-0.08	0.64	0.02	0.19	-0.58	1.00									
Total	0.24	-0.44	-0.04	-0.13	-0.49	-0.11	0.04	-0.27	0.69	-0.41									
Zn	-0.03	-0.26	0.11	-0.03	-0.25	-0.74	-0.28	-0.04	0.52	-0.78	1.00								
Ga	-0.37	0.45	0.63	-0.05	-0.62	0.58	-0.35	0.45	-0.33	0.10	-0.16	1.00							
Rb	-0.45	0.03	0.36	0.22	0.01	-0.61	-0.40	0.19	0.90	-0.42	0.52	-0.09	1.00						
Y	-0.29	-0.18	0.27	0.45	-0.49	-0.31	-0.78	-0.02	0.31	-0.53	0.70	0.29	0.42	1.00					
Zr	-0.27	-0.21	0.31	0.27	-0.52	-0.38	-0.73	0.03	0.57	-0.33	0.68	0.13	0.73	0.84	1.00				
Nb	0.02	-0.48	0.00	0.39	-0.59	-0.22	-0.64	-0.30	0.33	-0.45	0.68	0.15	0.35	0.94	0.85	1.00			
Pb	-0.63	0.29	0.64	0.46	-0.50	0.08	-0.90	0.37	0.04	-0.13	0.23	0.69	0.30	0.80	0.64	0.63	1.00		
Ce	-0.80	0.46	0.73	0.45	-0.25	-0.20	-0.91	0.53	0.07	-0.22	0.34	0.52	0.36	0.77	0.59	0.52	0.93	1.00	
Th	-0.75	0.29	0.61	0.46	-0.12	-0.46	-0.93	0.43	0.38	-0.15	0.43	0.14	0.65	0.71	0.78	0.54	0.75	0.86	1.00

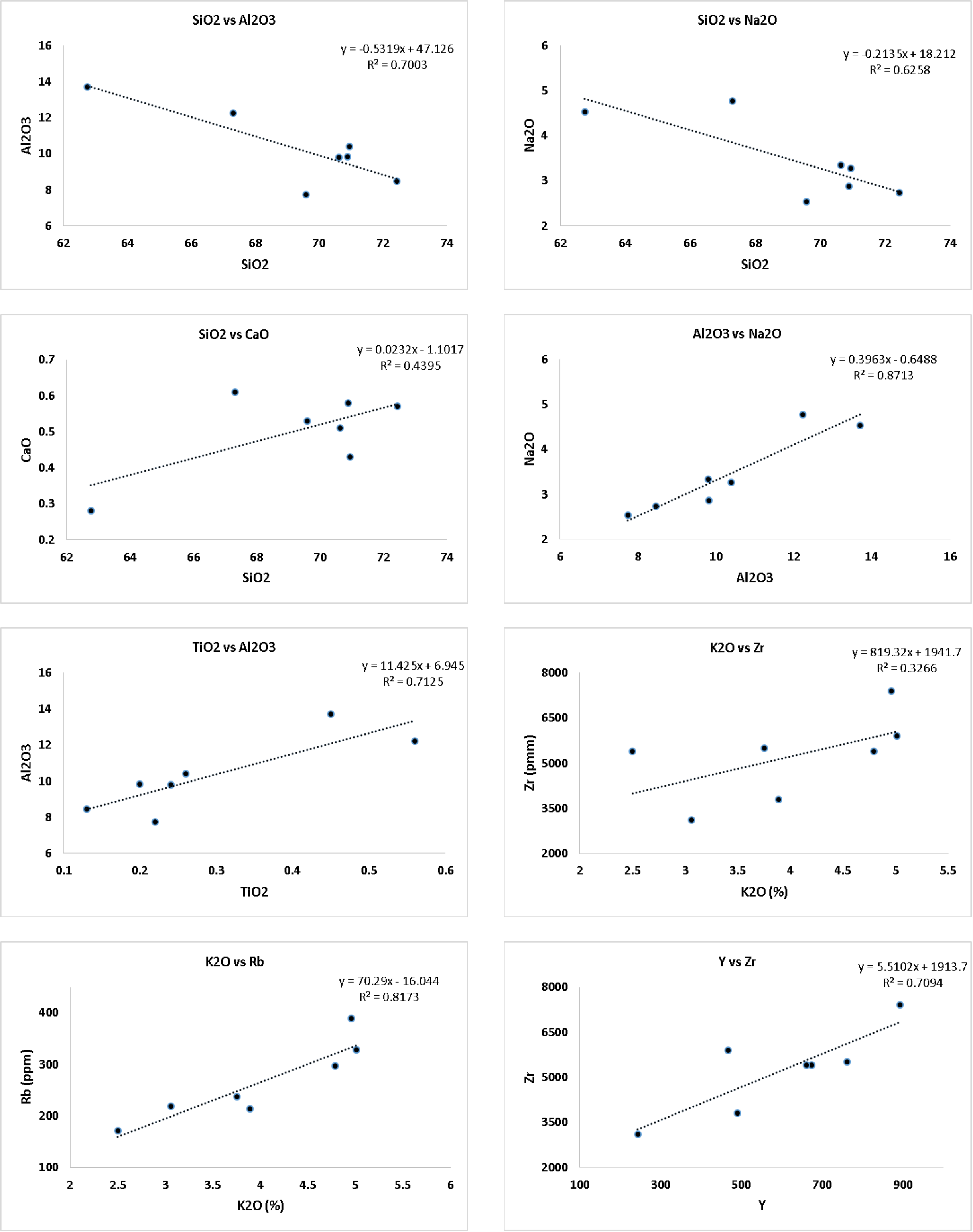

Figure 5. 13 Variation diagrams (Harker type) between major oxides (%) and trace elements (ppm) in agglomerate

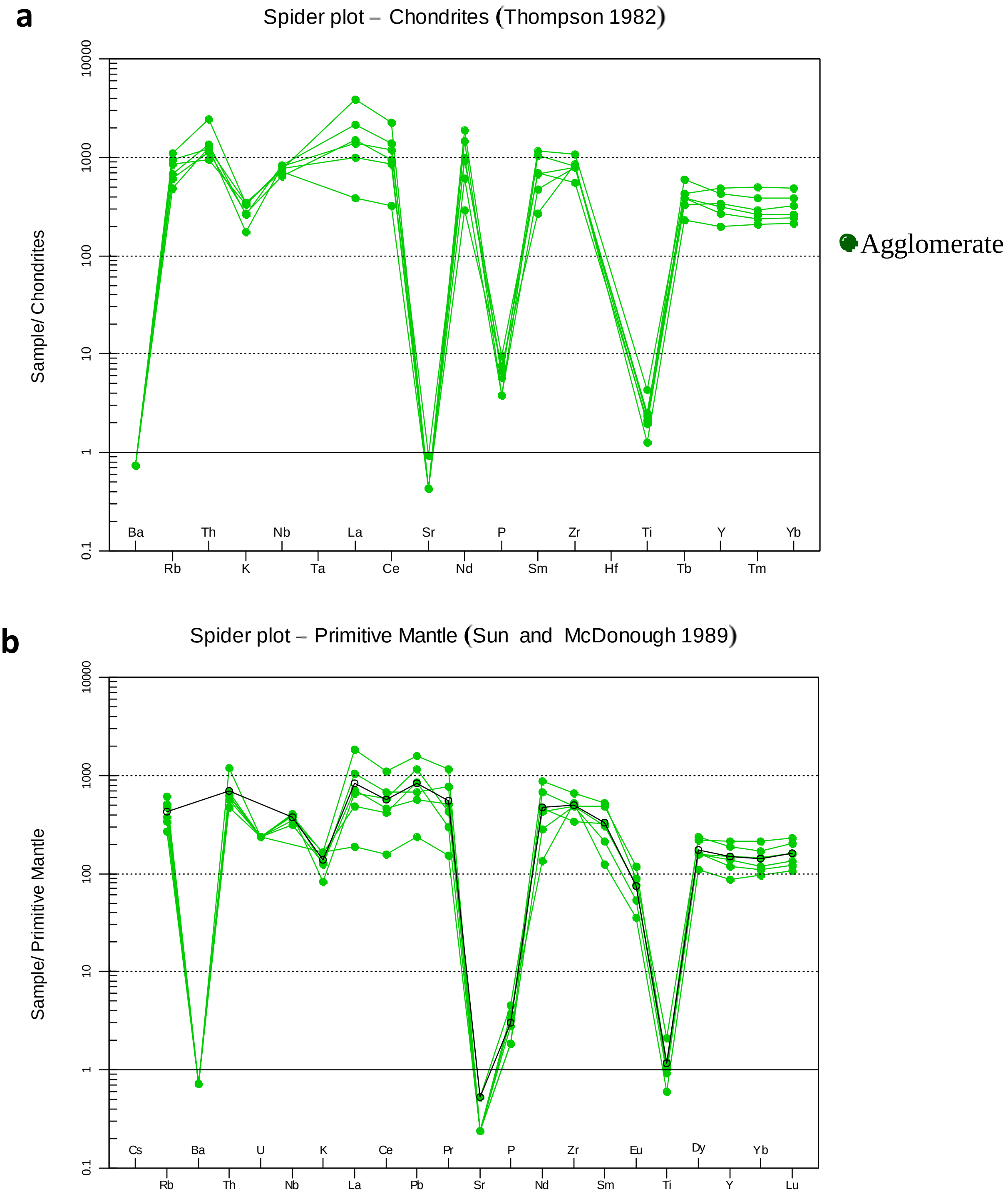

Figure 5. 14 Spider diagram for trace elements in agglomerate a) Chondrite normalized (Thompson, 1982) b) Primitive mantle normalized (Sun and Mc Donough 1989)

5.5.2 REE in Agglomerate

REE value raw data of (n=6) sample of tuff has been tabulated in the *Table 5.12*. All the samples display uniform REE patterns, parallel to sub-parallel, slightly LREE enriched over HREE. The REE fractionation pattern having $(La/Yb)_N$= 1.84-8.17, $(La/Sm)_N$=1.46-3.44 and $(Gd/Yb)_N$=1.13-2.09 shows almost similar but a little higher degree of fractionation than tuff. Negative Eu anomaly, Eu/Eu*=0.23-0.30 could be attributed to plagioclase fractionation which is also being supported by negative strontium anomaly *(Figure 5.14).* The average TREO (total rare earth oxide) of 6 samples is 4360ppm varying from 2000ppm to 7500ppm. The HREO concentration of 1420ppm accounts to 33% of TREO

Table 5. 12 Representative analysis of REE of Agglomerate

REE in Agglomerate (ppm)						
REE	**BDW 23**	**BDW 31**	**BDW 32**	**BDW 33**	**BDW 34**	**BDW 35**
La	455	1285	490	716	331	128
Ce	1037	1942	829	1212	746	281
Pr	117	318	140	211	82	42
Nd	579	1188	622	926	384	184
Sm	137	235	142	215	96	55
Eu	13	15	13	20	9	6
Gd	140	165	133	197	104	66
Tb	20	22	20	31	17	12
Dy	119	163	115	175	116	80
Ho	21	35	23	34	24	15
Er	56	112	70	93	71	45
Tm	8	17	9	13	10	7
Yb	54	106	58	84	71	47
Lu	9	17	10	15	12	8
Y	542	962	630	864	675	392
$(La/Sm)_N$	2.09	3.44	2.17	2.09	2.17	1.46
$(La/Yb)_N$	5.68	8.17	5.70	5.75	3.14	1.84
$(Gd/Yb)_N$	2.09	1.26	1.85	1.89	1.18	1.13
Eu/Eu*	0.29	0.23	0.29	0.30	0.28	0.30
TLREO	2719	5812	2600	3836	1917	807
THREO	1193	1969	1317	1857	1355	826
TREO	3913	7781	3917	5692	3272	1633

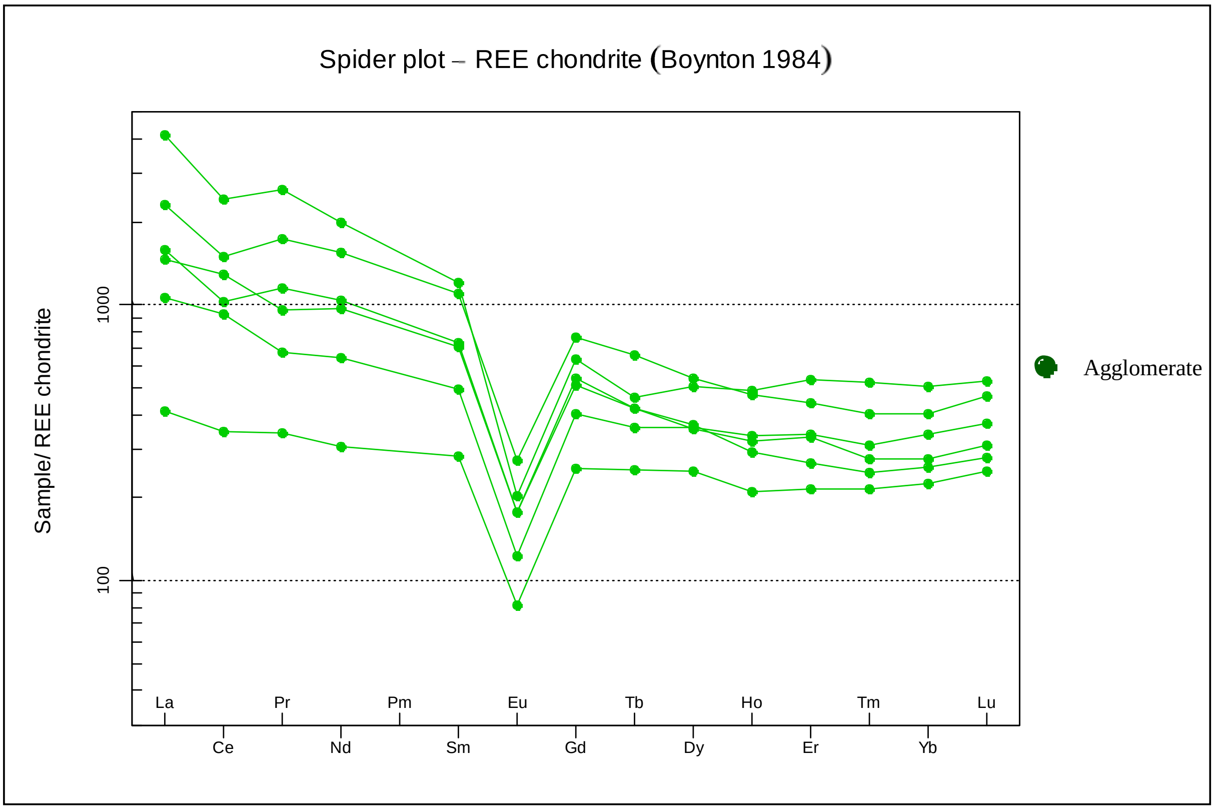

Figure 5. 15 Spider diagram of REE Chondrite normalized after (Boynton,1984) for agglomerate

5.6 Geochemical analysis of Porphyritic Rhyolite

The chemical data with major, minor and trace elements of porphyritic rhyolite are tabulated in *Table 5.13* depicting the major and trace element while analyzed REE data is tabulated in *Table 5.16*.

5.6.1 Major oxide and Trace Elements in Porphyritic Rhyolite

Seven samples (n=7) for porphyritic rhyolite have been considered for analyzing geochemistry. These samples are characterized by high concentration of SiO_2, Na_2O, K_2O, Zr, Nb, Y &REE and lower concentration of MgO, Fe_2O_3 (t), CaO, Cr, Ni &Sr. SiO_2 from 63.36 to 70.65%; Al_2O_3 from 8.93 to13.39%; Fe_2O_3(t) from 6.14 to 13.53%; MgO from 0.10 to 0.41%; CaO from 0.19 to 0.56; Na_2O from 1.79 to 7.24%; K_2O from 1.93 to 5.36%; MnO from 0.04 to 0.28; TiO_2 from 0.26 to 0.47% and P_2O_5 values from 0.04 to 0.96%. Among the trace elements U varies from 6 to 7ppm, Th varies from 23 to 33ppm Zn from 260 to 418 ppm; Pb from 38 to 47ppm; Ba from 32 to 74ppm; Nb from 76 to 151 ppm; Rb from 80 to 267ppm; Cr from 62 to117 and Zr in range of 1125 to 4237 ppm*(Table5.14).*

Range (maxima- minima), median and standard deviation has been calculated for the major, minor and trace element in porphyritic rhyolite (n=7). The statistical data is given in *Table 5.14* and its graphical representation given in the bar diagram *(Figure 5.16).*

Table 5. 13 Representative Major Oxide and trace elemental compositions of Porphyritic rhyolite from Buriwara

	BDW 21	BDW 22	BDW 25	BDW 26	BDW 27	BDW 36	BDW 37
Major oxides (wt%) of Porphyritic rhyolite							
SiO_2	69.86	66.29	69.2	70.65	63.36	70.44	68.99
TiO_2	0.39	0.4	0.46	0.29	0.47	0.26	0.43
Al_2O_3	12.29	9.75	11.44	9.88	13.39	8.93	10.69
Fe_2O_3(t)	6.14	13.53	7.9	8.87	10.58	10.03	8.86
MgO	0.28	0.28	0.17	0.41	0.14	0.19	0.1
MnO	0.04	0.23	0.13	0.14	0.19	0.09	0.28
CaO	0.19	0.53	0.45	0.51	0.3	0.56	0.33
Na_2O	1.79	3.85	2.86	3.53	7.24	2.72	4.07
K_2O	5.32	4.72	5.36	3.68	1.93	4.5	4.19
P_2O_5	0.04	0.08	0.07	0.96	0.04	0.47	0.08
Trace elements (ppm) of porphyritic rhyolite							
Cr	87	113	117	62	79	<10	<10
Ni	<10	<10	<10	<10	<10	<10	<10
Cu	5	<5	<5	<5	<5	<10	<10
Zn	260	382	376	385	388	418	298
Ga	20	16	21	24	29	20	21
Rb	267	215	202	170	80	237	216
Sr	11	11	19	12	<10	<10	15
Y	179	246	352	390	279	414	454
Zr	1125	2676	2743	4237	2366	2832	2352
Nb	76	119	114	145	114	151	102
Pb	<25	<25	<25	<25	<25	38	47
Ba	44	74	57	67	32	37	38
Ce	507	1040	644	1114	746	414	729
Th	24	23	25	28	29	33	32
U	<5	<5	6	7	<5	<10	<10
Total	96.60	100.15	98.51	99.59	98.06	98.65	98.45

Table 5. 14 Statistical evaluation of major, minor (in %) and trace (in ppm) elements of Porphyritic rhyolite

Porphyritic rhyolite (n=7)	**Range**		**Mean**	**Std dev**
	Min	**Max**		
Major oxide (wt%)				
SiO_2	63.36	70.65	68.40	2.46
TiO_2	0.26	0.47	0.39	0.08
Al_2O_3	8.93	13.39	10.91	1.45
Fe_2O_3(t)	6.14	13.53	9.42	2.15
MgO	0.10	0.41	0.22	0.10
MnO	0.04	0.28	0.16	0.08
CaO	0.19	0.56	0.41	0.13
Na_2O	1.79	7.24	3.72	1.60
K_2O	1.93	5.36	4.24	1.09
P_2O_5	0.04	0.96	0.25	0.32
Trace element (ppm)				
Cr	62.00	117.00	91.60	20.78
Ni	0.00	0.00		
Cu	5.00	5.00	5.00	0.00
Zn	260.00	418.00	358.14	52.55
Ga	16.00	29.00	21.57	3.74
Rb	80.00	267.00	198.14	55.57
Sr	11.00	19.00	13.60	3.07
Y	179.00	454.00	330.57	91.79
Zr	1125.00	4237.00	2618.71	849.31
Nb	76.00	151.00	117.29	23.51
Pb	38.00	47.00	42.50	4.50
Ba	32.00	74.00	49.86	15.06
Ce	414.00	1114.00	742.00	238.98
Th	23.00	33.00	27.71	3.61
U	6.00	7.00	6.50	0.50

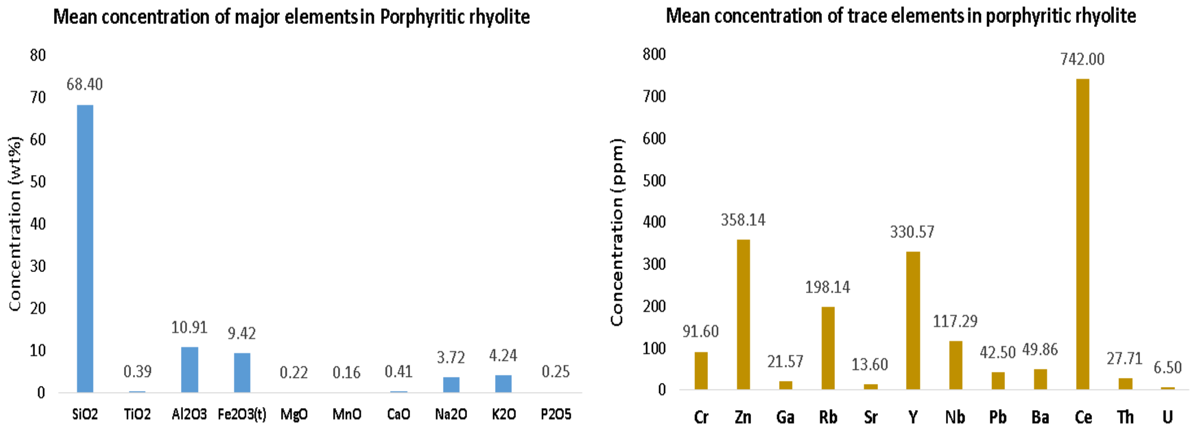

Figure 5. 16 Bar diagram of mean concentration of major, minor and trace element of porphyritic rhyolite

In between the different major and trace element of tuff the correlation matrix *Table 5.15* has been prepared and those pairs of elements which is showing the strong positive or negative correlation has been plotted in Harker diagram *(Figure 5.17).* Very strong positive correlation has been observed in between CaO vs Zn, Nb; K_2O vs Rb; Zn vs Nb. Moderate positive correlation between SiO_2 vs K_2O, Rb; TiO_2 vs Al_2O_3; Fe_2O_3 vs CaO, Zn; CaO vs Zr, Ba and Y vs Zr,Nb,Th; and strong negative correlation between SiO_2vsNa_2O; Al_2O_3 vs CaO; Na_2O vs K_2O, Rb; while moderately negative correlation between TiO_2 vs Nb; SiO_2 vs TiO_2, Al_2O_3, Fe_2O_3(t); TiO_2 vs CaO, Nb; Al_2O_3 vs Y, Zr, Nb; Ba vs Th is observed.

The spider diagram of trace elements are plotted in order to understand their relative concentration with respect to Chondrite (Chondrite values after Thompson 1982) and Primitive mantle (Primitive mantle values after Sun and Mc. Donough 1989) *(Figure 5.18).* It has been noticed that Ba, Sr, K and Ti shows a negative anomaly which indicates mobility of these elements. Other trace elements like Mo, V, Ni, Co and Ta are also very low in concentration which supports element mobility. This may lead to the conclusion that events like magma mixing or heterogeneity in magma had been taken place where these elements had escaped from the system.

Table 5. 15 Correlation matrix of geochemical data of major, minor (in %) and trace elements (in ppm) of porphyritic rhyolite (n=7)

Correlation of different major and minor elements in porphyritic rhyolite																					
	SiO2	TiO2	Al2O3	Fe2O3(t)	MgO	MnO	CaO	Na2O	K2O	P2O5	Cr	Zn	Ga	Rb	Sr	Y	Zr	Nb	Ba	Ce	Th
SiO2	1.00																				
TiO2	-0.64	1.00																			
Al2O3	-0.57	0.75	1.00																		
Fe2O3(t)	-0.56	-0.02	-0.36	1.00																	
MgO	0.37	-0.56	-0.32	-0.02	1.00																
MnO	-0.47	0.42	-0.07	0.58	-0.38	1.00															
CaO	0.22	-0.55	-0.83	0.57	0.28	0.12	1.00														
Na2O	-0.86	0.46	0.46	0.48	-0.36	0.57	-0.12	1.00													
K2O	0.66	-0.14	-0.37	-0.33	0.15	-0.36	0.11	-0.92	1.00												
P2O5	0.52	-0.81	-0.56	-0.03	0.68	-0.22	0.55	-0.17	-0.14	1.00											
Cr	-0.36	0.49	0.39	0.10	0.29	-0.14	-0.07	0.01	0.20	-0.32	1.00										
Zn	-0.20	-0.32	-0.40	0.61	0.08	0.07	0.81	0.33	-0.35	0.42	0.02	1.00									
Ga	-0.41	0.22	0.61	-0.18	-0.16	0.02	-0.33	0.71	-0.84	0.15	-0.11	0.17	1.00								
Rb	0.72	-0.36	-0.47	-0.32	0.15	-0.36	0.03	-0.92	0.90	-0.06	-0.14	-0.46	-0.84	1.00							
Sr	0.30	0.43	0.04	-0.37	-0.22	0.18	0.01	-0.29	0.48	-0.19	0.26	-0.20	-0.19	0.18	1.00						
Y	0.39	-0.32	-0.52	0.00	-0.27	0.36	0.46	0.03	-0.11	0.45	-0.71	0.32	0.11	-0.05	0.31	1.00					
Zr	0.20	-0.47	-0.55	0.32	0.45	0.20	0.76	0.13	-0.26	0.82	-0.12	0.69	0.17	-0.34	0.08	0.58	1.00				
Nb	0.18	-0.66	-0.67	0.45	0.26	0.03	0.88	0.10	-0.25	0.74	-0.32	0.88	0.09	-0.24	-0.22	0.58	0.85	1.00			
Ba	0.16	-0.15	-0.43	0.34	0.70	0.10	0.53	-0.29	0.37	0.32	0.57	0.21	-0.49	0.16	0.25	-0.17	0.49	0.22	1.00		
Ce	-0.22	0.01	-0.18	0.49	0.55	0.52	0.34	0.31	-0.29	0.39	0.32	0.22	0.04	-0.38	0.03	0.01	0.63	0.25	0.74	1.00	
Th	0.16	-0.36	-0.26	-0.02	-0.44	0.19	0.15	0.24	-0.41	0.30	-0.93	0.23	0.35	-0.16	-0.21	0.79	0.24	0.46	-0.65	-0.32	1.00

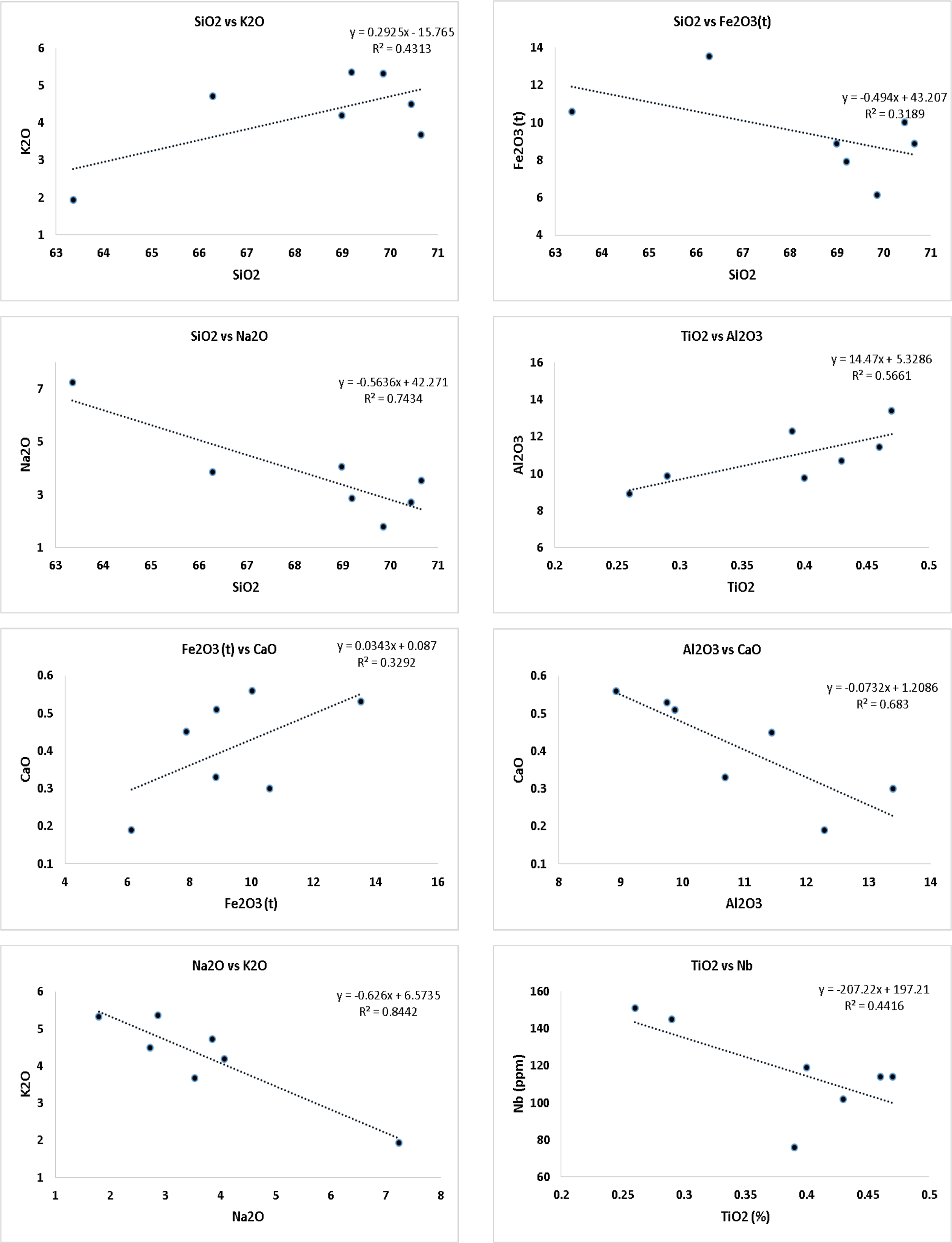

Figure 5. 17 Variation diagrams (Harker type) between major, minor oxides (in %) and trace (ppm) for porphyritic rhyolite

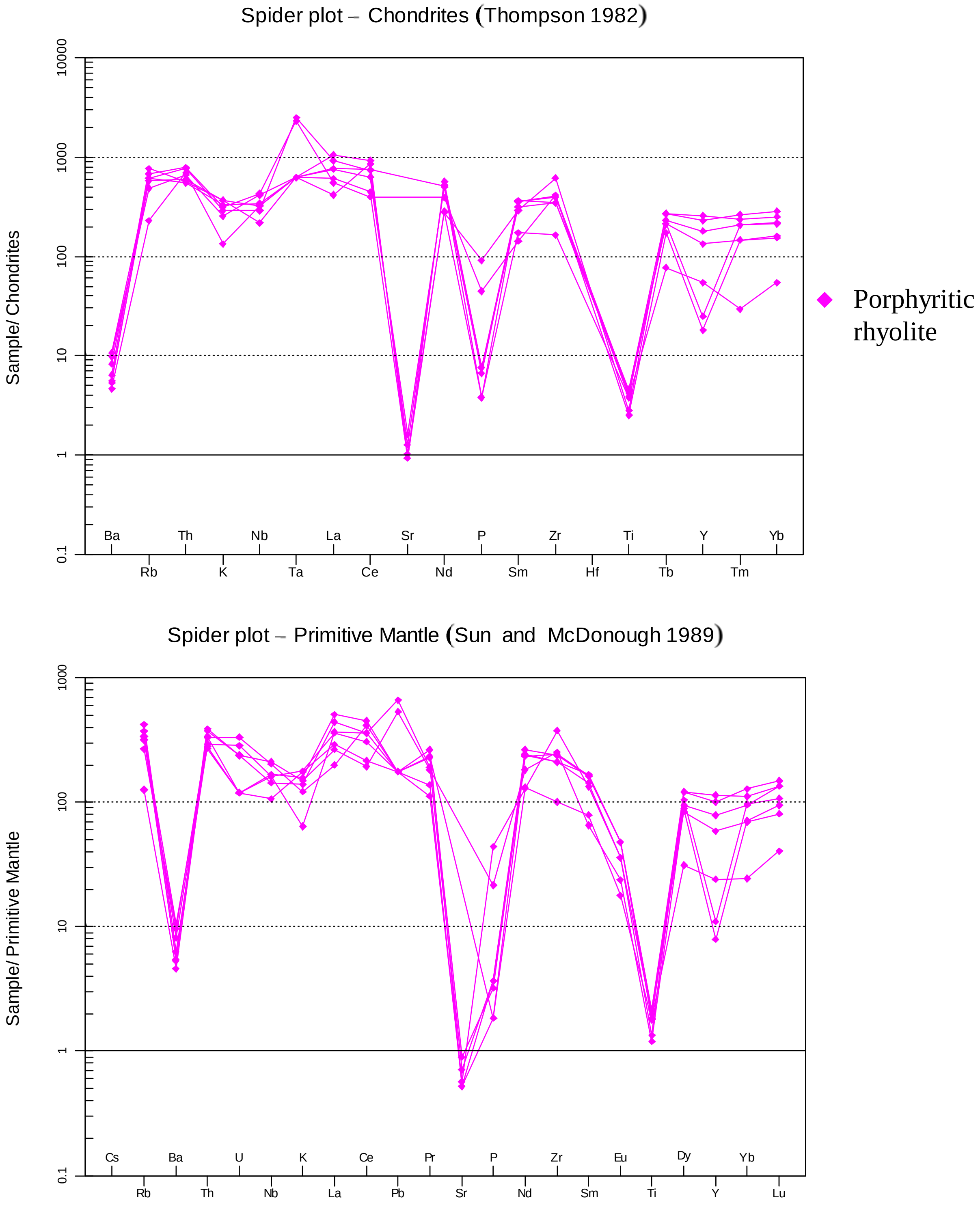

Figure 5. 18 Spider diagram for trace elements in porphyritic rhyolite a) Chondrite normalized (Thompson, 1982) b) Primitive mantle normalized (Sun and Mc Donough 1989)

5.6.2 REE in Porphyritic rhyolite

REE raw data of (n=7) sample of porphyritic rhyolite has been tabulated in *Table 5.16*. All the samples display uniform REE patterns, parallel to sub-parallel, slightly LREE enriched over HREE. The REE fractionation pattern *(Figure 5.19)* having $(La/Yb)_N$= 1.68-5.02, $(La/Sm)_N$=1.46-3.95 and $(Gd/Yb)_N$=1.04-2.15 is almost showing a similar pattern with massive rhyolite but a slight lower $(La/Yb)_N$ indicates lesser HREE fractionation than massive rhyolite. Negative Eu anomaly, Eu/Eu*=0.26-0.34 could be attributed to plagioclase fractionation which is also being supported by negative strontium anomaly *(Figure 5.18)*. The average TREO of 7 samples is 2042ppm varying from 1226ppm to 2700ppm, of which 30%, i.e. 625ppm is HREO.

Table 5. 16 Representative analysis of REE in Porphyritic rhyolite

REE in Porphyritic rhyolite							
REE	**BDW 21**	**BDW 22**	**BDW 25**	**BDW 26**	**BDW 27**	**BDW 36**	**BDW 37**
La	200	347	248	137	253	182	303
Ce	385	800	545	738	644	345	638
Pr	38	73	63	31	65	50	53
Nd	179	358	318	175	325	247	329
Sm	35	72	73	59	74	29	64
Eu	3	8	8	6	8	4	6
Gd	32	70	81	84	69	52	73
Tb	4	12	14	14	11	9	11
Dy	23	70	90	89	62	66	77
Ho	4	15	20	18	12	12	16
Er	12	43	59	53	32	36	54
Tm	1	7	9	8	5	5	7
Yb	12	47	63	55	34	35	48
Lu	3	10	11	10	6	7	8
Y	109	358	458	517	267	-	-
$(La/Sm)_N$	3.59	3.03	2.14	1.46	2.15	3.95	2.98
$(La/Yb)_N$	11.24	4.98	2.65	1.68	5.02	3.51	4.26
$(Gd/Yb)_N$	2.15	1.20	1.04	1.23	1.64	1.20	1.23
Eu/Eu*	0.27	0.34	0.32	0.26	0.34	0.31	0.27
TLREO	979	1930	1459	1334	1592	998	1623
THREO	246	778	989	1043	613	305	407
TREO	1226	2708	2447	2377	2205	1303	2030

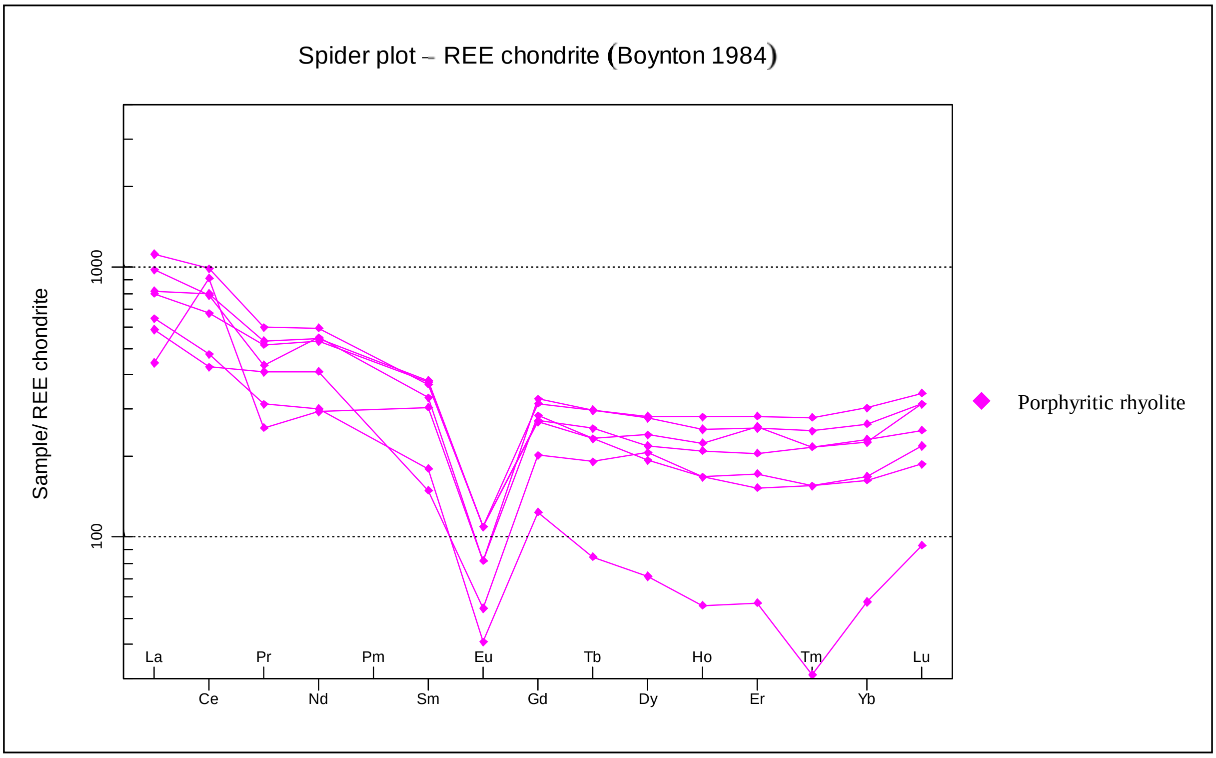

Figure 5. 19 Spider diagram of REE Chondrite normalized after (Boynton,1984) for porphyritic rhyolite

5.7 Alteration studies

From megascopic as well as petrographic study, intense ferrugenisation is observed in tuff which is due to post magmatic hydrothermal alteration. Detailed alteration studies in such a fine grained rock is very difficult. So, the elemental analysis plots and their relative concentration study is adopted in order to decipher the alteration characteristics. The ternary diagram with end members Al_2O_3, $CaO+Na_2O$ and K_2O (Nesbitt and Young 1984, 1989) has been used where alteration trends towards common alteration mineral assemblages viz. K-feldspar, muscovite, illite and kaolinite in hydrothermally altered plutonic rocks and their corresponding volcanic rocks could be studied *(Figure 5.20).* It has been observed that agglomerate and rhyolite samples plot and clustered nearly at average rhyolite whereas the tuff samples are seen to be following a trend towards illite and muscovite which are hydrous mineral phases. Thus, the alteration process involved removal of alkali elements Na and K with influx of acidic fluid in the system. Thus, evidence of sericitisation alongwith ferrugenisation of tuff could also be understood from the plot.

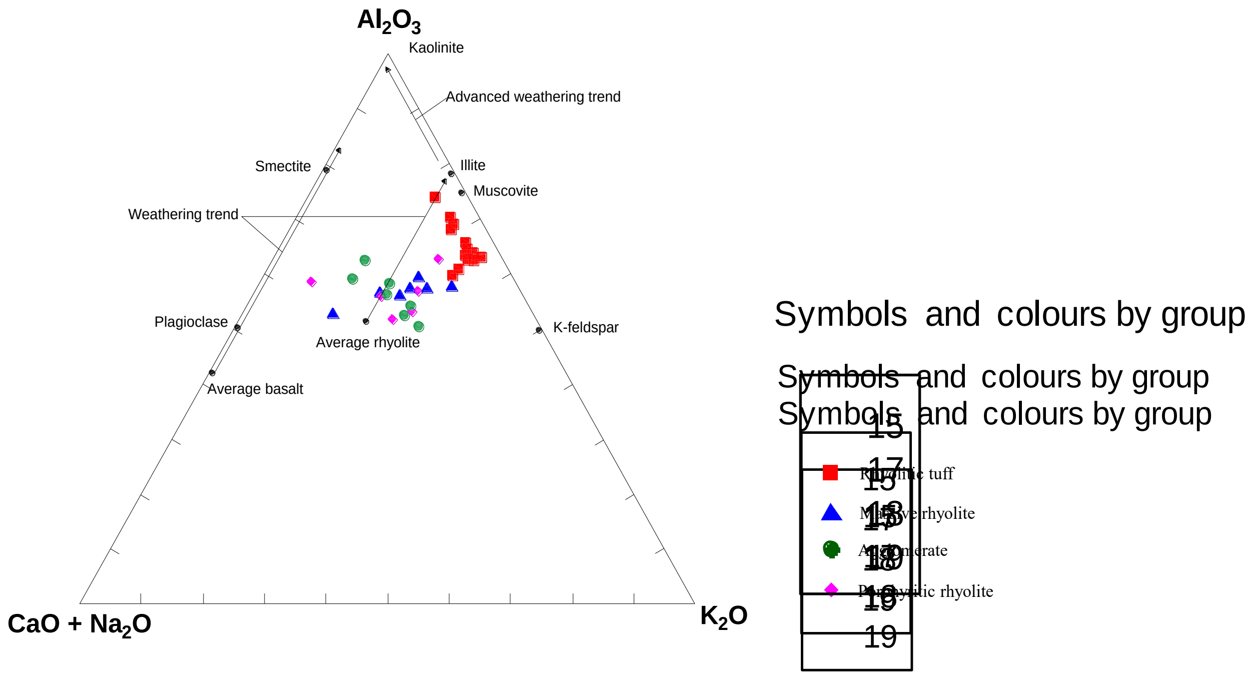

Figure 5. 20 (Na_2O+Cao)-Al_2O_3-CaO diagram of Nesbitt and Young (1984, 1989) showing alteration trends for average rhyolite and average basalt

5.7.1 Elemental behaviour during alteration

SiO_2 vs Na_2O: In the SiO_2 vs Na_2O plot, Na_2O is showing negative correlation with SiO_2. This indicates depletion of Na concentration with successive evolution of magma. But in case of the altered tuff, significant change is noticed and Na_2O is highly depleted and almost flattened with respect to silica. This clearly implies that Na was mobile and have escaped from the system during hydrothermal event *(Figure 5.21a).*

Al_2O_3 vs TiO_2: Al and Ti are immobile during low temperature hydrothermal alteration. Therefore, it has been observed that the Al_2O_3 and TiO_2 are having a positive correlation irrespective of the altered tuff or unaltered rhyolite and agglomerate. As the tuff is silica enriched and more evolved, it is having a relatively lower concentration of Al_2O_3 as compared to rhyolites, but the ratio of TiO_2 remains invariably same with Al_2O_3 concentration. This also concludes that both Al_2O_3 and TiO_2 behaved in a similar manner during magma fractionation process *(Figure 5.21b).*

Zr vs Nb: Zr and Nb are well known as resistive minerals that are normally unaffected by low temperature hydrothermal alterations. It is observed that both are positively correlated and their ratio also remains constant in all the lithotypes. This clearly suggest that Zr and Nb in all cases behaved in geochemically similar fashion. It has been noticed that the tuff and agglomerate samples are showing elevated Nb and Zr values, with tuff samples being higher in Zr. Thus, subsequent hydrothermal process possibly added Zr in the tuff and Zr was significantly mobile during alteration process *(Figure 5.21c).*

Y vs Nb: Y and Nb also behave in a similar geochemical manner during the evolution of rocks. The tuff samples are forming clusters while in rhyolites and agglomerate a positive correlation is seen. This implicates that there might be a minor affect on Y concentration during alteration event but overall concentration of Y and Nb in tuff and agglomerate is higher which could be potential for REE exploration *(Figure 5.21d).*

U vs Th: The U and Th concentration varies extremely for altered and unaltered rocks. In the altered tuff, U ranges from 20-50ppm, Th ranges from 72-104ppm. Whereas, in rhyolite U and Th are below 10ppm (most of them are below detection limit) and 40ppm respectively. In agglomerate, Th ranges from 40 to 100ppm, but concentration of U is <10ppm. It might be so that the tuff are having higher intrinsic U and Th, for which U/Th ratios has been checked. It is observed that the altered tuff are having higher U/Th ratio ranging from 0.20-0.58 whereas in unaltered rhyolite and agglomerate U/Th ratio is smaller and ranges from 0.10-0.20. U/Th plot of tuff are also forming a scatter which suggest that alteration has affected their concentration. U behaved as mobile element and were variably concentrated in altered rocks during post-magmatic hydrothermal alteration resulting in higher U content and U/Th ratio. Again, the samples show high Fe_2O_3 (4.5-11.26%), whereas FeO content is comparatively less (0.2-1.06%). This might indicate that uranium was transported as U^{+6} in oxidizing solutions and precipitated through oxidation of the reduced species of Fe (Fe^{+2}). The U might be present in adsorbed form in ferrugenised matrix as no radioactive phase was identified during petrographic study. Taking into consideration of all the factors, the alteration plays a role in the mobility of U where Th remained relatively immobile *(Figure 5.21e)*.

Table 5. 17 U and Th ratio of rhyolitic tuff samples from Buriwara

Sample no	Rock type	U (ppm)	Th (ppm)	U/Th ratio
BDW 1	Rhyolitic tuff	25	104	0.24
BDW 2	Rhyolitic tuff	26	98	0.27
BDW 3	Rhyolitic tuff	31	90	0.34
BDW 4	Rhyolitic tuff	30	80	0.38
BDW 5	Rhyolitic tuff	50	86	0.58
BDW 6	Rhyolitic tuff	25	90	0.28
BDW 7	Rhyolitic tuff	32	96	0.33
BDW 8	Rhyolitic tuff	25	94	0.27
BDW 9	Rhyolitic tuff	22	88	0.25
BDW 10	Rhyolitic tuff	20	100	0.20
BDW 11	Rhyolitic tuff	40	72	0.56
BDW 12	Rhyolitic tuff	30	80	0.38
BDW 13	Rhyolitic tuff	43	84	0.51
BDW 14	Rhyolitic tuff	25	58	0.43
BDW 15	Rhyolitic tuff	31	76	0.41
BDW 16	Rhyolitic tuff	34	92	0.37

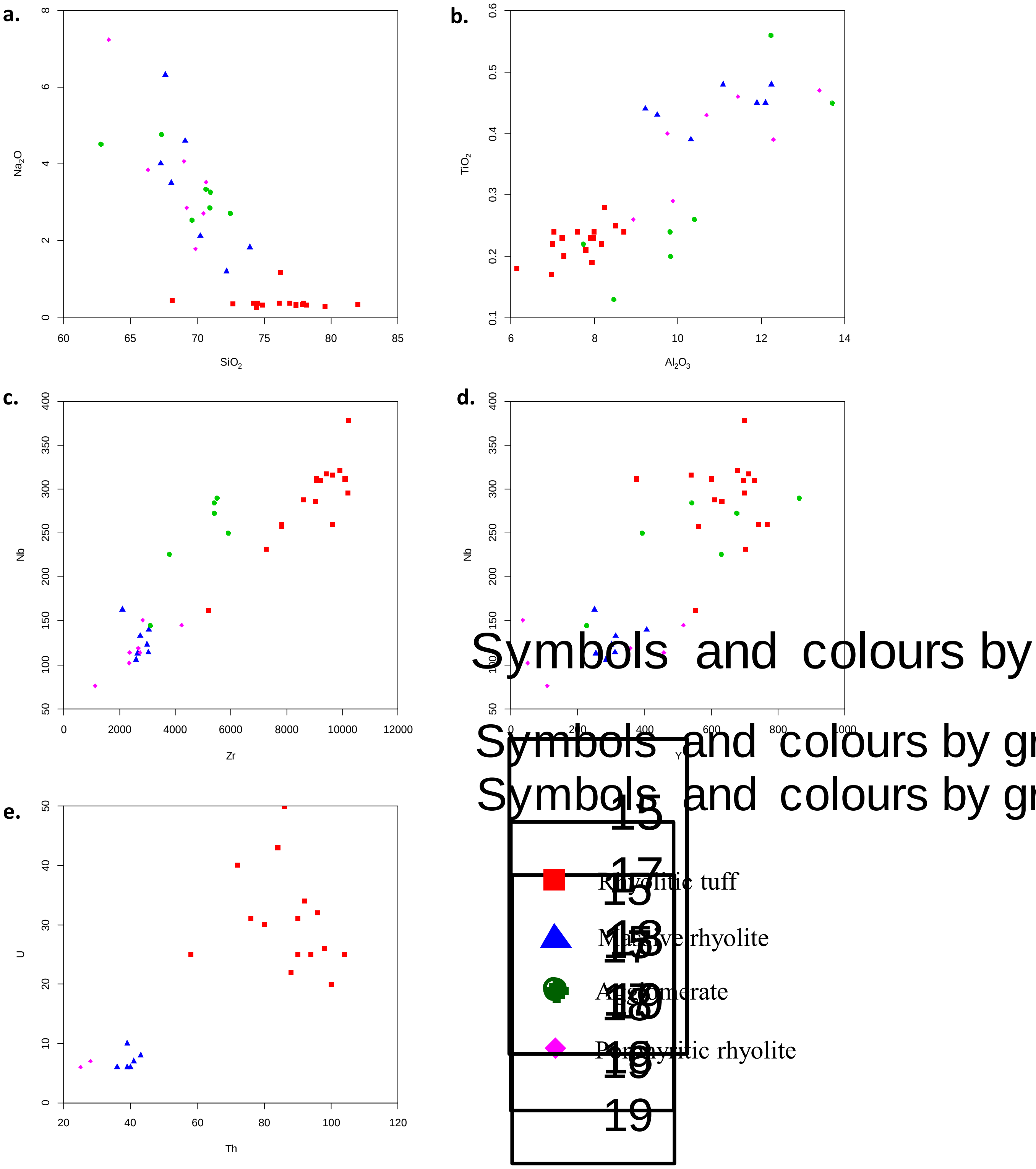

Figure 5. 21 Bivariate plots of major oxide and trace element behavior for altered and unaltered rocks

CHAPTER 6

RARE EARTH ELEMENT (REE) MINERALISATION

Representative samples collected from all the lithotypes were analyzed for REE in chemical laboratory which were discussed in previous sections for individual lithotypes. Potential REE mineralisation is hosted in the tuff and agglomerate in Buriwara. A comparative analysis of the average values of REO from Tuff, Agglomerate, Massive rhyolite and Porphyritic rhyolite is as follows:

Table 6. 1 Average REO concentration in different lithotypes of Buriwara

Rocktype	**Tuff (n=16)**	**Agglomerate (n=6)**	**Massive rhyolite (n=7)**	**Porphyritic rhyolite (n=7)**
Average REO (ppm)	3200	4360	2270	2040

The chondrite normalized plot for the average REE from all the lithotypes is showing similar fractionation pattern which concludes that they are genetically correlated and are enriched in HREE *(Figure 6.1)*. It is observed that the agglomerate is having an elevated concentration of REE followed by tuff. This gives a clear indication that REE mineralisation in Buriwara is mainly associated with pyroclastic host. The tuff is composed of homogeneous rhyolitic pyroclast and is masked by ferrugenised matrix. It is rich in intrinsic REE with further enrichment after hydrothermal event. Previous R&D work reported REE minerals like bastnaesite and monazite in tuff samples from Buriwara (Upadhyay and Banerjee, 2011). The agglomerate consists of angular pyroclastic fragments of rhyolite binded within silicious matrix. The REE enrichment is supposed to be in the matrix part as petrographic studies revealed that the rhyolite fragments is similar to that of the surrounding rhyolite. Along with REE, Nb enrichment is also associated with these two lithotypes. Thus, the pyroclastic formations of Buriwara, viz. tuff and the agglomerate together could be a promising host rock for Rare Metal and Rare Earth exploration, especially for HREE like Dy which ranges from 116-175 ppm in agglomerate.

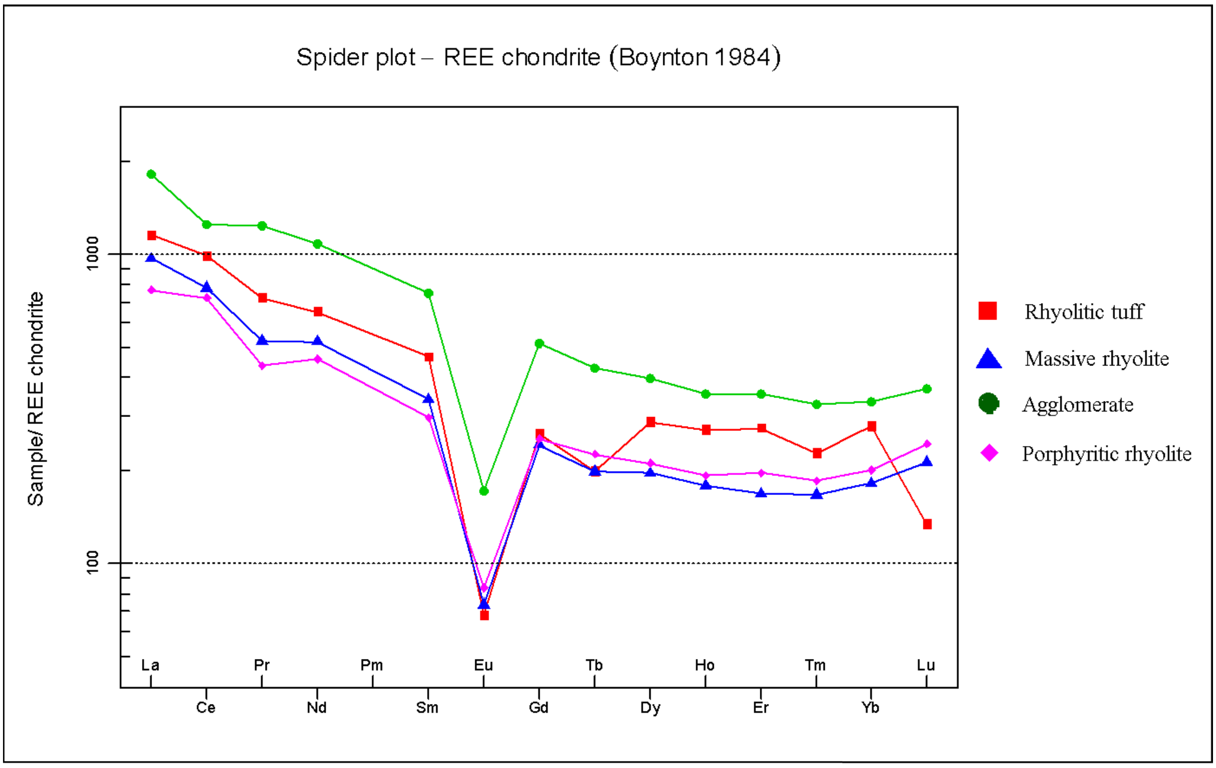

Figure 6. 1 Chondrite normalized plot (Boynton, 1984) for average REE from different lithotypes from Buriwara

CHAPTER 7

RADIOACTIVE ANOMALIES

7.1 Radioactive anomaly in rhyolitic tuff

Detailed radiometric survey has indicated anomalous radioactivity in the ferrugenised rhyolitic tuff which is exposed towards eastern part for an area of nearly 1 sq km as well as in two small isolated hillocks towards north. Consistent radioactivity of the order 2-3 times of background was encountered. The samples analysed eU_3O_8 from 73-94 ppm and ThO_2 from 102-126 ppm *(Table7.1)*. U is enriched by hydrothermal activity and adsorbed on hematite & hydrous Fe Oxide (Upadhyay and Banerjee, 2011)

7.2 Radioactive anomaly in agglomerate

Detailed radiometric survey has indicated anomalous radioactivity in the agglomerate which is exposed as thin outcrop of 5-10 m width for a distance of nearly 1.5 km trending N-S and separating the massive and porphyritic rhyolite. Consistent radioactivity of the order 2-3 times of background was encountered. The samples analysed eU_3O_8 from 49-55 ppm and ThO_2 from 66-76 ppm *(Table7.1)*.

Table 7. 1 Physical assay result of radioactive tuff and agglomerate samples from Buriwara

Sample Name	**Lithotype**	**eU_3O_8**	**ThO_2**	**Ra(eU_3O_8)**	**K**
		ppm			**%**
BDW-1	Rhyolitic Tuff	74	102	20	2.7
BDW-2		77	113	16	3.2
BDW-4		73	108	17	3.3
BDW-5		94	113	36	3.3
BDW-6		92	122	27	4.5
BDW-7		93	126	31	3.4
BDW-9		83	123	22	3.3
BDW-12		78	107	21	3.3
BDW-13		89	116	30	3.3
BDW-16		81	111	22	3.4

Sample Name	**Lithotype**	**eU_3O_8**	**ThO_2**	**Ra(eU_3O_8)**	**K**
		ppm			**%**
BDW-23	Agglomerate	49	66	11	2.6
BDW-32		50	67	11	3.6
BDW-33		55	76	12	3.1
BDW-34		54	69	13	3.9

7.3 Anomalous concentration of High Field Strength (HFS) elements in Tuff and Agglomerate

Both the tuff and agglomerate are enriched in HFS elements like Y, Zr, Nb and Ce which is a good indication of potential Rare Metal (RM) and Rare Earth Element(REE) mineralisation. Tuff samples (n=16) analyzed Y (upto 768 ppm), Zr (upto 10220 ppm), Nb (upto 378 ppm) and Ce (upto 1498 ppm) whereas the agglomerate samples (n=6) analysed Y (upto 962 ppm), Zr (upto 7400 ppm), Nb (upto 290 ppm) and Ce (upto 1942 ppm). High Ce and Y is attributed to higher degree of REE fractionation whereas high Zr concentration could be due to several reasons. Geochemical study revealed that Zr was mobile to some extent during hydrothermal alteration and in that process it might have become enriched. Petrographic study did not give a clear indication of mineral phase due to higher degree of ferrugenisation. However, previous XRD data from R&D works has reported the presence of Baddeleyite in Buriwara. Other Zr bearing phases like Gittinsite, Zaktzerite (Li-Na-Zr Silicate), Vlasovite occurring as secondary Zr minerals has also been reported. It has also being noticed that the tuff and agglomerate which are evolved in REE is also enriched with HFS elements. Thus, a positive correlation could be established between these elements with respect to both the lithotypes. A comparative assessment of HFS from tuff and agglomerate with crustal abundance (ppm) (*crustal abundance values from Haynes et.al. 2016-17*) is shown in *Table 7.2* and diagrammatically depicted in the bar diagram *(Figure 7.1).*

Table 7. 2 Average concentration of HFS elements in tuff and agglomerate from Buriwara and average concentration in continental crust

	Average concentration (ppm)		**Crustal abundance (ppm)**
HFS	**Tuff (n=16)**	**Agglomerate(n=6)**	
Ce	800	1008	66.5
Y	644	678	33
Nb	289	265	20
Zr	8895	5567	250

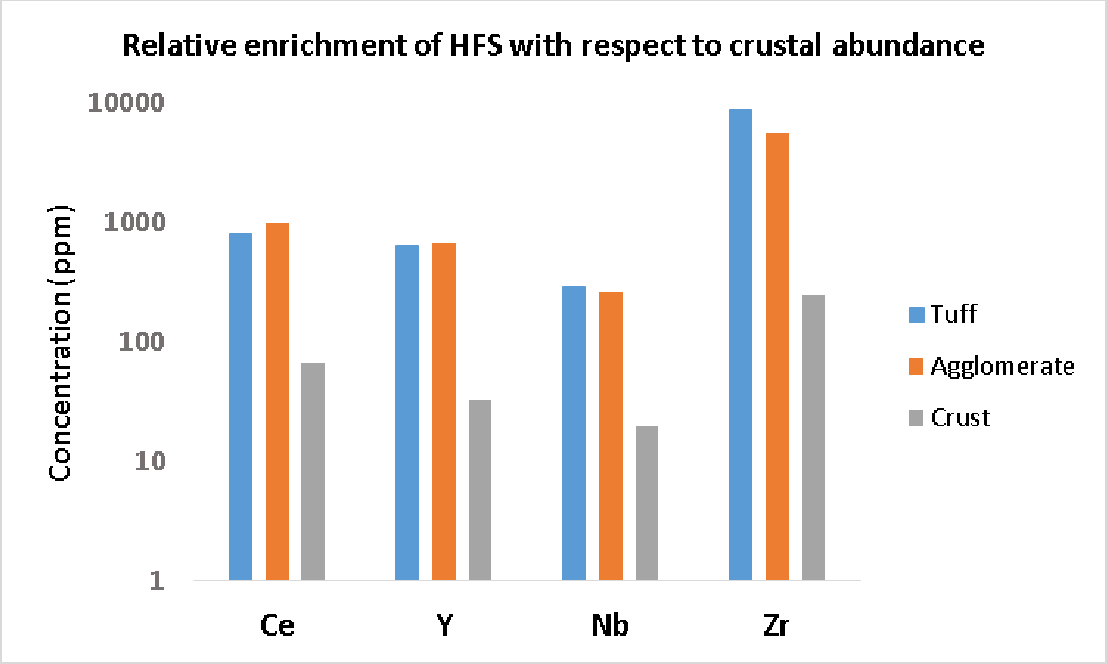

Figure 7. 1 Bar diagram depicting relative enrichment of HFS elements in tuff and agglomerate plotted with respect to average crustal abundance, described in logarithmic scale.

It has been observed that the concentration of Zr in tuff is relatively higher than in agglomerate. The possible reason could be magmatic fractionation. Zr being an incompatible element might have enriched in the residual magma and highly concentrated in the later evolved phases such as tuff. Another possibility could be homogeneity in compositions. While tuff is composed of very fine grained homogeneous ash sized particles, agglomerate on the other hand is having lithic fragments as well as fine matrix. In this study, the agglomerate analysis is on the basis of whole rock sample including both fragment and matrix. From the petrographic study, the rock fragments are identified to be similar to that of surrounding rhyolite, having lower REE and Zr concentration which might be a reason for dilution of concentration. Thus, to understand their respective Zr compositions, sampling from matrix and fragment parts have been carried out separately which would be taken up as future work from the current M.Tech study.

CHAPTER 8

STUDY OF TECTONIC ENVIRONMENT

We are all aware that peralkaline silicic rocks are characteristics of epirogenic uplift and rift formation on the continents but they may also form in several other tectonic settings such as oceanic islands, during their later stage of orogenic cycles, as isolated occurrence in active mobile belts and in areas of extensional tectonics at or near continental plate margins. Their emplacement is effected during periods of dominantly tensional stress. Pearce et al (1984) proposed a classification of granite types according to tectonic setting. This classification involves geochemistry of HFS elements as their concentration and relative abundances are stable during weathering, low grade hydrothermal activity and metamorphism. This phenomenon has also been observed in the present geochemical study with altered vs unaltered rock. *Figure 8.1* presents tectonic setting discrimination diagrams based on trace elements Rb, Nb and Y. Most of the studied rocks are projected on the within-plate magmatism area for both Rb vs Y+Nb as well as Nb vs Y. Also, the rocks in Buriwara are enriched with radioactive mineral U and Th along with REE, RM and HFSE which are characteristics of a typical within plate magmatic tectonic setting. Within plate magmatism is generally encountered in intracontinent ring complexes, attenuated continental crust and in oceanic islands (Rollinson, 1993). Our study area itself is a ring complex which is a part of Malani Igneous Suite (MIS). MIS owes its origin to intraplate hotspot tectonics (Pareek, 1981; Kochhar, 1984; Bhushan and Chandrasekaran, 2002; Vallinayagam, 2004). The age of MIS, 771-751 Ma (Torsvik et. al, 2001) is also contemporaneous with a major Pan African event of widespread intraplate, anorogenic magmatism represented by acid volcanics. Thus from the trace element diagrams (Pearce et al, 1984) the study area Buriwara which is a part of Siwana Ring Complex is concluded to be of intraplate origin evolved during a palaeo-tensional stress condition characterised by felsic peralkaline rocks.

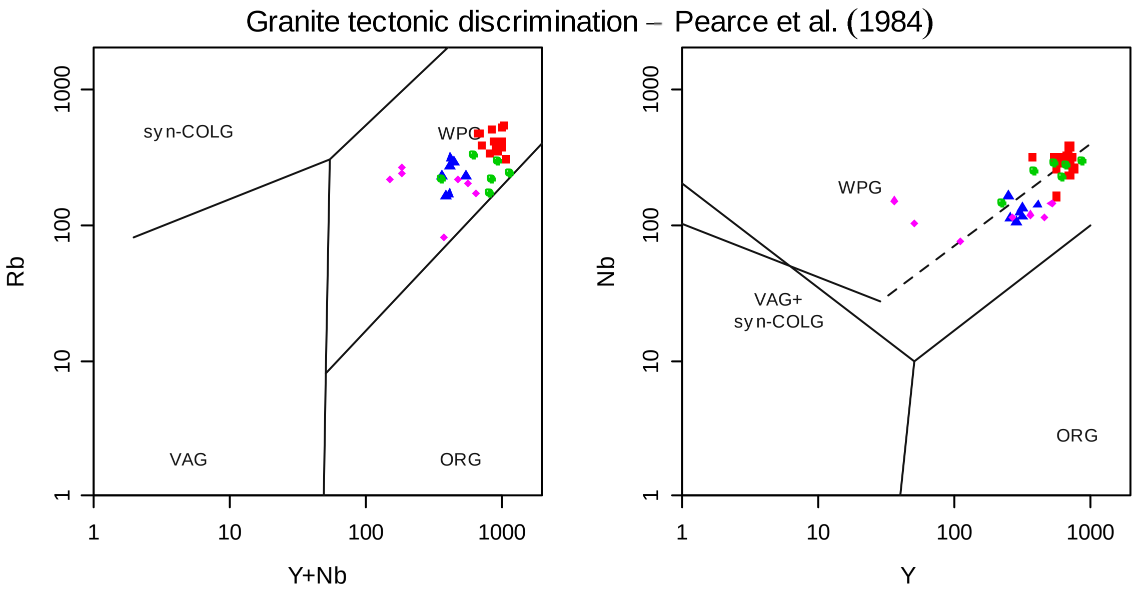

Figure 8. 1 Tectonic discrimination diagram by Pearce et. al. (1984)

CHAPTER 9

DISCUSSION

Siwana Ring Complex (SRC) of South Western Rajasthan is a well preserved caldera in Malani Igneous Suite (MIS) (~750Ma) comprising predominantly of peralkaline acid volcanics and intrusive ring dyke granite. Multiple phases of magmatism is deciphered in SRC, manifested by basalt-rhyolite-tuff sequences intruded by ring dykes of granite along ring fractures developed due to collapse of the caldera. Microgranite dykes and veins occur as intrusives within the bimodal volcanics and granite. These microgranite veins and pyroclastic tuff behave as host rock for REE in different areas within SRC.

This study was carried out in the western part of the ring complex at Buriwara area which comprises of tuff and rhyolite. Detailed geological mapping and radiometric survey shows variation within rhyolite, viz. massive and porphyritic separated by a thin layer of agglomerate. The tuff is composed of homogeneous fine ash sized pyroclast (<2mm) and is intensely ferrugenised whereas agglomerate is composed of angular rhyolitic clast having maximum size of upto 10 cm embedded within siliceous matrix. Both tuff and rhyolite are radioactive, recorded upto *0.06 to 0.12 µR/hr* (2-4x BG). Ferruginisation, kaolinisation and sericitisation are the prominent alterations in tuff. Presence of alkali feldspar phenocryst in porphyritic rhyolite gives an indication of hypersolvus origin and crystallization at low water pressure. Structural features mainly include three sets of joints NE-SW, NW-SE and E-W with columnar joints found in rhyolite. Flow banding is distinguished by alternate siliceous and dark bands which is mainly having easterly flow with dip ranging from 30° to 50°. Signatures of caldera collapse faulting indicated by striation marks plunging towards the centre of the ring is also marked. Other volcanic textures like lithophysae and spherulites in rhyolite supported volcanic origin.

Petro-mineralogical study was carried out to understand the texture and rock characterization. The rhyolites are mainly quartzo-feldspathic with occasional presence of tabular microlaths of aegirine. Perthitisation of alkali feldspar in porphyritic rhyolite is commonly observed. The massive rhyolite is having interlocking and hypidomorphic texture. Compositionally, the tuff is similar to rhyolite, so they are identified as rhyolitic tuff. The texture is non-welded and intense ferrugenisation has imparted a reddish and masky appearance. The agglomerate is having lithic fragments of rhyolite and crystal fragments of alkali feldspar supported by siliceous matrix where flow structures, volcanic textures are prominent. Non-undulose quartz, perlitic cracks, spherulitic quartz etc. are common volcanic signatures present invariably in all the lithotypes. Flow banding is also distinctly observed and signature of faulting is also marked by these bandings by offset along micro-cracks.

Geochemical characterizations on different variants of litho-units present in the study area are as follows:

- The tuff and the associated rocks are rhyolitic and falls in the Comendite (Al-rich) and Pantellerite (Fe-rich) variety of rhyolite. They are characterized by high concentration of SiO_2, Na_2O, K_2O, Zr, Nb, Y & REE and low concentration of MgO, Fe_2O_3 (t), CaO, Cr, Ba, Ni & Sr.
- Geochemical study of individual lithotype suggest that the tuff, rhyolite and agglomerate are genetically correlated. From major, minor and trace element analysis they are found to have evolved from fractional crystallization of the parental magma. Strong negative europium anomalies in chondrite-normalized REE plots and highly depleted Sr in chondrite normalized trace elemental plots are suggestive of the fractionation of plagioclase feldspar. The REE fractionation pattern having $(La/Yb)_N$= 2.14-6.87, $(La/Sm)_N$=1.81-3.80 and $(Gd/Yb)_N$=0.64-1.17 is forming a slightly negative slope which also supports magmatic fractionation. Again, such a lower slope is entitled

to enrichment of HREE, which also indicates that no significant fraction of HREE bearing phase such as garnet had taken place. The primary magmatic evolution trend is also depicted by other trace/minor elements viz. positive correlation between Al_2O_3 and TiO_2, Y and Nb, Zr and Nb etc.

- Alteration studies revealed that the tuff is altered where ferruginisation, silicification, sericitization and kaolinisation are prominent. Although, alteration of other lithotypes cannot be totally denied but major part is unaltered whereas the tuff is homogeneously affected by ferrugenisation. Blebs of kaoline could also be seen megascopically. Geochemical plot of alteration studies revealed sericitisation in tuff from the ternary diagram proposed by Nesbitt and Young (1984, 1989) where trends towards commonly altered minerals with end members $(CaO+Na_2O)$, Al_2O_3 and K_2O is studied. The alteration had affected geochemistry of the rock where alkali elements, especially Na had been significantly depleted. It has also affected the concentration of K and Al and thus it is seen that the tuff is peraluminous whereas the unaltered lithotypes are peralkaline. A distinct linear correlation from peralkaline to peraluminous field in A/NK vs A/CNK plot thus illustrates that the parental magma was peralkaline and the tuff has attained peraluminous nature because of mobility of these element. Thus the primary variations in the compositions of tuff are a function of magmatic evolution which was accentuated by later hydrothermal alterations and it had also impacted the enrichment of REE and U. U/Th plot of tuff are also forming a scatter which suggest that alteration has affected their concentration. U behaved as mobile element and were variably concentrated in altered rocks during post-magmatic hydrothermal alteration resulting in higher U concentration and U/Th ratio. The tuff which was initially rich in intrinsic REE have become more enriched by the alteration as REE and U are occurring in adsorbed state on ferrugenised matrix.

- Al_2O_3 vs TiO_2, Nb vs Zr, Y vs Nb shows positive correlation irrespective of altered as well as unaltered samples. Thus, being high field strength elements they are unaffected by alteration and so they could be taken into consideration for rock characterization as well as tectonic environment study.

As far as REE mineralisation is concerned, the tuff and agglomerate could be potential rock for hosting REE. The chondrite normalized plot for the average REE has indicated that the agglomerate is having an elevated concentration of REE followed by tuff. Samples from agglomerate (n=6) have analyzed 4300ppm REO and tuff (n=16) have analyzed 3200ppm REO. This gives a clear indication that REE mineralisation in Buriwara is mainly associated with pyroclastic host. The tuff being altered and highly ferrugenised has been further enriched on its intrinsic REE by hydrothermal event. The agglomerate consists of angular pyroclastic fragments of rhyolite bound within silicious matrix and the REE enrichment is suspected to be in the matrix part. As the analysis is based on whole rock, exact mode of mineralisation is difficult to understand but since the lithic fragments are of non-mineralised rhyolite (as identified during petrographic study), the possibility is in favour of the matrix part. Along with REE, Nb enrichment is also associated with these two lithotypes. Thus, the pyroclastic formations of Buriwara, viz. tuff and the agglomerate together could be a promising host rock for Rare Metal and Rare Earth exploration, especially for HREE like Dy which anlysed upto175 ppm in agglomerate and 140ppm in tuff. Along with REE, the tuff and agglomerate are also enriched in HFS elements like Y, Zr, Nb and Ce .Tuff samples (n=16) analyzed Y upto 768 ppm, Zr upto 10220 ppm, Nb upto 378 ppm and Ce upto 1498 ppm whereas the agglomerate samples (n=6) analysed Y upto 962 ppm, Zr upto 7400 ppm, Nb upto 290 ppm and Ce upto 1942 ppm. Thus REE and HFS are positively correlated which is a good indication of potential Rare Metal (RM) and Rare Earth Element(REE) mineralisation in pyroclastic rocks of Buriwara.

Implication about tectonic environment was made using the relatively immobile HFS elements. In the trace element diagrams (Pearce et al, 1984) the samples from all the lithotype plots in the within plate granitic field which are generally hotspot related magmatism. The study area Buriwara which is a part of Siwana Ring Complex is concluded to be of intraplate origin evolved during a palaeo-tensional stress condition. Also peralkaline silicic rocks itself are characteristics of extensional tectonics settings associated with epirogenic uplift and rift formation.

CHAPTER 10

CONCLUSION AND FUTURE SCOPE OF WORK

The bimodal volcano-plutonic rocks in Siwana Ring Complex is peralkaline, which makes it unique from other equivalent rocks of Malani Igneous Suite. The later phase of microgranite dykes and felsic tuff are highly evolved and enriched. Buriwara area lying in the western part of SRC is composed of tuff, massive rhyolite, porphyritic rhyolite and agglomerate. Geochemical study reveals that they are peralkaline, but the tuff being affected by post magmatic hydrothermal alteration has experienced alkali element mobility, due to which it has shown peraluminous nature. The alteration has also affected the U/Th ratio in tuff which implies that U was significantly mobile. However, the genesis of all the lithotypes is from a single parental magma and their evolution is attributed to magmatic fractionation. Magmatic fractionation is supported by strong negative Eu anomaly indicating plagioclase fractionation. The high intrinsic concentrations of the valuable elements could be enrichment in late residual magma. Ferrugenisation, sericitisation, kaolinisation and silicification are prominent alterations. Detailed geological mapping and radiometric survey revealed another REE bearing lithotype i.e. agglomerate trending N-S which is exposed as a thin outcrop separating the massive and porphyritic rhyolite. So the pyroclastic rocks, tuff and agglomerate are potential host rock in Buriwara which are also showing radioactivity upto *0.06 to 0.12 µR/hr* (2-4x BG). Joints are the primary structural elements and flow warping was also occasionally noticed. Evidence of faulting is preserved by slickensides which are caldera collapse generated faults. Thus, structural features might have control on mineralisation. REE results of detailed survey sample indicates the average concentration in agglomerate as 0.43% REO, 0.034% Nb_2O_5 which is exposed over an area of 1km x 0.01 km and the rhyolitic tuff have average REO 0.32%, 0.041% Nb_2O_5 exposed over an area of 1.4 km x 0.3 km. An important aspect to be noted is that this area is favourable for HREE exploration as REE fractionation pattern indicates HREE enrichment and valuable HREE such as Dy is having a significant grade of 0.020 % in agglomerate and 0.016% in tuff, which is considered as economic grade worldwide. Along with REE, the tuff and agglomerate are also enriched in HFS elements like Y, Zr, Nb and Ce. Hence, it is concluded that the pyroclastic rock, agglomerate and tuff in Buriwara are likely to yield favourable result with respect to REE and Nb in further sub-surface exploration. Also, as a future scope of work, separate sampling from the matrix and fragment part of agglomerate would insight upon a better understanding of their respective compositions and nature of occurrences of REE, Nb and Zr.

REFERENCES

Anderson, A.T., Davis, A.M. and Lu, F (2000). Evolution of Bishop Tuff Rhyolitic Magma based on melt and magnetite inclusions and zoned phenocrysts. Journal of petrology, Vol.41(3), pp.449–473

Annual report FS 2011-12, Siwana Ring Complex, Atomic Minerals Directorate for Exploration and Research, WR, (Unpublished)

Banerjee, A. (2013). Petro-mineralogy and geochemistry of volcano-sedimentary suite of rocks with special emphasis on the alteration zones around the central part of Siwana ring complex, Barmer district, Rajasthan. Thesis for M.Tech under Homi Bhabha National Institute. (Unpublished)

Bhushan, S.K. (2000). Malani Rhyolites — A Review, Gondwana Research 3(1), pp.65-77

Bhushan, S.K. and Chandrasekaran, V. (2002). Geology and geochemistry of the magmatic rocks of the Malani Igneous Suite and Tertiary Alkaline Province of Western Rajasthan. Memoirs of Geological Survey of India, Vol.126, pp. 1-129

Bidwai, R. and Krishnamurty, P. (1996). Radioelement abundances in some acid rocks of Neoproterozoic Malani Igneous Suite in parts of western Rajasthan and implications. Journal of atomic mineral science, Vol.4, pp.21-27

Bidwai, R. and Krishnamurthy, P. (1997). Possible lava channels and tubes from the Siwana Caldera Sequence, Siwana, Barmer District, Rajasthan. Jour. Geol. Soc. India, Vol.50(3), pp.303-305.

Bidwai R (2001). Geological, structural and geochemical characterization of the Siwana Ring Complex, Barmer district, Rajasthan for favourable volcanogenic, caldera related uranium and rare metal mineralization, PhD Thesis, Osmania University. (Unpublished)

Blanford, W. T. (1877). Geological notes on the Great Indian Desert bctwccn Sind and Rajputana: India. Geological Survey Records, Vol.10, pt. 1, p.17

Boynton, W.V. (1984). Cosmochemistry of the rare earth elements: meteorite studies. Rare Earth Element Geochemistry, Ed by P. Henderson, Elsevier, Amsterdam, pp, 63-114

Coulson, A.L. (1933). The Geology of the Sirohi state Rajputana. Mem.Geol.Surv of India, Vol.63(1), p.1-133

Cuney, M. and Kyser, K. (2008). Recent and not so recent developments in uranium deposits and implications for exploration, Mineralogical association of Canada, Short course series, Vol.39, Joint publication of MAC and SGA.

Davies, J.F. and Whitehead, R.E. (2006). Alkali-alumina and MgO-alumina molar ratios of altered and unaltered rhyolites: Exploration and Mining Geology, Vol.15, p. 77–90.

Dostal, J. (2017). Rare Earth Element Deposits of Alkaline Igneous Rocks. Resources 2017, 6, 34

Elliot, B. A. (2018). Petrogenesis of Heavy Rare Earth Element Enriched Rhyolite: Source and Magmatic Evolution of the Round Top Laccolith, Trans-Pecos, Texas. The Bureau of Economic Geology, The University of Texas at Austin, Austin, TX 78712, USA

Fisher, R.V. (1966). Rocks Composed Of Volcanic Fragments And Their Classification. Earth-Science Reviews - Elsevier Publishing Company, Amsterdam, pp.287-298

Goodell, P.J. (1985). Classification and model of uranium deposits in volcanic environments in International Atomic Energy Agency, Uranium deposits in volcanic rocks: International Atomic Energy Agency Panel Proceedings of a Technical Committee Meeting, El Paso Texas April 2–5, pp. 1–17.

Goswami, S., Dey, S., Zakaulla, S. and Verma, M.B. (2020). Active rifting and bimodal volcanism in Proterozoic Papaghni sub-basin, Cuddapah basin (Andhra Pradesh), India, J. Earth Syst. Sci. Vol.129 21

Haynes, W.M., Lide, D.R. and Bruno, T.J (2016-17). CRC Handbook of Chemistry and Physics: A ready reference book of Chemical and Physical data, CRC Press, 97th edition.

Holohan, E.P., Walter, T.R., Martin, P.J., Schöpfer, John, J., Walsh, Benjamin van Wyk de Vries and Valentin R. Troll (2013). Origins of oblique-slip faulting during caldera subsidence. Journal of Geophysical Research: Solid Earth, Vol. 118, pp.1778–1794

Jain, R.S., Miglani, T.S., Kumar, S., Swarnkar, B.M. and Singh, R. (1996). Rare metal and rare earth rich peralkaline, agpaiitic granitoid dykes of Siwana Ring Complex, District Barmer, Rajasthan. Curr. Sci., Vol.70, pp.854-858.

Kochhar, N. (1984). Malani igneous suite; hot-spot magmatism and cratonization of the Northern part of the Indian Shield. Journal of the Geological Society of India, Vol.25, pp.155-161

Kochar N., Vallinayagam, G. and Gupta, L. N. (1991). Zircon from the granitic rocks of the Malani Igneous Suite: Morphological and chemical studies, Jour Geol Soc Ind, Vol. 38, No 6, pp.561-576.

Kochhar, N. (1999). Rare metal potential of the A type Malani granites, northwestern peninsular India, Indian Minerals.

Kochhar, N. (2000). Attributes and significance of the A type Malani magmatism, North-western Peninsular India. Crustal evolution and metallogeny in the North Western Indian shield. M Deb (Ed), New Delhi, Chapter 9, pp.158-188.

Kochaar, N. (2001). Anorogenic magmatism, mantle plume and assembly of the Late Proterozoic Malani supercontinent, NW Indian shield. Gondwana ResearchGroup Misc, Publiaction, Vol.12, pp.23-27

Krishnan, M.S. and Jacob, K. (1956). Malani beds: Lexique startigraphic international, Congres Geologique International Commision de Stratigraphic, Vol.3, ASIE, Fascicule,8a, p.165.

La Touche, T.H.D. (1902). Geology of western Rajputana. Mem. Geol. Surv. India, Vol. 35(1), pp. 1-116.

Leat, P.T., Jackson, S.E., Thorpe, R.S. and Stillman, C.J. (1986). Geochemistry of bimodal basalt-subalkaline/peralkaline rhyolite provinces within the Southern British Caledonides. Journal of the Geological Society, Vol.143, pp.259-273.

Macdonald, R., Baginski, B., Ronga, F., Dzierżanowski, P., Lustrino, M., Marzoli, A. and Melluso, L. (2012). Evidence for extreme fractionation of peralkaline silicic magmas, the Boseti volcanic complex, Main Ethiopian Rift. Miner Petrol 104, pp.163–175

Middlemost, E.A.K., (1994). Naming materials in the magma/igneous rock system. Earth-Science Reviews Vol.37, pp.215-224

Motoki, A., Sichel, S.E., Vargas, T., Melo, D.P., and Motoki, K.F (2015). Geochemical behaviour of trace elements during fractional crystallization and crustal assimilation of the felsic alkaline magmas of the state of Rio de Janeiro, Brazil. Anais da Academia Brasileira de Ciências 87(4)

Narayan Das, G.R., Begchi, A.K., Chaube, D.N., Sharma, C.V. and Naveneetham, K.V. (1978). Rare metal content, geology and tectonic setting of the alkaline complexes across the Trans- Aravalli region, Rajasthan, India: Verma, P.K., Verma, V.K. (Eds.), Recent researches in Geology. Hindustan Publishing Corporation, Delhi, Vol.7, pp.201-217.

Nash JT (2010). Volcanogenic Uranium Deposits: Geology, Geochemical processes and criteria for resource assessment, Open-File Report 2010–1001, U.S. Department of the Interior U.S. Geological Survey.

Nelson Eby, G. and Kochhar, N. (1990). Geochemistry and petrogenesis of Malani Igneous suite, North peninsular India. Journal of Geological society of India, Vol.36, pp.109-130

Nesbitt, H.W. and Young, G.M. (1984). Prediction of some weathering trends of plutonic and volcanic rocks based on thermodynamic and kinetic considerations. Geochemica et Cosmochimica Acta, Vol.48, pp.1523-1534

Pareek, H.S. (1981). Petrochemistry and Petrogenesis of the Malani Igneous Suite, India. Geological Society of America Bulletin, no.2 Part II, pp.206-273

Pascoe, E.H. (1960). Manual of the geology of India and Burma, Geoi. Sum. Ind., Vol. 2, pp. 553-560.

Pearce, J.A., Harris, N.B.W., Tindle, A.G. (1984).Trace Element Discrimination Diagrams for the Tectonic Interpretation of Granitic Rocks. Journal of Petrology, Vol.25, Issue 4, pp.956–983

Rollinson, H. (1993). Using geochemical data: Evaluation, presentation, interpretation. 1st edition. British Library Cataloguing-in-publication Data.

Ronga, F. Lustrino, M. Marzoli, A. and Melluso, L (2010). Petrogenesis of a basalt-comendite-pantellerite rock suite: the Boseti Volcanic Complex (Main Ethiopian Rift). Miner Petrol, pp.227–243

Shand, S.J. (1943). The eruptive rocks: 2nd edition, John Wiley, New York, p.444

Singh, A.K. and Vallinayagam, G. (2004). Geochemistry and petrogenesis of anorogenic basic volcanic-plutonic rocks of the Kundal area of Malani Igneous Suite, Western Rajasthan, India. Proc. Ind. Acad. Sci. (Earth Planetary Science), Vol.113, pp. 667-681.

Singh, L.S. and Vallinayagam, G. (2013). Geochemistry and Petrogenesis of Acid Volcano-plutonic Rocks of the Siner Area, Siwana Ring Complex, Northwestern Peninsular India. Journal Geological Society of India, Vol.82, pp.67-79

Sinha Roy, S., Malhotra, G. and Mohanty, M. (1998). Geology of Rajasthan, Mem Geol Soc India.

Sun, S. S. and McDonough, W. F. (1989) Chemical and isotopic systematics of oceanic basalts: implications for mantle composition and processes. Magmatism in Ocean Basins (ed. A. D. Saunders and M. J. Norry); Geol. Sot. Spec. Pd. 42, pp.313-345.

Thompson, R. N. (1982). Magmatism of the British Tertiary Volcanic Province, Scott. J. Geol. Vol.18, pp.49–107

Torsvik, T.H., Ashwal, L.D., Tucker, R.D., Eide, E.A. (2001). Geochronology and palaeomagnetism of the Seychelles microcontinent: the India link. Precamb. Res. (in press).

Upadhyay, D and Banerjee, A. (2011). Evaluating the potential of Malani Igneous Suite rocks, Rajasthan for Uranium using petrological & geochemical proxies, A BRNS R&D project. (Unpublished)

Vallinayagam, G. (1998). Rare metal bearing and barren distinction of alkali granites, Piplun area, Siwana ring complex, Rajasthan, India: petrological and geochemical evidences. In: B.S. Paliwal, (Ed.), The Indian Precambrian, Scientific Publisher, Jodhpur, pp.492-501.

Vallinayagam, G. (1999). Nb, Zr, Y, REE rich dyke rocks, Piplun area, Siwana Ring Complex, Rajasthan. In: B.S. Paliwal (Ed.), Proc. Geological Evolution of Northwestern India, Scientific publisher, Jodhpur, pp.94-102.

Vallinayagam, G. (2004). A report on rare metals and rare earths in the Siwana Ring Complex, Rajasthan. Jour. Applied Geochemistry, Vol.6(2), pp.387-391.

Winchester, J.A. and Floyd, P.A. (1977). Geochemical discrimination of different magma series and their differentiation products using immobile elements. Chem. Geol., Vol.20 pp.325--343.